Molecular Therapy
Original Article

mRNA-LNP vaccines tuned for systemic immunization induce strong antitumor immunity by engaging splenic immune cells

Sanne Bevers,[1,7,9] Sander A.A. Kooijmans,[2,9] Elien Van de Velde,[1] Martijn J.W. Evers,[2] Sofie Seghers,[1] Jerney J.J.M. Gitz-Francois,[2] Nicky C.H. van Kronenburg,[3] Marcel H.A.M. Fens,[3] Enrico Mastrobattista,[3] Lucie Hassler,[4] Helena Sork,[5] Taavi Lehto,[5,6] Kariem E. Ahmed,[6] Samir El Andaloussi,[6] Katja Fiedler,[1] Karine Breckpot,[7] Michael Maes,[1] Diane Van Hoorick,[1] Thierry Bastogne,[4,8] Raymond M. Schiffelers,[2] and Stefaan De Koker[1]

[1]eTheRNA Immunotherapies, 2845 Niel, Belgium; [2]CDL Research, University Medical Center Utrecht, 3508 GA Utrecht, the Netherlands; [3]Department of Pharmaceutics, Utrecht Institute for Pharmaceutical Sciences, Utrecht University, 3584 CG Utrecht, the Netherlands; [4]CYBERnano, 54000 Nancy, France; [5]Institute of Technology, University of Tartu, 50411 Tartu, Estonia; [6]Department of Laboratory Medicine, Karolinksa Institutet, 141 52 Huddinge, Sweden; [7]Laboratory for Molecular and Cellular Therapy (LMCT), Free University of Brussels, 1090 Jette, Belgium; [8]CRAN, Université de Lorraine, CNRS, INRIA BIGS, 54506 Vandœuvre-lès-Nancy, France

mRNA vaccines have recently proved to be highly effective against SARS-CoV-2. Key to their success is the lipid-based nanoparticle (LNP), which enables efficient mRNA expression and endows the vaccine with adjuvant properties that drive potent antibody responses. Effective cancer vaccines require long-lived, qualitative CD8 T cell responses instead of antibody responses. Systemic vaccination appears to be the most effective route, but necessitates adaptation of LNP composition to deliver mRNA to antigen-presenting cells. Using a design-of-experiments methodology, we tailored mRNA-LNP compositions to achieve high-magnitude tumor-specific CD8 T cell responses within a single round of optimization. Optimized LNP compositions resulted in enhanced mRNA uptake by multiple splenic immune cell populations. Type I interferon and phagocytes were found to be essential for the T cell response. Surprisingly, we also discovered a yet unidentified role of B cells in stimulating the vaccine-elicited CD8 T cell response. Optimized LNPs displayed a similar, spleen-centered biodistribution profile in non-human primates and did not trigger histopathological changes in liver and spleen, warranting their further assessment in clinical studies. Taken together, our study clarifies the relationship between nanoparticle composition and their T cell stimulatory capacity and provides novel insights into the underlying mechanisms of effective mRNA-LNP-based antitumor immunotherapy.

INTRODUCTION

Messenger RNA (mRNA) vaccines are extremely versatile, as mRNA sequences can be easily tailored to encode any antigen of interest, enabling both rapid and mass-scale vaccine development against emerging pathogens as well as personalized vaccine design against cancers. Key to the success of the currently approved SARS-CoV2 mRNA vaccines and of many mRNA-based prophylactic vaccines in clinical development are lipid-based nanoparticles (LNPs), delivery vehicles that mediate efficient mRNA expression *in situ* and endow the vaccine with intrinsic adjuvant properties.[1] LNPs are composed of an ionizable lipid, a phospholipid, cholesterol, and a PEGylated lipid, with the ionizable lipid being considered the most important driver of mRNA expression. In contrast to their predecessors having a cationic charge across a wide variety of pH ranges, ionizable lipids are pH-sensitive lipids that endow the LNPs with a positive, membrane fusion-promoting charge at endosomal pH while having a neutral charge at physiological pH.[2] The ionizable lipid is required to encapsulate the mRNA and drives endosomal escape. The PEGylated lipid improves LNP stability and controls the interaction of the LNPs with blood proteins and cells. Cholesterol and the phospholipid contribute to LNP stability and endosomal membrane destabilization.[2] Intramuscular[3] or subcutaneous[4] administration of mRNA-LNPs has been reported to elicit CD8 T cell responses against the mRNA encoded antigen. In these strategies, mRNA is delivered to local antigen-presenting cells (APCs), resulting in low to moderate antigen-specific CD8 T cell levels in the circulation. However, to effectively combat tumors (especially at distant locations) potent, long-lasting, and systemic CD8 T cell responses are required. Intravenous (i.v.) delivery of mRNA vaccines has been described to confer enhanced T cell responses and antitumor immunity,[5–7] which is likely related to its capacity to mobilize the large pools of APCs present in the spleen. Induction of strong CD8 T cell responses has been confirmed clinically, upon i.v. immunization of metastatic melanoma

Received 2 December 2021; accepted 9 July 2022;
https://doi.org/10.1016/j.ymthe.2022.07.007.

[9]These authors contributed equally

Correspondence: Stefaan De Koker, eTheRNA Immunotherapies NV, 2845 Niel, Belgium.
E-mail: stefaan.dekoker@etherna.be

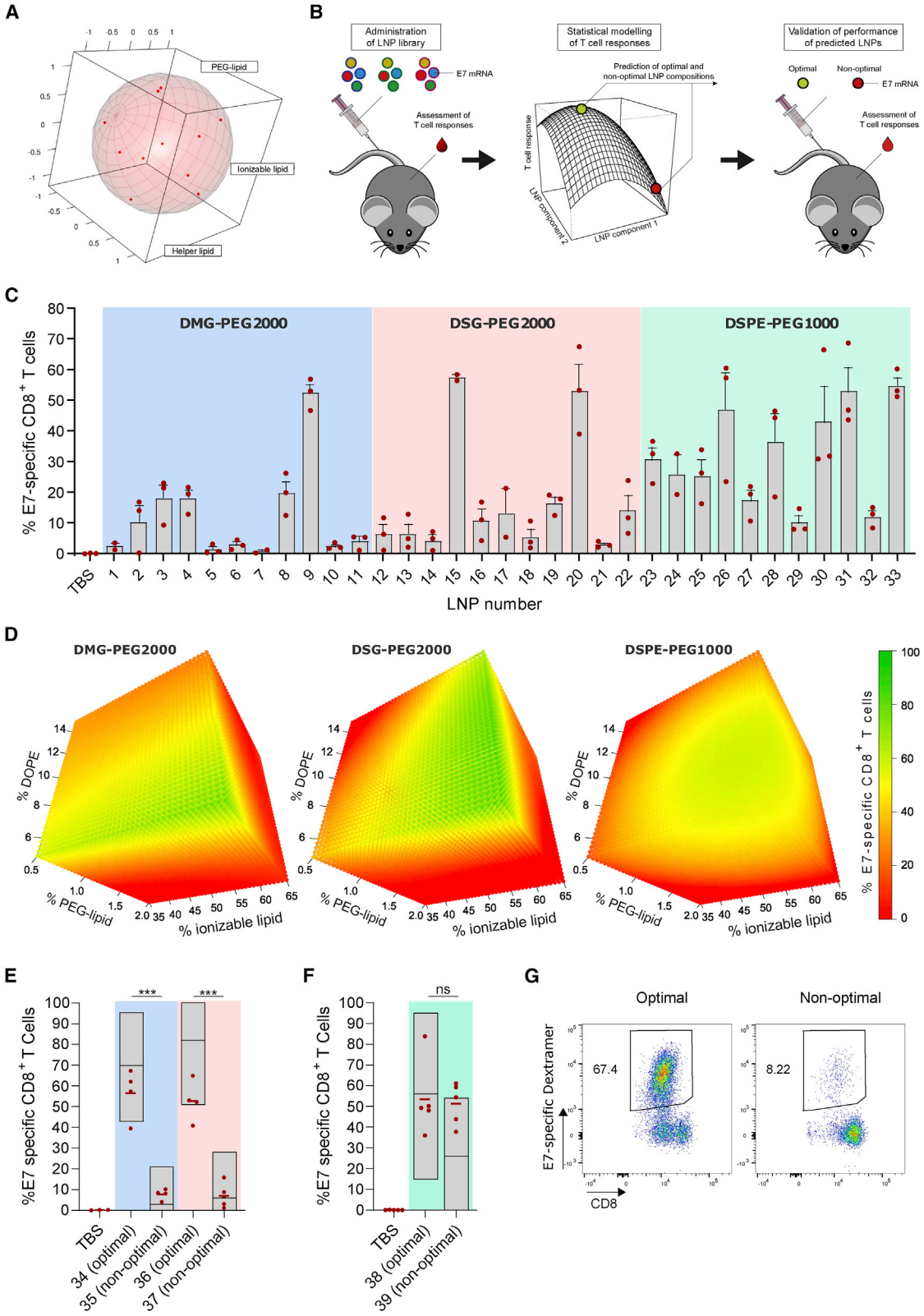

(legend on next page)

patients with mRNA lipoplexes composed of 1,2-dioleoyl-*sn*-glycero-3-phosphoethanolamine (DOPE) and the cationic lipid DOTMA,[8] but no LNP-based formulation has yet been used in the clinic for i.v. therapeutic cancer vaccination. LNPs might show even further improved activity compared with lipoplexes given their enhanced intrinsic potential to transfect cells. Nonetheless, standard LNP formulations typically deliver RNA to hepatocytes upon i.v. delivery,[9–11] instead of the APCs needed to instigate CD8 T cells. In this study, we speculated that LNPs could be tailored toward systemic vaccination through optimization of the molar ratio between the four lipids and selection of an appropriate polyethylene glycol (PEG) lipid. These parameters are known to impact LNP features such as size, ζ potential, pharmacokinetics, and biodistribution, which ultimately will determine *in vivo* immunogenicity.[4,9,12–16] To design and screen a virtually unlimited variety of potential LNP compositions in a time- and cost-effective manner, we adopted a quality-by-design approach based on a statistical design-of-experiment (DOE) coupled to Bayesian regression modeling. This strategy enabled us to identify the key composition parameters that determine immunogenicity and to predict optimal LNP compositions within a single round of *in vivo* immunogenicity assessment. Optimal LNP compositions (within the constraints of the design space) resulted in strong CD8 T cell responses that could be boosted by repeated administration and conveyed antitumor efficacy in a syngeneic mouse TC-1 tumor model. Mechanistic studies revealed that the T cell response was dependent on initial mRNA expression by various APCs in the spleen and on the induction of type I interferons (IFNs). Surprisingly, we also discovered a previously unrecognized role of B cells in instigating antigen-specific CD8 T cell responses upon intravenous mRNA-LNP vaccination.

RESULTS

DOE-driven optimization of LNP composition maximizes T cell responses

We aimed to maximize the T cell response elicited by antigen-encoding mRNA-LNPs composed of the ionizable lipid Coatsome SS-EC,[17] cholesterol, DOPE, and a PEGylated lipid. The human papillomavirus 16 (HPV16) oncoprotein E7 was used as the antigen of choice. HPV16 is a frequent cause of cervical, anal, and oropharyngeal cancer. The oncogenic potential of HPV is driven by persistent expression of the viral oncoproteins E6 and E7, which cause degradation of the tumor-suppressor proteins p53 and Rb.[18] Whereas E6 is not immunogenic in standard inbred mice strains,[19] E7 contains a well-established class I epitope recognized in C57BL/6 mice, making it a highly relevant and suitable antigen to assess the potency of vaccine platforms in mice. Using DOE methodology, an LNP library was designed to address the impact of lipid molar ratio and PEG-lipid chemistry on the T cell response. Three PEGylated lipids (DMG-PEG2000, DSG-PEG2000, and DSPE-PEG1000) that differ in length and chemistry of the acyl chain and/or the molecular weight of PEG were explored. Per PEG-lipid chemistry, LNPs were formulated at 11 different molar ratios of the four lipid components, yielding a library of 33 LNPs (Table S1). These 11 molar ratios were derived from a Roquemore hybrid design[20] in which the molar percentage of ionizable lipid, DOPE, and PEG lipid each had five levels. Cholesterol was used as a "filler" variable that completed the total molar percentage to 100% (Figure 1A). This design is particularly suited for the generation of quadratic response surface models and more economic than traditional central composite or Box-Behnken designs (15 and 13 conditions required, respectively). The composition and properties (size, polydispersity index, percentage of mRNA, encapsulation, and ζ potential) of the LNPs are shown in Table S1. All LNPs remained stable at 4°C for 1 month (Figure S1). LNPs were administered i.v. three times at weekly intervals. Five days after the third injection, the percentage of E7-specific CD8 T cells in blood was determined. Data were subjected to Bayesian statistical modeling to identify the LNP components critical for activity (Figure 1B). Results showed that the magnitude of the CD8 T cell response heavily depends on the LNP composition (Figure 1C). Bayesian effect analysis (supplemental methods) identified PEG-lipid chemistry and molar percentage of PEG lipid as the most critical LNP attributes. In the cases of DSG-PEG2000- and DSPE-PEG1000-based LNPs, the percentage of ionizable lipid also had a critical impact. Interaction effects were found between the percentages of DOPE and the PEG lipids, indicating that LNP optimization required fine-tuning of all lipid components simultaneously. Bayesian regression modeling was applied to predict the immunogenicity of LNP compositions not included in our initial library (Figure 1D). For all PEG-lipid types, the predicted optimal T cell response region corresponded to high percentages of the ionizable lipid SS-EC (>50%) and low percentages of PEG lipid (<0.6%) and DOPE (<10%). To validate the predictive value of the models, we tested six new LNP compositions (LNP34–LNP39, Table S1) *in vivo*. T cell responses higher than or equal to the best performers of the original library were predicted for mice immunized with LNP34 (DMG-PEG2000), LNP36 (DSG-PEG2000), and LNP38 (DSPE-PEG1000) (optimal LNPs), whereas poor T cell responses

Figure 1. LNP composition was optimized for maximal T cell responses using DOE methodology

(A) Plot showing the uniform distribution of the 11 LNP compositions (with variable lipid ratios) over the experimental domain. An LNP library was prepared covering these 11 lipid ratios for three different PEG lipids (DMG-PEG2000, DSG-PEG2000, and DSPE-PEG1000), yielding a total of 33 LNPs. (B) Schematic representation of LNP optimization approach. (C) Percentage of E7-specific CD8 T cells in blood after three immunizations (weekly intervals, 10 μg of E7 mRNA) with the indicated mRNA-LNP compositions, as determined by MHC class I tetramer stain (n = 3). E7 mRNA was used as antigen of choice encoded by the mRNA. (D) Response surface plots modeled from the data in (C), showing LNP compositions with high (green) and low (red) predicted capacity to elicit CD8 T cell responses. (E and F) Percentage of E7-specific CD8 T cells in blood measured after three immunizations (weekly intervals, 10 μg of E7 mRNA) with predicted optimal and non-optimal DMG-PEG2000, DSG-PEG2000 (E), and DSPE-PEG1000 (F) LNPs. (G) Representative flow cytometry scatterplots of E7-specific CD8 T cells in blood after three immunizations (weekly intervals, 10 μg of E7 mRNA) with LNP34 (optimal) or LNP35 (non-optimal). In (C), (E), and (F), mean ± SD is shown with individual data points in red. In (E) and (F), statistics were assessed by one-way ANOVA with Sidak's multiple comparison test. ***$p < 0.001$; ns, not significant.

were predicted for LNP35 (DMG-PEG2000), LNP37 (DSG-PEG2000), and LNP39 (DSPE-PEG1000) (non-optimal LNPs). The experimental data largely matched the predictions and validated the models in the cases of DMG-PEG2000 and DSG-PEG2000 LNPs (Figures 1E and 1G; supplemental methods). In contrast to the predictions, LNP39 elicited T cell responses nearly equal to those of LNP38 (Figure 1F), meaning that the DSPE-PEG1000 LNP model could not be validated. Because of this unpredictable behavior and visual toxicity in mice (lethargy, pain symptoms) DSPE-PEG1000 LNPs were excluded from further assessment.

mRNA-LNP vaccines induce qualitative T cell responses and tumor regression

The success of cancer immunotherapy is determined by a multitude of factors, including the T cell phenotype and functionality. We first assessed the quality of the T cell response evoked by the optimal LNPs (LNP34 and LNP36). Therefore, mice received three weekly immunizations followed by a final immunization at day 50. E7 mRNA was supplemented with TriMix, which a mix of three mRNAs encoding murine CD70, murine CD40L, and a constitutively active TLR4, which increases the strength of the T cell response.[21] Expression of all four co-formulated mRNAs was confirmed by *in vitro* transfection (data not shown). For both LNPs, the kinetics and phenotypic traits of the T cell response were similar. Following three immunizations with E7-TriMix LNPs, over 70% of CD8 T cells in blood were E7 specific (Figure 2A). Five weeks after the third immunization (day 49), the percentage of E7-specific CD8 T cells remained highly elevated (approximately 40%, Figure 2A) with the majority displaying a short-lived effector cell phenotype (KLRG1$^+$ CD127$^-$) (Figures 2B and 2C). However, a noteworthy population (~10%) of memory precursor effector cells (KLRG1$^-$ CD127$^+$) was present as well. Functional memory conversion was evidenced by the rapid re-expansion of E7-specific CD8 T cells after the day-50 booster immunization (Figures 2A and 2C). IFN-γ concentrations in serum increased with every immunization (Figure 2D), indicating increased systemic immune stimulation. To assess T cell functionality, we performed an intracellular cytokine staining on splenocytes obtained from mice after three immunizations. Polyfunctional CD8 T cells, which produce more than one cytokine simultaneously, are associated with better control of infectious diseases[22,23] and tumors[24–26] and accounted for approximately 11% of CD8 T cells for both optimal LNPs (Figures 2E and 2F). To assess whether the activity of the LNPs also extended to other antigens, mRNA encoding the MC38 colon carcinoma-derived neo-epitope Adpgk or the B16-F10-derived melanocyte differentiation antigen Trp-2 was mixed with TriMix and encapsulated in LNP36. Augmented T cell responses were observed after two immunizations with LNPs containing both types of antigen-encoding mRNAs, especially when combined with TriMix (Figure S2). Next, therapeutic antitumor efficacy was assessed in mice bearing subcutaneous TC-1 tumors, which express HPV16 E7 antigen.[27] Treatment was initiated when tumors reached a mean diameter of 52 ± 4 mm^3 (Figure 2G). E7-TriMix treatment resulted in profound tumor growth inhibition of the established TC-1 tumors (Figure 2H) and significantly prolonged survival time (Figure 2I), yet tumors relapsed after cessation of treatment. We additionally assessed the capacity of mRNA-LNP-elicited T cells to reach the tumor bed. Two i.v. injections with the mRNA-LNPs led to a strong infiltration of CD8$^+$ tumor-infiltrating lymphocytes (TILs) into the tumor (Figures 2J and 2K), with over 70% being specific for E7 (Figure 2L). Treatment with LNP36 delivering TriMix without E7 or containing an irrelevant mRNA (Firefly luciferase [Fluc]) did not induce regression of tumors, nor did it result in increased percentages of E7-specific CD8 T cells in the tumor (Figures S3A and S3B). To understand why tumors relapse despite the high numbers of vaccine-elicited E7-specific CD8 T cells, we compared tumor E7 expression levels in LNP36 versus Tris-buffered saline (TBS)-treated tumors. Tumors that relapsed after vaccination with E7-TriMix delivered by LNP36 showed a profound decrease in E7 expression levels compared with TBS (Figure S3C), suggesting loss of antigen expression as a major mechanism of immune escape. Moreover, at the time of relapse (day 35) tumors were less infiltrated by E7-specific CD8 TILs compared with 2 days after the second immunization (day 17, regression phase) (Figure S3B). In addition, TILs in regressing tumors showed proliferative potential (Ki67$^+$) and cytolytic capacities (granzyme B$^+$), whereas TILs present in relapsing tumors predominantly had a non-proliferative (Ki67$^-$), non-cytolytic (granzyme B$^-$) phenotype and expressed high levels of the immune-checkpoint PD-1 (Figures S3D and S3E). This "non-reactive" phenotype might be inflicted by immune-suppressive factors present in the tumor microenvironment or driven by the lack of E7 presence. Further immunophenotyping revealed no significant increases in the levels of myeloid-derived suppressor cells, regulatory T cells, or M2 macrophages in relapsing tumors compared with regressing tumors (Figure S3F), arguing against a major role of these cells in the observed tumor escape.

Early LNP association with splenic APCs correlates with immunogenicity

To address whether the magnitude of the T cell responses after the third immunization can be correlated to the initial biodistribution of mRNA uptake and expression at organ level and cell-type level, we encapsulated a mixture of Cy5-labeled (25% substituted cyanine-5 uridine-5′-triphosphate [Cy5-UTP], 75% substituted 5-methoxy UTP), and unlabeled (and without nucleoside modification) Fluc mRNA in the LNPs screened in the original immunogenicity assessment (Figure 3A). Fluc activity was measured in liver, spleen, lung, heart, and kidney homogenates 4 h after LNP injection. LNP composition had a strong impact on the intensity and organ specificity of mRNA expression (Figure 3B). Across the library, Fluc expression was highest in the liver, followed by the spleen (Figure 3C), but the liver-to-spleen ratio differed strongly between LNPs. The magnitude of the E7-specific CD8 T cell responses positively correlated with absolute (DSG-PEG2000 LNPs) and relative (DMG-PEG2000 LNPs) spleen expression (Table S2). The importance of organ-specific mRNA delivery was further highlighted by the absence of correlation between total expression and T cell responses (Table S2). Significant correlations were also identified between LNP size (in turn strongly dependent on lipid composition) and relative expression in the spleen (Figure S4A) and between LNP size and

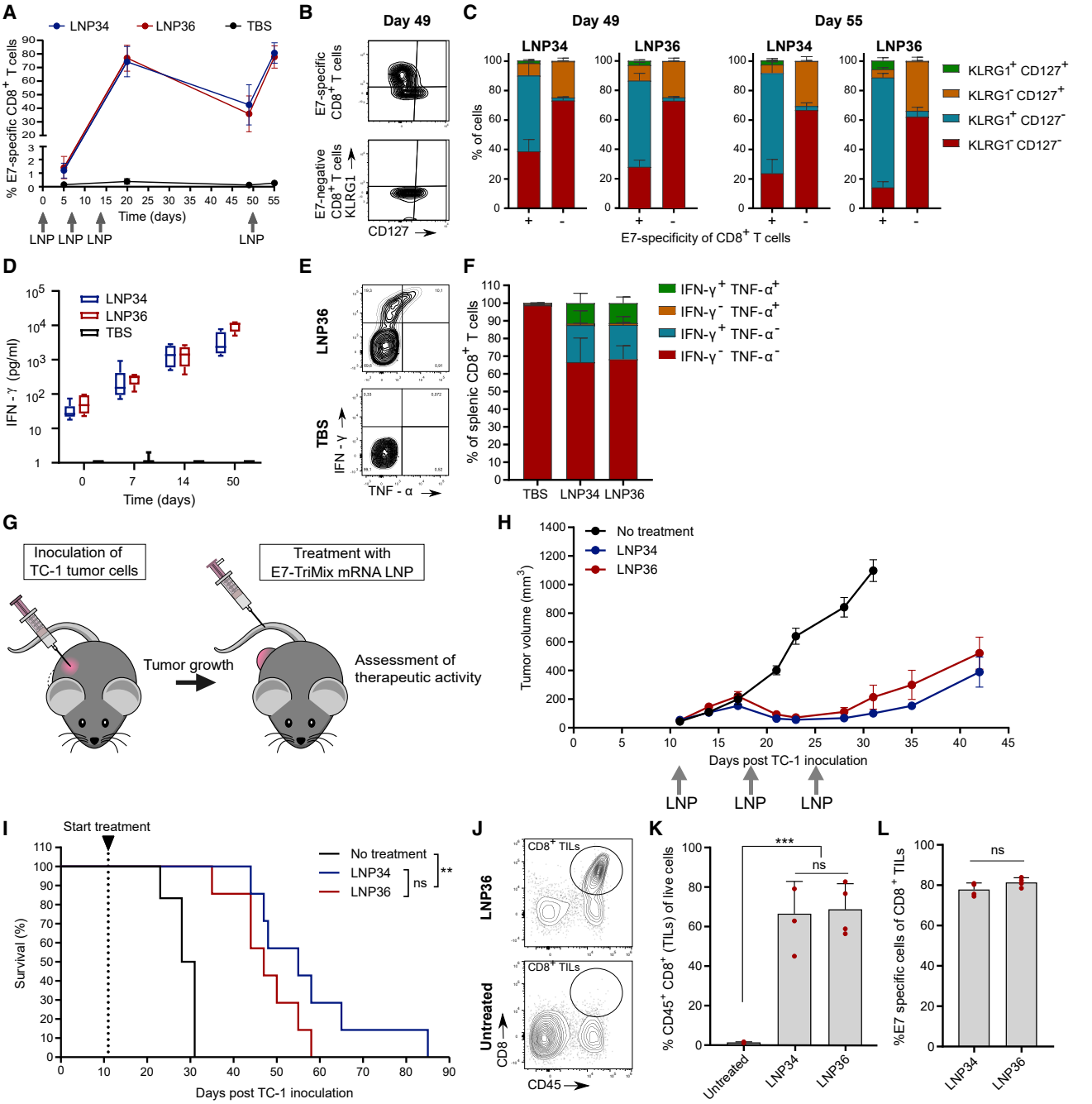

Figure 2. Optimal mRNA-LNPs induce qualitative T cell responses and strong antitumor efficacy

(A) Mice were immunized with optimal LNPs encapsulating 5 μg of E7 and 5 μg of TriMix mRNA at days 0, 7, 14, and 50. Blood CD8 E7-specific T cell responses were determined at days 5, 20, 49, and 55. (B and C) Differential expression of KLRG1 and CD127 on blood E7-specific (+) and non-specific (–) CD8 T cells at day 49 and day 55. Representative contour plots (B, day 49) and quantification (C, mean ± SD [n = 4]) of KLRG1 and CD127 expression are shown. (D) IFN-γ levels in serum were measured 6 h after each immunization (n = 4–6). (E and F) IFN-γ and TNF-α expression by splenic CD8 T cells after three immunizations with TBS or mRNA-LNPs (weekly intervals, 10 μg of E7-TriMix). Representative contour plots (E) and quantification (F: mean ± SD [n = 3 for TBS, n = 5 for LNPs]) is shown. (G) When TC-1 tumors reached a mean volume of 52 mm^3, mice were injected i.v. with 5 μg of E7-TriMix mRNA-LNPs (weekly intervals). (H) TC-1 growth curves in mice. Data are shown as mean ± SEM (n = 6–7). (I) Kaplan-Meier survival curves of TC-1-bearing mice. (J and K) Representative contour plots (J) and graph (K, mean ± SD [n = 4] with individual data points shown in red) quantifying the infiltration of CD8 T cells in TC-1 tumors. (L) E7 specificity of CD8 TILs in TC-1 tumors. Data are shown as mean ± SD with individual data points in red (n = 4). Statistical differences were assessed using a Mantel-Cox log-rank test with Bonferroni multiple testing correction (I), one-way ANOVA with Tukey post hoc test (J), or two-way Student's t test (L).**$p < 0.01$, ***$p < 0.001$; ns, not significant.

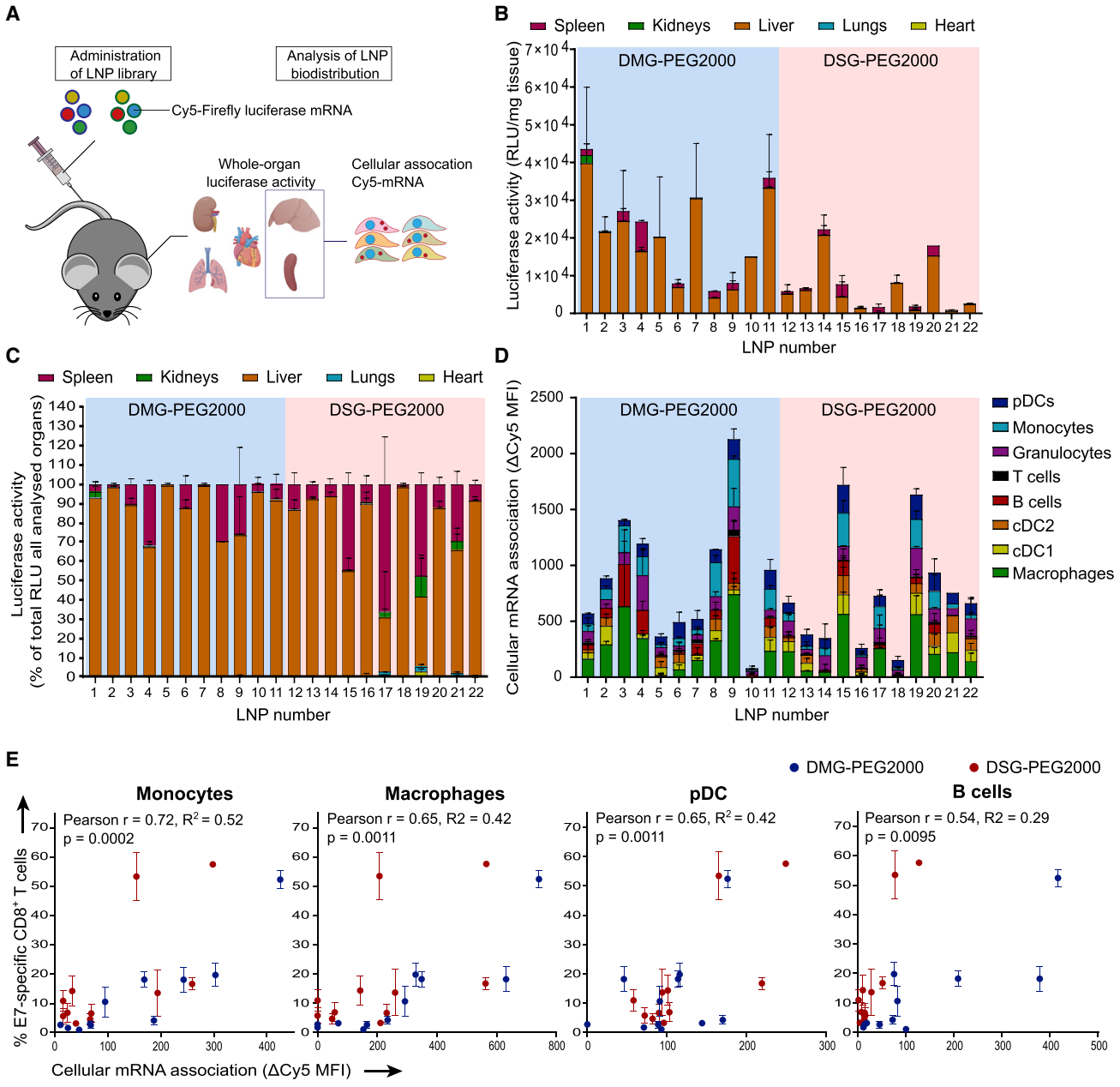

Figure 3. LNP immunogenicity correlates with splenic immune cell association

(A) A mixture of 5 μg Cy5-labeled (25% substituted Cy5-UTP, 75% substituted 5-methoxy UTP) and 5 μg unlabeled (and without nucleoside modifications) Fluc mRNA in LNPs was injected i.v. (n = 2–4). After 4 h, kidneys, lungs, heart, liver, and spleen were isolated. A part of spleens and livers was kept for immediate flow cytometry analysis to assess Cy5 association with multiple cell types. Remaining tissues were homogenized and assayed for luciferase activity. (B) Luciferase activity per mg of tissue. (C) Luciferase activity (expressed as percent of luciferase activity per mg in all assayed organs) was mainly localized in liver and spleen. (D) Association of Cy5-mRNA with immune cell types in the spleen, expressed as difference in Cy5 mean fluorescence intensity between cells of LNP-injected mice and vehicle-injected mice (ΔCy5 MFI). (E) Correlations of ΔCy5 MFI after first LNP administration with T cell response after three immunizations (Figure 1C) were strongest for monocytes, pDCs, macrophages, and B cells based on Pearson's correlation coefficients. In (B), (C), and (D), mean ± SD is shown. RLU, relative light unit.

the E7-specific CD8 T cell response (Figure S4B). Using Cy5-labeled mRNA as a fluorescent reporter molecule, we further assessed whether T cell responses can be linked to early (4 h post administration) mRNA uptake by specific immune cell types in the spleen (Figure 3D). Significant correlations were observed between the T cell response and early mRNA association with splenic monocytes,

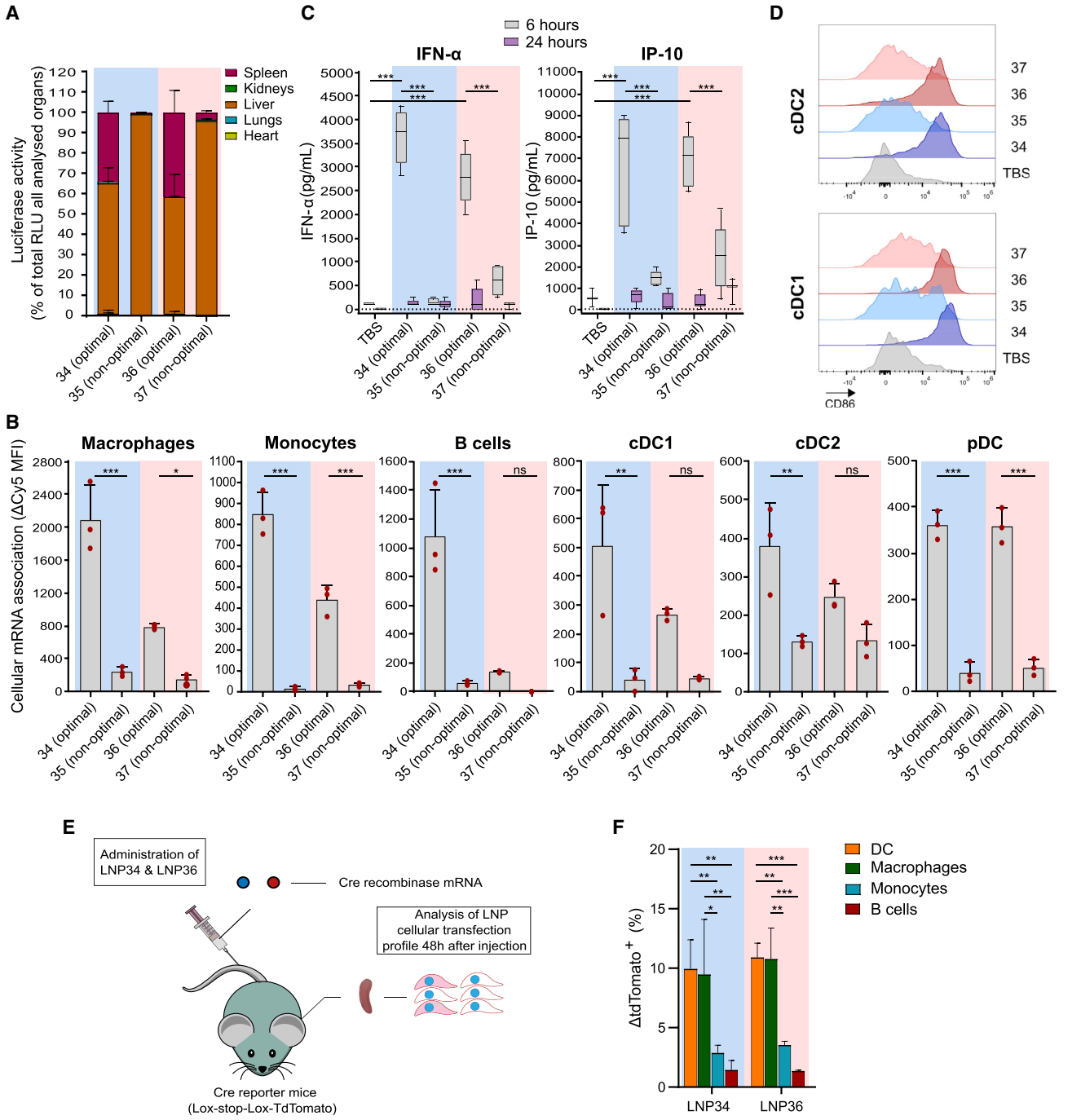

Figure 4. Optimal LNPs show increased splenic immune cell transfection and activation compared with non-optimal LNPs

(A) Fluc expression distribution over organs 4 h after injection of 10 μg of Fluc mRNA encapsulated in optimal (LNP34 and LNP36) or non-optimal LNPs (LNP35 and LNP37). Mean ± SD is shown (n = 3). (B) Association of optimal LNPs with various splenic immune cell subsets is stronger compared with non-optimal LNPs. Mean ± SD is shown with individual data points in red (n = 3). (C) Transient increases in IFN-α and IP-10 cytokine levels in serum were observed after injection of optimal, but not suboptimal LNPs (n = 5 for E7 LNPs [10 μg], n = 3 for TBS). (D) CD86 expression on splenic cDC1 and cDC2 is weakly upregulated by non-optimal LNPs and strongly upregulated by optimal LNPs (n = 5 for E7-TriMix LNPs [5 μg], n = 4 for TBS). (E) Cre mRNA (10 μg) in optimal LNPs was injected i.v. into transgenic Cre reporter mice (ROSA-loxP-STOP-loxP-tdTomato). After 48 h, spleens were isolated and assayed for tdTomato fluorescence in immune cell types. (F) In spleen, optimal LNPs mainly

(legend continued on next page)

macrophages, plasmacytoid dendritic cells (pDCs), and B cells (Figure 3E). In contrast, such correlations could not be established between T cell responses and mRNA association with non-parenchymal liver cells (Figures S4C and S4D).

Optimal LNP compositions increase mRNA uptake by splenic immune cells and trigger enhanced innate responses

To further validate these findings, we compared the organ-specific and splenic cell distribution of the optimal, highly immunogenic LNPs (LNP34 and LNP36) with the non-optimal, poorly immunogenic LNPs (LNP35 and LNP37) following the same method as for the DOE library LNPs (Figure 3A). Compared with the non-optimal LNPs, LNP34 and LNP36 showed increased splenic mRNA expression (Figure 4A) and mRNA association with splenic macrophages, monocytes, B cells, and dendritic cells (DCs) (Figure 4B). The increased association of optimal LNPs with innate immune cells translated to stronger innate activation, illustrated by enhanced IFN-α and IFN-γ-induced protein 10 (IP-10) levels in blood (Figure 4C) and invigorated expression of the co-stimulatory molecules CD86 (Figures 4D, S5A, and S5B) and CD40 (Figures S5A and S5B) on conventional DC (cDC1 and cDC2) subsets. To fully elucidate which splenic cell types translate the LNP-delivered mRNA, we injected LNPs with Cre recombinase mRNA into ROSA-loxP-STOP-loxP-tdTomato (Ai9) mice (Figure 4E). Of the cell types analyzed, DCs and macrophages showed the highest percentage of transfected cells (Figure 4F). These cell types are potent APCs and hence presumably contribute to the observed T cell responses elicited by antigen mRNA-LNPs. Despite their strong association with Cy5 mRNA, mRNA expression by monocytes and B cells was comparatively low, which might reflect either limited mRNA internalization or poor endosomal release in these cell types.

PEG-lipid chemistry differentially affects LNP biodistribution upon repeated administration

Intravenous administration of mRNA-LNPs[28] has been reported to trigger antibody production against the PEG moiety, a response driven by the activation of splenic PEG-specific B cells.[29–31] Presence of anti-PEG antibodies has presumably opposing impacts on the T cell response: it results in decreased expression of the delivered mRNA but also shifts LNP uptake from hepatocytes to phagocytic cells[14] that can function as APCs. We therefore determined whether the optimized LNPs we identified—characterized by different PEG-lipid chemistries—induce the generation of anti-PEG antibodies and whether this impacts the intensity and biodistribution of mRNA expression upon repeated administration. I.v. administration of LNP34 and LNP36 provoked a pronounced B cell activation, as evidenced by a strong upregulation of the B cell activation markers CD69 (Figure 5A), CD86, and CD40 (Figure S5C), with the presence of mRNA in the LNPs being a clear prerequisite for B cell activation. Anti-PEG immunoglobulin M (IgM) and IgG became detectable in the serum of mice after respectively the first and second immunization with E7-TriMix LNPs (Figure 5B), and antibodies were still readily detectable 40 days after the last immunization (Figure S6A). Titers were more elevated after treatment with LNP36 compared with LNP34, especially at the later time point (Figure S6A). We observed reduced mRNA expression upon weekly administrations of Fluc mRNA in LNP34 and LNP36, both in liver and spleen (Figure 5C). In the case of DSG-PEG2000-containing LNP36, this reduced expression was accompanied by a relative shift in mRNA expression from liver to spleen, with the spleen/liver ratio increasing from 0.8 at the first injection to 3 after the third injection. The relative increase in splenic expression observed after the third injection was mirrored by an increased association of Cy5-mRNA with splenic macrophages, monocytes, DCs, and B cells (Figure 5D). Despite a drop in the intensity of mRNA expression, the relative distribution of mRNA uptake and expression at the organ and cellular level, in contrast, remained relatively constant in the case of the DMG-PEG2000-stabilized LNP34 (Figures 5C and 5D). We next assessed whether the differential behavior of LNP36 compared with LNP34 could be explained by qualitative changes in the protein corona adsorbed to the LNPs upon repeated administration. LNP34 and LNP36 were incubated with plasma from either naive mice or mice immunized twice with the matching LNPs ("immune plasma") and subsequently recovered using differential centrifugation. Proteomics analysis identified abundant plasma proteins, i.e., albumin, apolipoprotein E and several immunoglobulins, in all samples (Figure S6B). Differential enrichment analysis showed different intensity of 25 precipitated proteins when LNP36 was incubated with plasma samples from LNP36-immunized mice compared with plasma of naive mice. On the other hand, only one protein was differentially enriched upon incubation of LNP34 with plasma from LNP34-immunized mice versus plasma from naive mice. The enriched proteins after incubation with immune plasma clustered together and were highly distinct from the proteins pelleted after incubation with naive plasma (Figure 5E), although the differences were clearly more pronounced for LNP36 compared with LNP34. Out of the 25 differentially enriched proteins identified for LNP36, 23 were increased in immune plasma compared with naive plasma and all represented immunoglobulins (Figure 5F). In the case of LNP34, Ighv3-6 was the only Ig family member enriched after incubation with immune plasma (Figure 5F). In addition, immunoglobulins in immune plasma make up a higher percentage of the total precipitated proteome for LNP36 compared with LNP34 (Figures S6C and S6D). We hypothesized that both LNP types bind anti-PEG antibodies, but that anti-PEG is released faster from LNP34 than from LNP36 due to the shorter acyl chain of its PEG lipid. Indeed, LNP34 and LNP36 showed a comparable initial opsonization by anti-PEG antibodies *in vitro*. However, upon incubation with mouse serum, the amount of anti-PEG antibody bound to LNP34 decreased over time,

transfected DCs and macrophages, as indicated by the difference between the percentage of tdTomato-positive cells in LNP-injected mice and the average of TBS-injected mice for each cell population (ΔtdTomato$^+$ (%)). Mean ± SD is shown (n = 3). In (B), (C), and (F) Statistics were assessed by one-way (B, C) or two-way (F) ANOVA with Sidak's multiple comparison test. *p < 0.05, **p < 0.01, ***p < 0.001; ns, not significant. RLU, relative light unit. Blue background: DMG-PEG2000-based LNPs, Pink background: DSG-PEG2000-based LNPs.

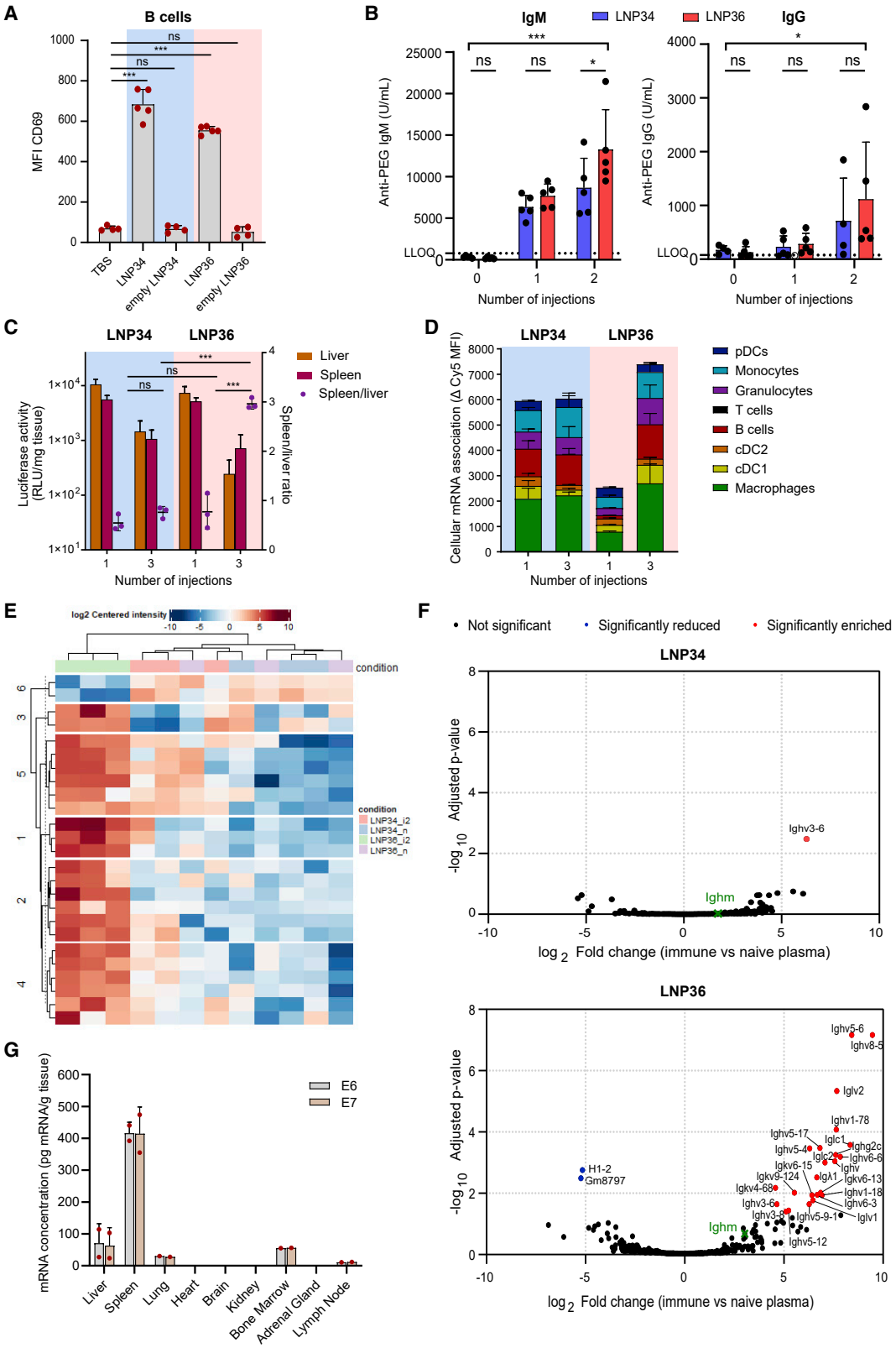

(legend on next page)

whereas it remained constant in the case of LNP36 (Figure S6E). The gradual loss of anti-PEG from LNP34—presumably due to shedding of the PEG lipid—coincided with an increase in LNP size (Figure S6F). In contrast, LNP36 size was relatively unaltered after 2 h incubation with serum, indicating DSG-PEG2000 was still incorporated in LNP and bound to anti-PEG antibodies. Taken together, these data strongly indicate that LNP36 becomes increasingly opsonized by antibodies upon repeated administration, potentially altering its biodistribution. In contrast, LNP34 shows only short-lived immunoglobulin opsonization.

The spleen-centered biodistribution of mRNA deposition is retained in non-human primates

To exclude species-specific differences in the biodistribution of LNPs that could hamper clinical translation, we assessed the biodistribution of LNP36-delivered mRNA in female and male cynomolgus monkeys. E6- or E7-encoding mRNA mixed with (human) TriMix were formulated in LNP36 and co-administered i.v. two times with a 1-week interval. The LNPs were well tolerated with no histopathological changes observed in major vital organs. Twenty-four hours after the second administration, tissues were collected to quantify mRNA content. Both mRNAs were mostly present in the spleen (based on pg mRNA per g of tissue), followed by the liver, bone marrow, draining lymph node, and lung (Figure 5G), irrespective of the administered dose (Figure S7). E6- and E7-mRNA levels in brain, heart, kidney, and adrenal gland were below quantifiable levels. Taken together, the spleen-centered biodistribution, which is linked to strong T cell responses in rodents, is preserved in non-human primates and warrants further clinical translation.

IFNAR signaling, phagocytes, and B cells are essential for eliciting mRNA-LNP-induced T cell responses

We next sought to determine whether the observed type I IFN response is vital for the T cell response elicited. Type I IFNs are pleiotropic cytokines that are typically induced upon sensing (viral) RNAs. Opposing effects of type I IFNs on the T cell response induced by mRNA vaccines have been reported.[5–7,32–34] As shown in Figure 4C, intravenous injection of E7 mRNA delivered by LNP34 and LNP36 resulted in a robust type I IFN response. This response was found to be critical for achieving T cell immunity, as blockade of the IFN-α/β receptor (IFNAR) prior to immunization—abrogating type I IFN signaling—had a profound negative impact on the CD8 T cell response (Figures 6A and 6B). In a parallel setup, we depleted pDCs (>80% depletion, Figures S8A and S8B), a cell type capable of producing large amounts of type I IFN in response to RNA sensing.[35] Although pDC depletion resulted in reduced yet not fully abrogated IFN-α titers in serum (Figure S8C), the impact of pDC depletion on T cell responses was moderate to non-significant in the case of LNP34 or LNP36, respectively. As our biodistribution studies showed correlations between T cell responses and early LNP association with phagocytic cells and B cells (Figure 3E), we decided to further assess the roles of these immune cells in the LNP-induced T cell response. Clodronate liposomes were used to deplete phagocytes in liver and spleen prior to each immunization.[36] We confirmed that this treatment resulted in strong reductions of macrophages in both organs, but also reduced numbers of monocytes and DCs in spleen (Figure S8D). After LNP immunization, strongly reduced E7-specific CD8 T cell responses were measured in the clodronate-pretreated mice (Figure 6D), indicating a vital role for phagocytic cell types in modulating T cell responses to mRNA-LNPs, either by antigen presentation or immunomodulation through cytokine production. However, cytokine levels were similar in clodronate-treated mice compared with wild-type mice after LNP immunization, supporting the former mechanism (Figure S6E). Given the association of mRNA with B cells observed in the biodistribution study, we also assessed the involvement of B cells in the T cell response via comparative immunization studies in wild-type mice versus μMT mice, which lack mature B cells.[37] With LNP-binding antibodies resulting in an increased uptake by splenic APCs upon repeated immunization with LNP36 but not LNP34, we speculated that B cells could be major mediators of the T cell response evoked by LNP36, yet not by LNP34. Surprisingly, however, μMT mice showed strongly reduced E7-specific CD8 T cell responses after immunization with both LNPs compared with wild-type mice, indicating a role of B cells in the T cell response that extends beyond antibody opsonization and altering biodistribution upon repeated immunization (Figure 6E). Of note, μMT mice showed preserved innate immune activation after mRNA-LNP injection compared with wild-type mice (Figure S8E), suggesting that the lack of response to mRNA-LNP immunization is not due to complete immunodeficiency.

DISCUSSION

Although LNPs are highly efficient carriers for mRNA delivery, they are not a one-size-fits-all solution, and their composition needs to be

Figure 5. PEG-lipid chemistry differentially affects mRNA biodistribution upon repeated administration

(A) mRNA-encapsulating LNPs (5 μg E7-TriMix), but not empty LNPs (equivalent lipids to hypothetical 5 μg mRNA), activate splenic B cells 4 h after a single administration, evidenced by upregulation of CD69. Mean ± SD is shown with individual data points in red (n = 4–5). Statistics were assessed by one-way ANOVA with Tukey's multiple comparison test. (B) Mice were immunized with 10 μg of E7-TriMix on days 0 and 7. Anti-PEG IgM and IgG titers were determined in plasma collected 6 days after each injection. Both LNPs induce the generation of anti-PEG IgM (left) and IgG (right) upon systemic injection. Mean ± SD is shown (n = 5). (C) Overall luciferase expression decreases with repeated administration of LNP34 and LNP36 encapsulating 10 μg of Fluc mRNA. Mean ± SD is shown (n = 3). Statistics were assessed by one-way ANOVA with Tukey's multiple comparison test. (D) Splenic cellular Cy5-mRNA association upon repeated administration (5 μg Fluc + 5 μg Cy5-Fluc) remains similar for LNP34, but increases in the case of LNP36. Mean ± SD is shown (n = 3). (E and F) Cluster analysis (E) and volcano plots (F) for differential enrichment (false discovery rate 5%, $\log_2$ fold change ≥ 1.5; $p_{adj} < 0.05$) of proteins in centrifuged pellets after incubation of LNP34 or LNP36 with plasma of naive mice or mice immunized twice with the respective LNP (10 μg E7-TriMix). LLOQ, lower limit of quantification. (G) After two immunizations with a 1:1 mixture of LNPs loaded with either E6 or E7 mRNA combined with TriMix (100 μg mRNA in total) in non-human primates, both mRNAs strongly accumulated in spleen. Mean ± SD is shown with individual data points in red (n = 2). Statistics in (D) were assessed by two-way ANOVA with Tukey's multiple comparison test. *p < 0.05, **p < 0.01, ***p < 0.001; ns, not significant.

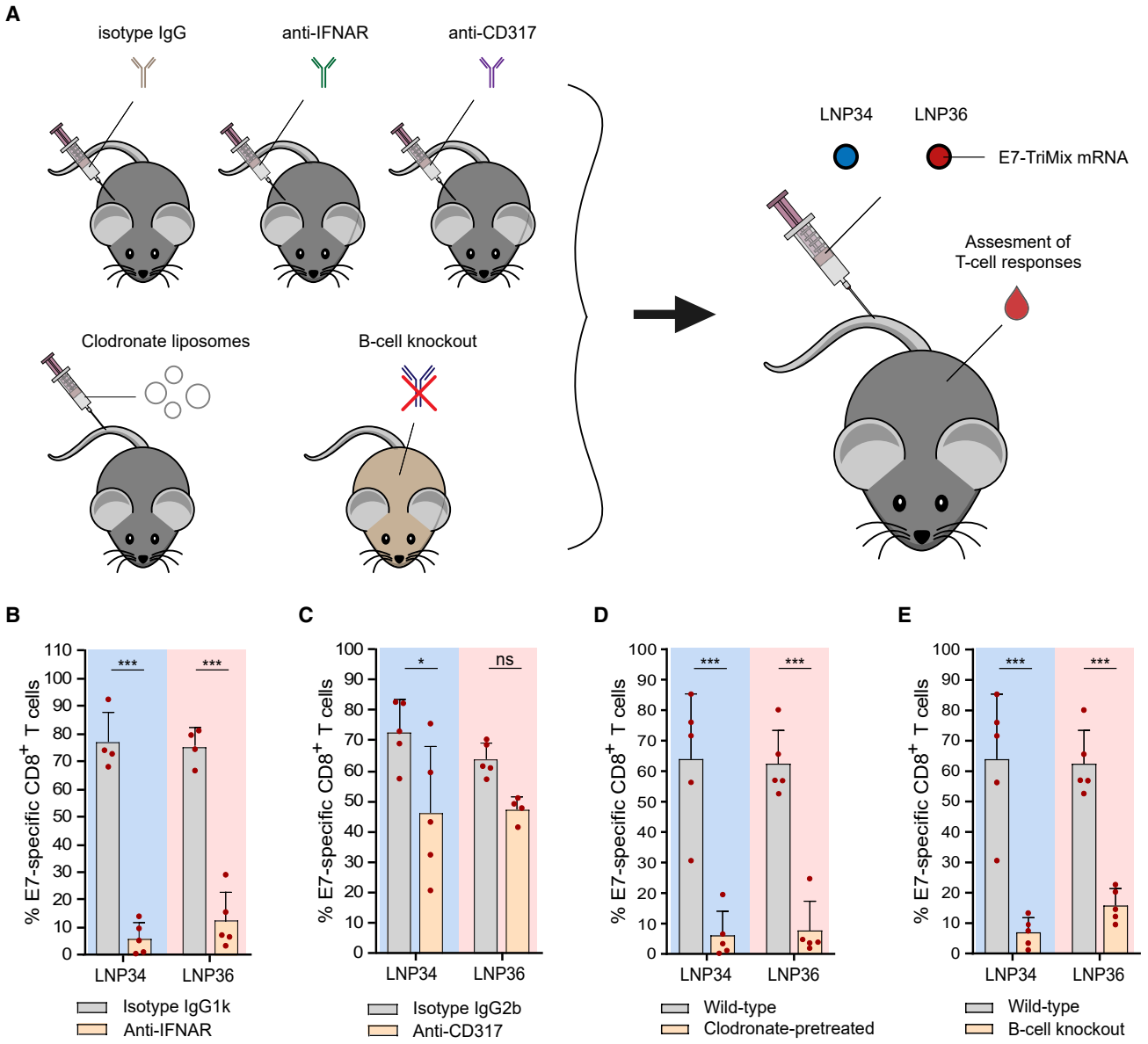

Figure 6. CD8 T cell responses are dependent on IFNAR signaling, phagocytes, and B cells

(A) Mice were pretreated with isotype antibodies, anti-CD317 pDC depleting antibody, anti-IFNAR blocking antibody, or clodronate liposomes. μMT mice were used as B cell knockout model. After two or three i.v. immunizations with 10 μg of E7-TriMix mRNA-LNP (weekly intervals), CD8 T cell responses were assessed in blood. (B) IFNAR blocking by i.p. administration of anti-IFNAR antibodies abrogated the E7-specific CD8 T cell response in blood after three immunizations. (C) Depletion of pDCs by i.p. administration of anti-CD317 antibodies had minor negative impact on the percentage of E7-specific CD8 T cells in blood after three immunizations. (D and E) Absence of phagocytes (clodronate-pretreated) (D) or B cells (knockout) (E) strongly reduced the percentage of E7-specific CD8 T cells in blood after two immunizations. In (B), (C), (D), and (E), mean ± SD is shown (n = 4–5). Statistics were assessed by two-way ANOVA with Sidak's multiple comparison test. *p < 0.05, ***p < 0.001; ns, not significant.

tailored toward the route of administration and the desired biological activity.[15,16,38–40] Here, we investigated whether mRNA-LNPs could be designed to induce strong CD8 T cell responses upon intravenous immunization by tailoring lipid ratios and PEG-lipid chemistry. A DOE methodology was used to set up and screen an initial library of 33 LNPs for their capacity to evoke CD8 T cell responses. Maximized T cell responses were predicted and confirmed for LNPs composed of low percentages of PEG lipid, high percentages of SS-EC ionizable lipid, and low percentages of DOPE. An increased T cell response by reduced mol % of PEG lipid is likely caused by the combined effects of reduced shielding and increased size resulting in increased LNP uptake by phagocytes,[41] as we observed in the

biodistribution studies. Aside of the chemistry of the ionizable lipid used, our initial library was highly similar, in terms of lipid ratios assessed, to the initial library described by Kauffman et al.[9] (DOPE: 4%–16%; DMG-PEG2000: 0.5%–2.5%), who optimized erythropoietin (EPO)-encoding mRNA-LNP compositions for maximal hepatic EPO production. Interestingly, the different goals and readouts of both studies led to the identification of different critical LNP attributes, second-order interactions, and predicted optimal LNP compositions. In the study of Kauffman et al., LNPs that were selected as optimal performers (i.e., achieving highest hepatic EPO production) contained high molar percentages of DOPE and PEG lipid and low percentages of ionizable lipid, which is opposite to the optimal mRNA-LNP composition we identified. Hence, DOE enables optimization of LNP compositions for the intended biological activity. Moreover, the design we employed proved to be cost effective, allowing single-step fine-tuning of all lipid components simultaneously *in vivo* with as little as 11 LNP compositions per PEG lipid. Early biodistribution of LNPs was linked to the magnitude of the T cell response, with mRNA uptake by splenic immune cells, including macrophages, monocytes, and pDCs, correlating positively with the T cell response evoked. By administering Cre mRNA formulated in optimal LNPs to tdTomato reporter mice, we identified splenic DCs and macrophages as the cell types showing the highest percentages of mRNA-expressing cells. Optimal LNPs led to an increased functional maturation of DCs in the spleen and to increased production of T cell stimulatory cytokines and chemokines such as IFN-α and IP-10. Opposing effects of type I IFNs on the T cell response induced by mRNA vaccines have been reported.[5–7,32–34] Type I IFN can promote DC activation and T cell differentiation but can also interfere with the expression of the mRNA encoded protein by inducing RNase activity and instigating translational arrest. A favorable impact of type I IFN is expected when type I IFN induction and T cell receptor triggering occurs simultaneously, i.e., by systemic immunization.[34] In this setting, blocking the type I IFN receptor IFNAR at the time of immunization had a strongly detrimental impact on the magnitude of the antigen-specific CD8 T cell response. Because the biodistribution studies also indicated a positive correlation between early mRNA association with splenic B cells and T cell response, we assessed the involvement of B cells at instigating the antigen-specific CD8 T cell response by conducting vaccination studies in μMT mice, which lack mature B cells. Surprisingly, the CD8 T cell response was nearly fully abrogated in these mice, pinpointing a crucial role of B cells in priming and/or expanding CD8 T cell responses. As B cells are not the typical APCs involved in priming CD8 T cells, we hypothesized that B cells might promote CD8 T cell responses via a more indirect mechanism involving the induction of anti-PEG antibodies, which would lead to LNP opsonization upon repeated administration, as has been postulated for PEGylated liposomes,[29,42] and subsequent increased uptake by conventional APCs such as DCs and macrophages. Repeated LNP injection indeed increased anti-PEG IgM and IgG levels in mouse serum, in line with other studies.[28] Anti-PEG titers were more elevated after treatment with LNP36 compared with LNP34, likely resulting from the more stable incorporation of DSG-PEG2000 compared with DMG-PEG2000 into the LNPs' surface, a phenomenon previously described for small interfering RNA LNPs.[14] Despite this induction of anti-PEG antibodies in mice, the vaccine-evoked T cell response was easily boostable by repeated immunization, which is of key importance given the increasing prevalence of anti-PEG antibodies in humans[43] and a substantial portion of the global population at risk of acquiring anti-PEG antibodies after vaccination with PEGylated LNPs in the context of the COVID-19 pandemic. We also evaluated how the protein corona of LNP34 and LNP36 changed upon repeated administration. For the DSG-PEG2000 stabilized LNP36, we observed a strong enrichment of immunoglobulins in the protein corona after repeated administration, which was absent in case of the DMG-PEG2000 stabilized LNP34. In line with these findings, LNP36 showed a shifted distribution toward the spleen compared with liver upon repeated injection, whereas LNP34 displayed a nearly unaltered biodistribution upon repeated administration, reflecting its minor immunoglobulin opsonization. Nonetheless, compared with wild-type mice, B cell knockout mice (μMT) showed strongly reduced E7-specific CD8 T cell responses after immunization with both LNPs, indicating a role of B cells in the T cell response that extends beyond antibody opsonization and altering biodistribution upon repeated immunization. The role of B cells in promoting antitumoral immune responses is increasingly recognized, with recent studies showing that B cells can act as APCs to T cells.[44–47] Hence B cell responses could enhance T cell responses to mRNA-LNP vaccines by multiple mechanisms, ranging from cytokine production to direct roles in antigen presentation themselves. Of note, as B cells contribute to the generation and maintenance of functional CD4 and CD8 T cells[48,49] and help in the organization of lymphoid organ architecture,[50] it cannot be ruled out that μMT mice are intrinsically less competent in responding to mRNA-LNP immunization compared with wild-type mice. Further work is needed to unravel the exact mechanism by which B cells contribute to the generation of antigen-specific CD8 T cell responses upon systemic mRNA-LNP vaccination.

In summary, the DOE approach enabled us to identify LNP compositions that induced high-magnitude CD8 T cell responses upon i.v. administration. This increased T cell response coincided with increased mRNA expression in splenic DCs and macrophages alongside augmented DC activation and cytokine release. Type I IFNs, phagocytes, and B cells were vital in instigating the antigen-specific CD8 T cell response. Repeated immunization resulted in high-magnitude and long-lasting tumor antigen-specific CD8 T cells that showed a high degree of multifunctionality, infiltrated subcutaneous antigen-expressing tumors, and provoked high antitumor efficacy. The promising immunogenicity data in mice combined with the beneficial biodistribution/tolerability results in non-human primates warrant further assessment in clinical studies.

MATERIALS AND METHODS

Animals

All experiments with mice were performed with approval from the Utrecht Animal Welfare Body of the UMC Utrecht or by the Animal Ethics Committee of Ghent University. Animal care was according to

established guidelines. All mice had unlimited access to water and standard laboratory animal chow. Female C57Bl/6J mice (20–25 g) were obtained from Charles River Laboratories (Germany/France). Female μMT B cell knockout and male and female B6.Cg-Gt(ROSA)26Sortm9(CAG-tdTomato)Hze/J mice (Ai9) were obtained from The Jackson Laboratory (USA). The study of non-human primates (two male and two female cynomolgus monkeys) was performed at Charles River Laboratories (France) according to local regulations.

Design of experiments and Bayesian-based analysis

A Roquemore hybrid design was used to select the LNP compositions to test in the initial library. The investigation model used to optimize the LNP composition was described by a quadratic response surface model structure. The posterior distributions of the model parameters were computed using the Hamiltonian Monte Carlo algorithm, a generalization of the Metropolis algorithm. After qualification of the model, the latter was used to predict mean CD8 T cell responses for all combinations of the three factors (%ionizable lipid, %PEG lipid, %DOPE) and select the lipid ratio predicted to result in maximal immunogenicity. Details of the statistical model, methods, and analysis can be consulted in supplemental methods.

mRNA synthesis and purification

Codon optimized E7, Adpgk, Trp-2, TriMix, and Firefly luciferase mRNAs were prepared by eTheRNA *in vitro* transcription (IVT) from eTheRNA plasmids. No nucleoside modifications were incorporated. The E7 mRNA used in the DOE was capped with anti-reverse cap analog. All later experiments were performed using CleanCapped mRNAs. After IVT, double-stranded RNA was removed by cellulose purification. mRNA quality was monitored by capillary gel electrophoresis (Agilent, Belgium). Cy5-labeled Firefly luciferase (Fluc) mRNA and Cre mRNA were purchased from TriLink Biotechnologies. Uridine is fully substituted with 5-methoxyuridine in the Cre mRNA. Cy5-labeled luciferase mRNA is transcribed with cyanine 5-UTP/5-methoxy-UTP at a ratio of 1:3.

LNP production and characterization

For biodistribution and cellular uptake studies, LNPs were loaded with a mixture of Fluc encoding mRNA (eTheRNA Immunotherapies) and CleanCap Cy5-labeled Fluc mRNA (TriLink Biotechnologies) in a 1:1 ratio. For the DOE immunogenicity study, LNPs were loaded with E7 mRNA. All other studies were performed with a mixture of E7 and TriMix (CD40L, CD70, and TLR4 mRNA) in a 3:1:1:1 ratio. The mRNA was diluted in 100 mM sodium acetate buffer (pH 4), and lipids were dissolved and diluted in ethanol. A nitrogen/phosphate ratio of 16 was employed for all LNPs. The mRNA and lipid solutions were mixed using a NanoAssemblr Benchtop microfluidic mixing system (Precision Nanosystems) at a flow rate of 9 mL/min and an aqueous/organic phase flow rate ratio of 2:1, followed by dialysis overnight against TBS (20 mM Tris, 0.9% NaCl, pH 7.4). Amicon Ultra Centrifugal Filters (Merck Millipore, 100 kDa molecular weight cutoff) were used for concentration of LNPs. Size, polydispersity index, and ζ potential were measured with a Zetasizer Nano (Malvern). mRNA encapsulation efficiency was determined via Quant-iT Ribogreen RNA assay (Thermo Fisher) by comparing lysed LNPs in 1% Triton X-100 (all RNA detectable) with LNPs in TE buffer (only non-encapsulated RNA detectable). The assay was performed according to manufacturer's recommendations. Composition and physicochemical properties of all LNPs are summarized in Table S1.

Biodistribution and cellular uptake

Mice were injected i.v. via the tail vein with 10 μg of mRNA in selected LNP formulations. After 4 h, mice were anesthetized with 250 μL of pentobarbital (6 mg/mL, intraperitoneal [i.p.]). Blood samples were collected in tubes with gel clotting factor (Sarstedt). Subsequently, the chest cavity was opened, the portal vein was cut, and mice were perfused with 7 mL of PBS through the heart's right ventricle. Organs were excised and snap-frozen in liquid nitrogen. For liver and spleen tissues, a part of the organ was kept in ice-cold PBS for immediate flow cytometry analysis. Non-human primates received two immunizations with a 1-week interval by a 30-min infusion of LNP36 (formulated as a 1:1 mixture of LNP36 containing either E6 or E7 mRNA and TriMix at total dose of 100 μg [Figure 5G] or 40 μg [Figure S7] mRNA). Twenty-four hours after the second LNP administration adrenal gland, bone marrow, brain, heart, kidney, liver, lung, spleen, and one lymph node were collected and immediately frozen in liquid nitrogen until completely frozen and solid, then transferred to −80°C. mRNA quantification in tissues was performed using a QuantiGene Singleplex assay (Thermo Fisher) with a custom-designed probe set hybridizing to E7 mRNA. In addition, tissues were histopathologically inspected by a trained pathologist from Charles River Laboratories (France).

Cellular association

Liver and spleen tissues were placed in Petri dishes with RPMI 1640 medium containing 1 mg/mL collagenase A (Roche) or 20 μg/mL Liberase (Roche), respectively, and 10 μg/mL DNAse I, grade II (Roche). Tissues were minced using surgical blades and incubated for 30 min at 37°C. Subsequently, tissue suspensions were passed through 100-μm nylon cell strainers. Liver suspensions were centrifuged for 3 min at 70 × *g* to deplete parenchymal cells. Supernatants and spleen suspensions were centrifuged 7 min at 500 × *g* to pellet cells. Red blood cells were lysed in ACK buffer (Gibco) for 5 min, inactivated with PBS, and subsequently passed through a 100-μm cell strainer. Cells were washed with RPMI 1640 containing 1% fetal bovine serum, mixed with trypan blue, and counted using a Luna-II Automated Cell Counter (Logos Biosystems). 3×10^5 (liver) or 6×10^5 (spleen) live cells were seeded in 96-well plates, pelleted for 5 min at 500 × *g*, and resuspended in 2% BSA in PBS (2% PBSA) containing 50% Brilliant Stain Buffer (BD Biosciences) and 2 μg/mL TruStain FcX (BioLegend). Cells were incubated for 10 min on ice and mixed 1:1 with 2% PBSA containing applicable antibodies (Table S3) in duplicate. Cells were incubated for 15 min at room temperature on a shaker, washed two times with 2% PBSA, and resuspended in 2% PBSA containing 0.25 μg/mL 7-AAD Viability Stain (BioLegend). Samples were acquired on a 4-laser BD LSRFortessa

flow cytometer. Analysis was carried out using FlowJo software. Gating strategies for all analyses are included in supplemental information.

Whole-body distribution

Approximately 50–100 mg of each tissue was dissected, weighed, and placed in 2-mL microtubes with a layer of approximately 5 mm of 1.4-mm ceramic beads (Qiagen). For each mg of tissue, 3 μL of cold Cell Culture Lysis Reagent (Promega) was added, and tissues were homogenized using a Mini-BeadBeater-8 (BioSpec) at full speed for 60 s at 4°C. Homogenates were stored at −80°C, thawed, centrifuged at 10,000 × *g* for 10 min at 4°C to remove beads and debris, and supernatants were stored again at −80°C. Ten microliters of each lysate was aliquoted in duplicate on a white 96-well plate. Using a SpectraMax iD3 platereader (Molecular Devices) equipped with injector, 50 μL of Luciferase Assay Reagent (Promega) was dispensed in each well while mixing, followed by a delay of 2 s and recording of luciferase emission for 10 s. Luciferase activity was normalized for background signal obtained from organ lysates of mice injected with TBS.

mRNA expression

Ai9 mice were injected intravenously in the tail vein with 10 μg of Cre mRNA encapsulated in selected LNPs. Forty-eight hours after administration, mice were anesthetized with pentobarbital and perfused with PBS as described above. Single-cell suspensions of spleen tissues were prepared and counted as described under "cellular association." Cells were stained with FcR blocking antibodies and Zombie Aqua viability dye prior to staining with antibodies in 1% PBSA. Subsequently cells were washed two times with 2% PBSA and analyzed using a 4-laser BD LSRFortessa flow cytometer. Analysis was carried out using FlowJo software. Gating strategies are included in supplemental information.

T cell response

Mice were immunized intravenously via the tail vein with 10 μg of mRNA in selected LNPs at weekly intervals. Blood for flow cytometry stainings was collected 5–7 days after immunizations. After lysing of red blood cells, the cells were incubated with FcR block and Zombie Aqua viability dye. After incubation and washing, APC-labeled tetramer/dextramer was added (E7: RAHYNIVTF; Adpgk: ASMTNRELM; or Trp-2: SVYDFFVWL) and incubated at room temperature for 30 min. Excess tetramer was washed away, and an antibody mixture for surface molecules CD3, CD8, KLRG1, and CD127 (Table S3) was added to the cells and incubated for 30 min at 4°C. Samples were acquired on a 3-laser AttuneNxt flow cytometer or a 4-laser BD LSRFortessa flow cytometer. Intracellular cytokine production was determined in spleen 7 days after the third immunization. Single-cell suspensions of splenocytes were prepared by crushing the spleens, lysing the red blood cells, and filtering the samples over a 40-μm cell strainer. Two million cells/well/sample were plated in duplicate in a 96-well plate. Four micrograms of E7 peptide (Genscript) was added for stimulation before cells were incubated at 37°C. After 1 h of peptide stimulation, GolgiPlug (BD Cytofix/Cytoperm kit; BD Biosciences) was added. Cells were incubated for another 4 h. Thereafter, cells were incubated with FcR block and viability dye. After incubation and washing, APC-labeled E7 (RAHYNIVTF)-tetramer was added and incubated at room temperature for 30 min. Excess tetramer was washed away, and an antibody mixture for surface molecules CD3 and CD8 (Table S3) was added to the cells and incubated for 30 min at 4°C. Further steps were according to the manufacturer's instructions of the BD Cytofix/Cytoperm kit (BD Biosciences). After permeabilization, cells were stained for IFN-γ and tumor necrosis factor α (TNF-α) (Table S3). Samples were acquired on a 4-laser BD LSRFortessa flow cytometer. Analysis was carried out using FlowJo software. Gating strategies are provided in supplemental information.

Immune cell activation

Mice were injected i.v. via the tail vein with 5 μg of E7-TriMix mRNA in selected LNPs. Spleens were harvested 4 h later for flow cytometry staining. Single-cell suspensions of splenocytes were prepared and incubated with digestion buffer (DMEM with DNAse-1 and collagenase-III) for 20 min with regular shaking. Thereafter, samples were incubated with Fc block and viability dye. After incubation and washing, cells were stained with cell lineage markers and activation markers (Table S3). Samples were acquired on a 3-laser AttuneNxt flow cytometer. Analysis was carried out using FlowJo software. Gating strategies are provided in supplemental information.

TC-1 tumor model

TC-1 cells were obtained from Leiden University Medical Center. TC-1 cells (0.5 million) in 50 μL of PBS were injected subcutaneously on the right flank of the mice. Tumor measurements were performed using a caliper. Tumor volume was calculated as (smallest diameter^2 × largest diameter)/2. For the TC-1 experiment shown in Figure 2, mice were injected i.v. via the tail vein with 5 μg of E7-TriMix mRNA in LNP34 or LNP36. Intravenous immunizations were started at a mean tumor volume of 52 mm^3 and performed weekly for a total of three times. For analysis of TILs, tumors were isolated 3 days after the second mRNA-LNP immunization and placed in a 24-well plate filled with MACS tissue storage buffer (Miltenyi Biotec). Tumors were minced and incubated in digestion buffer for 1 h with regular shaking. Thereafter, red blood cells were lysed and all samples were filtered over a 70-μm cell strainer. Lymphocytes were enriched by Ficoll-Paque density gradient purification before proceeding with staining. First, the cells were incubated with FcR block and viability dye. After incubation and washing, APC-labeled E7 (RAHYNIVTF) tetramer was added and incubated at room temperature for 30 min. Excess tetramer was washed away, and an antibody mixture for surface molecules CD45 and CD8 (Table S3) was added to the cells and incubated for 30 min at 4°C. Samples were acquired on a 3-laser AttuneNxt flow cytometer or a 4-laser BD LSRFortessa flow cytometer. Analysis was carried out using FlowJo software. Gating strategies are provided in supplemental information. For the TC-1 experiment shown in Figure S2, the complete method (flow cytometry and qPCR) is provided in supplemental information.

Cell depletion or receptor blocking

pDC depletion was achieved by i.p. injection of anti-CD317 depleting antibody (BioXcell), starting 1 week before the first immunization (for schedules and depletion efficiency, see Figures S8A and S8B). To deplete phagocytes, mice were injected intravenously via the tail vein with 200 μL of clodronate liposomes (Liposoma) 1 day before the immunization (for depletion efficiency, see Figure S8D). To block IFNAR, mice were injected with 100 μg of IFNAR blocking antibody (BioXcell) 1 h before each immunization.

Anti-PEG ELISA

Blood samples were collected in tubes with EDTA or clotting activator (Sarstedt) 5 days after immunization. Blood samples were centrifuged for 10 min at 1,000 × *g* to obtain plasma (EDTA tubes) or 5 min at 10,000 × *g* to obtain serum (clotting activator tubes). Samples were stored at −80°C until analysis. ELISA for anti-PEG IgM (Life Diagnostics, PEGM-1) and anti-PEG IgG (Life Diagnostics, PEGG-1) was performed according to kit protocol. Readout was carried out on a TECAN Infinite 200 Pro plate reader.

Inflammatory cytokines

Blood samples were collected in tubes with gel clotting factor (Sarstedt). Clotted blood samples were centrifuged for 5 min at 10,000 × *g* to obtain serum. Serum samples were stored at −80°C until analysis. ProcartaPlex multiplex assay (Thermo Fisher) was used to determine concentrations of IFN-γ, IFN-α, and IP-10. Serum samples were diluted three times in assay buffer and incubated with fluorescently labeled beads for 120 min. Further steps were performed according to protocol. Samples were acquired on a MagPix instrument (Luminex). Data were analyzed using ProcartaPlex Analyst software.

LNP protein corona

Mice were immunized two times intravenously via the tail vein with 10 μg of E7-TriMix mRNA in selected LNPs at a weekly interval. Blood samples were collected in tubes with EDTA (Sarstedt) 6 days after the second immunization. In addition, blood was collected from naive (non-immunized) mice. Blood samples were centrifuged for 10 min at 1,000 × *g* to obtain plasma. LNPs were prepared as described above. Plasma samples and LNPs were shipped to Karolinska Institutet (Sweden) for protein corona analysis. The full method is described in supplemental methods. In brief, 10% plasma in PBS adjusted to 10 mM sodium citrate to prevent coagulation was prepared from naive mice, LNP34–immunized, and LNP36-immunized mice. Next, LNP34 and LNP36 were mixed with 10% immune plasma (from mice immunized with the respective LNP) or naive plasma. The mixture was incubated for 1 h at 37°C. The LNP-corona complexes were spun at 20,000 × *g* at 4°C for 1 h, the supernatant was discarded, and the pellet was resuspended and washed twice with PBS. Next, proteins were precipitated and digested to peptides. Samples were injected into an Ultimate 3000 RSLCnano system (Dionex) using a C18 trap-column (Dionex) and an in-house packed (3 μm C18 particles, Dr. Maisch) analytical 50 cm × 75 μm internal diameter emitter column (New Objective). Peptides were eluted at 200 nL/min with an 8%–40% B 120 min gradient (buffer B: 80% acetonitrile + 0.1% formic acid; buffer A: 0.1% formic acid) to a Q Exactive Plus (Thermo Fisher Scientific) mass spectrometer. Mass spectrometric raw files were analyzed with the MaxQuant software (version 1.6.15.0). Search was performed against the UniProt *Mus musculus* reference proteome database. Protein and LFQ ratio count (i.e., number of quantified peptides for reporting a protein intensity) was set to 1. Differential enrichment analysis was performed on the LFQ intensity values by using differential enrichment analysis of proteomics data (DEP version 1.10.0 [3]), R version 4.0.2, and RStudio version 1.3.1073.

Statistical analysis

GraphPad Prism software 8.0 and 9.0 was used for the statistical analyses indicated in figure legends. Significant differences are indicated as *p < 0.05, **p < 0.01, ***p < 0.001; ns denotes no significance.

SUPPLEMENTAL INFORMATION

Supplemental information can be found online at https://doi.org/10.1016/j.ymthe.2022.07.007.

ACKNOWLEDGMENTS

This research was supported by the Applied and Engineering Sciences domain of the Dutch Research Council (NWO) HTSM grant ("TORNADO") no. 16169 (S.A.A.K., R.M.S., J.J.J.M.G.-F., S.D.K.) European Union research and innovation Horizon 2020 grant ("EXPERT") grant no. 825828 (R.M.S., S.D.K., T.B., L.H.), Flanders Innovation & Entrepreneurship (VLAIO, Baekeland grant) no. 2017.0572 (S.B.), and Estonian Research Council grant PSG226 (T.L.).

AUTHOR CONTRIBUTIONS

S.B., S.A.A.K., and S.D.K. designed the experiments. S.B and S.A.A.K. performed the experiments and analyzed the results. S.S., E.V.d.V., J.J.J.M.G.-F., M.J.W.E., N.C.H.v.K., and M.H.A.M.F. helped with experiment execution. T.B. and L.H. designed the DOE and performed related statistical analysis. H.S. and K.E.A. analyzed LNP protein corona. M.M. and D.V.H. provided non-human primate data. R.M.S., S.D.K., E.M., K.B., S.E.A., T.L., and K.F. supervised the work. S.B., S.A.A.K., and S.D.K. wrote the manuscript. All authors have given approval to the final version of the manuscript.

DECLARATION OF INTERESTS

S.B., E.V.d.V., S.S., M.M., D.V.H., and S.D.K. are employees of eTheRNA Immunotherapies NV. S.B., S.A.A.K., R.M.S., and S.D.K. have applied for patents related to this study.

REFERENCES

1. Alameh, M.-G.G., Tombácz, I., Bettini, E., Lederer, K., Sittplangkoon, C., Wilmore, J.R., Gaudette, B.T., Soliman, O.Y., Pine, M., Hicks, P., et al. (2021). Lipid nanoparticles enhance the efficacy of mRNA and protein subunit vaccines by inducing robust T follicular helper cell and humoral responses. Immunity *54*, 2877–2892.e7.

2. Reichmuth, A.M., Oberli, M.A., Jeklenec, A., Langer, R., and Blankschtein, D. (2016). mRNA vaccine delivery using lipid nanoparticles. Ther. Deliv. *7*, 319–334.

3. Cafri, G., Gartner, J.J., Zaks, T., Hopson, K., Levin, N., Paria, B.C., Parkhurst, M.R., Yossef, R., Lowery, F.J., Jafferji, M.S., et al. (2020). mRNA vaccine–induced

neoantigen-specific T cell immunity in patients with gastrointestinal cancer. J. Clin. Invest. *130*, 5976–5988.

4. Oberli, M.A., Reichmuth, A.M., Dorkin, J.R., Mitchell, M.J., Fenton, O.S., Jaklenec, A., Anderson, D.G., Langer, R., and Blankschtein, D. (2017). Lipid nanoparticle assisted mRNA delivery for potent cancer immunotherapy. Nano Lett. *17*, 1326–1335.
5. Kranz, L.M., Diken, M., Haas, H., Kreiter, S., Loquai, C., Reuter, K.C., Meng, M., Fritz, D., Vascotto, F., Hefesha, H., et al. (2016). Systemic RNA delivery to dendritic cells exploits antiviral defence for cancer immunotherapy. Nature *534*, 396–401.
6. Broos, K., Van der Jeught, K., Puttemans, J., Goyvaerts, C., Heirman, C., Dewitte, H., Verbeke, R., Lentacker, I., Thielemans, K., and Breckpot, K. (2016). Particle-mediated intravenous delivery of antigen mRNA results in strong antigen-specific T-cell responses despite the induction of type I interferon. Mol. Ther. Nucleic Acids *5*, e326.
7. Van Der Jeught, K., De Koker, S., Bialkowski, L., Heirman, C., Tjok Joe, P., Perche, F., Maenhout, S., Bevers, S., Broos, K., Deswarte, K., et al. (2018). Dendritic cell targeting mRNA lipopolyplexes combine strong antitumor T - cell immunity with improved inflammatory safety. ACS Nano *12*, 9815–9829.
8. Sahin, U., Oehm, P., Derhovanessian, E., Jabulowsky, R.A., Vormehr, M., Gold, M., Maurus, D., Schwarck-Kokarakis, D., Kuhn, A.N., Omokoko, T., et al. (2020). An RNA vaccine drives immunity in checkpoint-inhibitor-treated melanoma. Nature *585*, 107–112.
9. Kauffman, K.J., Dorkin, J.R., Yang, J.H., Heartlein, M.W., Derosa, F., Mir, F.F., Fenton, O.S., and Anderson, D.G. (2015). Optimization of lipid nanoparticle formulations for mRNA delivery in vivo with fractional factorial and definitive screening designs. Nano Lett. *15*, 7300–7306.
10. Ramaswamy, S., Tonnu, N., Tachikawa, K., Limphong, P., Vega, J.B., Karmali, P.P., Chivukula, P., and Verma, I.M. (2017). Systemic delivery of factor IX messenger RNA for protein replacement therapy. Proc. Natl. Acad. Sci. USA *114*, E1941–E1950.
11. Pardi, N., Tuyishime, S., Muramatsu, H., Kariko, K., Mui, B.L., Tam, Y.K., Madden, T.D., Hope, M.J., and Weissman, D. (2015). Expression kinetics of nucleoside-modified mRNA delivered in lipid nanoparticles to mice by various routes. J. Control. Release *217*, 345–351.
12. Chen, S., Tam, Y.Y.C., Lin, P.J.C., Sung, M.M.H., Tam, Y.K., and Cullis, P.R. (2016). Influence of particle size on the in vivo potency of lipid nanoparticle formulations of siRNA. J. Control. Release *235*, 236–244.
13. Chen, D., Ganesh, S., Wang, W., and Amiji, M. (2019). The role of surface chemistry in serum protein corona-mediated cellular delivery and gene silencing with lipid nanoparticles. Nanoscale *11*, 8760–8775.
14. Suzuki, T., Suzuki, Y., Hihara, T., Kubara, K., Kondo, K., Hyodo, K., Yamazaki, K., Ishida, T., and Ishihara, H. (2020). PEG shedding-rate-dependent blood clearance of PEGylated lipid nanoparticles in mice: faster PEG shedding attenuates anti-PEG IgM production. Int. J. Pharm. *588*, 119792.
15. Hassett, K.J., Benenato, K.E., Jacquinet, E., Lee, A., Woods, A., Yuzhakov, O., Himansu, S., Deterling, J., Geilich, B.M., Ketova, T., et al. (2019). Optimization of lipid nanoparticles for intramuscular administration of mRNA vaccines. Mol. Ther. Nucleic Acids *15*, 1–11.
16. Hassett, K.J., Higgins, J., Woods, A., Levy, B., Xia, Y., Hsiao, C.J., Acosta, E., Almarsson, Ö., Moore, M.J., and Brito, L.A. (2021). Impact of lipid nanoparticle size on mRNA vaccine immunogenicity. J. Control. Release *335*, 237–246.
17. Akita, H., Noguchi, Y., Hatakeyama, H., Sato, Y., Tange, K., Nakai, Y., and Harashima, H. (2015). Molecular tuning of a vitamin E-scaffold pH-sensitive and reductive cleavable lipid-like material for accelerated in vivo hepatic siRNA delivery. ACS Biomater. Sci. Eng. *1*, 834–844.
18. Pal, A., and Kundu, R. (2020). Human Papillomavirus E6 and E7: the cervical cancer hallmarks and targets for therapy. Front. Microbiol. *10*, 3116.
19. Grunwitz, C., Salomon, N., Vascotto, F., Selmi, A., Bukur, T., Diken, M., Kreiter, S., Türeci, Ö., Sahin, U., Grunwitz, C., et al. (2019). HPV16 RNA-LPX vaccine mediates complete regression of aggressively growing HPV-positive mouse tumors and establishes protective T cell memory. Oncoimmunology *8*, e1629259.
20. Lewis, G.A., Mathieu, D., and Phan-Tan-Lu, R. (1999). Pharmaceutical Experimental Design (Marcel Dekker, Inc).
21. Bonehill, A., Tuyaerts, S., Van Nuffel, A.M., Heirman, C., Bos, T.J., Fostier, K., Neyns, B., and Thielemans, K. (2008). Enhancing the T-cell stimulatory capacity of human dendritic cells by co-electroporation with CD40L, CD70 and constitutively active TLR4 encoding mRNA. Mol. Ther. *16*, 1170–1180.
22. Almeida, J.R., Price, D.A., Papagno, L., Arkoub, Z.A., Sauce, D., Bornstein, E., Asher, T.E., Samri, A., Schnuriger, A., Theodorou, I., et al. (2007). Superior control of HIV-1 replication by CD8+ T cells is reflected by their avidity, polyfunctionality, and clonal turnover. J. Exp. Med. *204*, 2473–2485.
23. Ciuffreda, D., Comte, D., Cavassini, M., Giostra, E., Bühler, L., Perruchoud, M., Heim, M.H., Battegay, M., Genné, D., Mulhaupt, B., et al. (2008). Polyfunctional HCV-specific T-cell responses are associated with effective control of HCV replication. Eur. J. Immunol. *38*, 2665–2677.
24. Wimmers, F., Aarntzen, E.H.J.G., Duiveman-deBoer, T., Figdor, C.G., Jacobs, J.F.M., Tel, J., and de Vries, I.J.M. (2016). Long-lasting multifunctional CD8+ T cell responses in end-stage melanoma patients can be induced by dendritic cell vaccination. Oncoimmunology *5*, e1067745.
25. Spranger, S., Koblish, H.K., Horton, B., Scherle, P.A., Newton, R., and Gajewski, T.F. (2014). Mechanism of tumor rejection with doublets of CTLA-4, PD-1/PD-L1, or IDO blockade involves restored IL-2 production and proliferation of CD8+ T cells directly within the tumor microenvironment. J. Immunother. Cancer *2*, 3.
26. De Groot, R., Van Loenen, M.M., Guislain, A., Nicolet, B.P., Freen-Van Heeren, J.J., Verhagen, O.J.H.M., Van Den Heuvel, M.M., De Jong, J., Burger, P., Van Der Schoot, C.E., et al. (2019). Polyfunctional tumor-reactive T cells are effectively expanded from non-small cell lung cancers, and correlate with an immune-engaged T cell profile. Oncoimmunology *8*, e1648170.
27. Lin, K.Y., Guarnieri, F.G., Staveley-O'Carroll, K.F., Levitsky, H.I., August, J.T., Pardoll, D.M., and Wu, T.C. (1996). Treatment of established tumors with a novel vaccine that enhances major histocompatibility class II presentation of tumor antigen. Cancer Res. *56*, 21–26.
28. Besin, G., Milton, J., Sabnis, S., Howell, R., Mihai, C., Burke, K., Benenato, K.E., Stanton, M., Smith, P., Senn, J., et al. (2019). Accelerated blood clearance of lipid nanoparticles entails a biphasic humoral response of B-1 followed by B-2 lymphocytes to distinct antigenic moieties. Immunohorizons *3*, 282–293.
29. Shimizu, T., Mima, Y., Hashimoto, Y., Ukawa, M., Ando, H., Kiwada, H., and Ishida, T. (2015). Anti-PEG IgM and complement system are required for the association of second doses of PEGylated liposomes with splenic marginal zone B cells. Immunobiology *220*, 1151–1160.
30. Kozma, G.T., Shimizu, T., Ishida, T., and Szebeni, J. (2020). Anti-PEG antibodies: properties, formation, testing and role in adverse immune reactions to PEGylated nano-biopharmaceuticals. Adv. Drug Deliv. Rev. *154–155*, 163–175.
31. Ishida, T., Wang, X.Y., Shimizu, T., Nawata, K., and Kiwada, H. (2007). PEGylated liposomes elicit an anti-PEG IgM response in a T cell-independent manner. J. Control. Release *122*, 349–355.
32. De Beuckelaer, A., Pollard, C., Van Lint, S., Roose, K., Van Hoecke, L., Naessens, T., Udhayakumar, V.K., Smet, M., Sanders, N., Lienenklaus, S., et al. (2016). Type I interferons interfere with the capacity of mRNA lipoplex vaccines to elicit cytolytic T cell responses. Mol. Ther. *24*, 2012–2020.
33. Pollard, C., Rejman, J., De Haes, W., Verrier, B., Van Gulck, E., Naessens, T., De Smedt, S., Bogaert, P., Grooten, J., Vanham, G., et al. (2013). Type I IFN counteracts the induction of antigen-specific immune responses by lipid-based delivery of mRNA vaccines. Mol. Ther. *21*, 251–259.
34. Van Hoecke, L., Roose, K., Ballegeer, M., Zhong, Z., Sanders, N.N., De Koker, S., Saelens, X., and Van Lint, S. (2020). The opposing effect of type I IFN on the T cell response by non-modified mRNA-lipoplex vaccines is determined by the route of administration. Mol. Ther. Nucleic Acids *22*, 373–381.
35. Patricia, F.-B., Jihong, D., and Sukhwinder, S. (2008). Plasmacytoid dendritic cells and type I IFN: 50 years of convergent history. Cytokine Growth Factor Rev. *19*, 3–19.
36. van Rooijen, N., and van Nieuwmegen, R. (1984). Elimination of phagocytic cells in the spleen after intravenous injection of liposome-encapsulated dichloromethylene diphosphonate - an enzyme-histochemical study. Cell Tissue Res. *238*, 355–358.
37. Kitamura, D., Roes, J., Kühn, R., and Rajewsky, K. (1991). A B cell-deficient mouse by targeted disruption of the membrane exon of the immunoglobulin μ chain gene. Nature *350*, 423–426.

38. Riley, R.S., Kashyap, M.V., Billingsley, M.M., White, B., Alameh, M.G., Bose, S.K., Zoltick, P.W., Li, H., Zhang, R., Cheng, A.Y., et al. (2021). Ionizable lipid nanoparticles for in utero mRNA delivery. Sci. Adv. *7*, eaba1028.

39. Arteta, M.Y., Kjellman, T., Bartesaghi, S., Wallin, S., Wu, X., Kvist, A.J., Dabkowska, A., Székely, N., Radulescu, A., Bergenholtz, J., et al. (2018). Successful reprogramming of cellular protein production through mRNA delivered by functionalized lipid nanoparticles. Proc. Natl. Acad. Sci. USA *115*, E3351–E3360.

40. Lokugamage, M.P., Vanover, D., Beyersdorf, J., Hatit, M.Z.C., Rotolo, L., Echeverri, E.S., Peck, H.E., Ni, H., Yoon, J.K., Kim, Y.T., et al. (2021). Optimization of lipid nanoparticles for the delivery of nebulized therapeutic mRNA to the lungs. Nat. Biomed. Eng. *5*, 1059–1068.

41. Kumar, V., Qin, J., Jiang, Y., Duncan, R.G., Brigham, B., Fishman, S., Nair, J.K., Akinc, A., Barros, S.A., and Kasperkovitz, P.V. (2014). Shielding of lipid nanoparticles for siRNA delivery: impact on physicochemical properties, cytokine induction, and efficacy. Mol. Ther. Nucleic Acids *3*, e210.

42. Shimizu, T., Abu Lila, A.S., Kawaguchi, Y., Shimazaki, Y., Watanabe, Y., Mima, Y., Hashimoto, Y., Okuhira, K., Storm, G., Ishima, Y., et al. (2018). A novel platform for cancer vaccines: antigen-selective delivery to splenic marginal zone B cells via repeated injections of PEGylated liposomes. J. Immunol. *201*, 2969–2976.

43. Hong, L., Wang, Z., Wei, X., Shi, J., and Li, C. (2020). Antibodies against polyethylene glycol in human blood: a literature review. J. Pharmacol. Toxicol. Methods. *102*, 106678.

44. Mathieu, M., Cotta-Grand, N., Daudelin, J.F., Boulet, S., Lapointe, R., and Labrecque, N. (2012). CD40-activated B cells can efficiently prime antigen-specific naïve CD8 + T cells to generate effector but not memory T cells. PLoS One *7*, 1–12.

45. Colluru, V.T., and McNeel, D.G. (2016). B lymphocytes as direct antigen-presenting cells for anti-tumor DNA vaccines. Oncotarget *7*, 67901–67918.

46. Wennhold, K., Shimabukuro-Vornhagen, A., and Von Bergwelt-Baildon, M. (2019). B cell-based cancer immunotherapy. Transfus. Med. Hemother. *46*, 36–46.

47. Sagiv-Barfi, I., Czerwinski, D.K., Shree, T., Lohmeyer, J.J.K., and Levy, R. (2022). Intratumoral immunotherapy relies on B and T cell collaboration. Sci. Immunol. *7*, eabn5859.

48. Bergmann, C.C., Ramakrishna, C., Kornacki, M., and Stohlman, S.A. (2001). Impaired T cell immunity in B cell-deficient mice following viral central nervous system infection. J. Immunol. *167*, 1575–1583.

49. Homann, D., Tishon, A., Berger, D.P., Weigle, W.O., von Herrath, M.G., and Oldstone, M.B.A. (1998). Evidence for an underlying CD4 helper and CD8 T-cell defect in B-Cell-Deficient mice: failure to clear persistent virus infection after adoptive immunotherapy with virus-specific memory cells from μMT/μMT mice. J. Virol. *72*, 9208–9216.

50. Lykken, J.M., DiLillo, D.J., Weimer, E.T., Roser-Page, S., Heise, M.T., Grayson, J.M., Weitzmann, M.N., and Tedder, T.F. (2014). Acute and chronic B cell depletion disrupts CD4 + and CD8 + T cell homeostasis and expansion during acute viral infection in mice. J. Immunol. *193*, 746–756.

YMTHE, Volume *30*

Supplemental Information

mRNA-LNP vaccines tuned for systemic immunization induce strong antitumor immunity by engaging splenic immune cells

Sanne Bevers, Sander A.A. Kooijmans, Elien Van de Velde, Martijn J.W. Evers, Sofie Seghers, Jerney J.J.M. Gitz-Francois, Nicky C.H. van Kronenburg, Marcel H.A.M. Fens, Enrico Mastrobattista, Lucie Hassler, Helena Sork, Taavi Lehto, Kariem E. Ahmed, Samir El Andaloussi, Katja Fiedler, Karine Breckpot, Michael Maes, Diane Van Hoorick, Thierry Bastogne, Raymond M. Schiffelers, and Stefaan De Koker

Supplementary method: Bayesian-based Quality by Design

A Bayesian implementation of the Quality by Design (QbD) good development practice (ICH Q8(R2))[1] was applied for the lipid based nanoparticle (LNP) optimization. The Bayesian inference is often qualified as more natural than the conventional frequentist statistics in the sense that science works namely the same way. In a scientific approach, today's prior is updated by new data to become a posterior distribution that will serve as tomorrow's prior, and so forth. The same applies to the Quality by Design cycle (Fig. 1) based on a deductive/inductive reasoning process. Any QbD cycle relies on an investigation model describing the cause-effect relationship between input factors (CMA: critical material attributes and CPP: critical process parameters) and output responses (CQA: critical quality attributes). The last three steps of the QbD cycle (experimentation, empirical modeling and knowledge) are detailed below. The Bayesian implementation of the empirical modeling was performed within the R statistical computing environment[2].

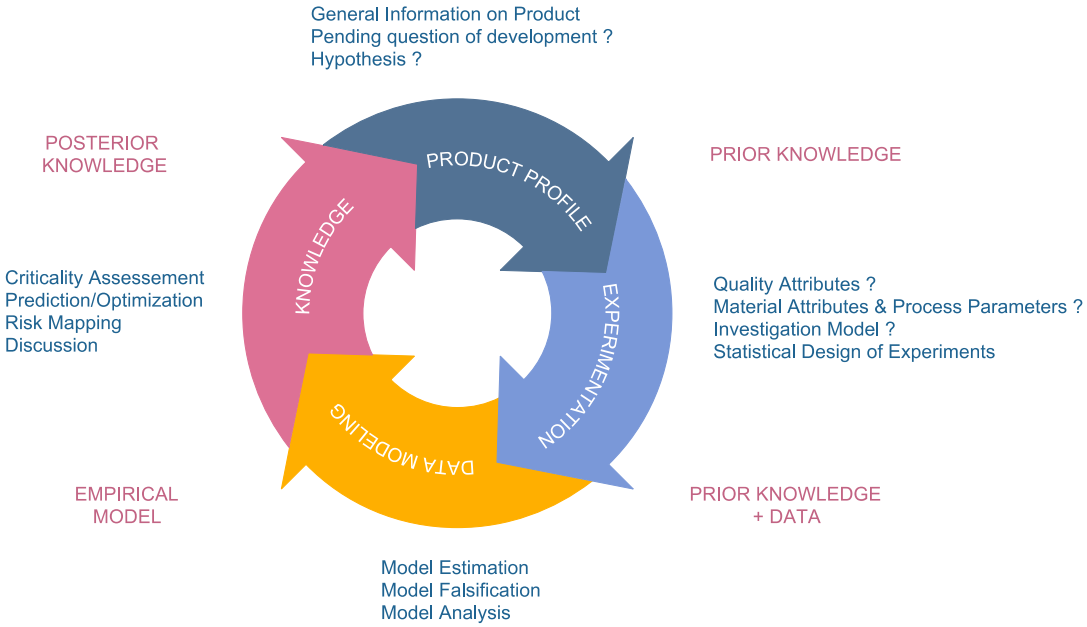

Figure 1: Quality by Design approach presented as a deductive/inductive reasoning process in which Bayesian statistics are introduced to estimate and assess models of investigation, but also to predict quality attributes (response variables) and risks to not meet expected specifications on CQA.

Pending Question & Quality Attribute

In this study we aimed to optimize the formulation of mRNA-lipid nanoparticles in order to achieve the maximal possible immune response. Accordingly, the critical quality attribute to be controlled is the CD8 T cell response, determined as %E7-specific T cells in blood of mice after three immunizations. The expected specification is to meet the minimum level of 50%.

Critical Material Attributes

Three constitutive lipid proportions were considered as three independent critical material attributes (CMA). The range of each lipid proportion was selected based on prior knowledge and is summarized in Table 1. Cholesterol (u4) constitutes the remainder of the lipid mix (fill molar proportion up to 100%).

Notation	Critical material attributes	Experimental domain (molar lipid proportion in %)
u1	Ionizable lipid	35 - 65
u2	PEG-lipid	0.5 - 2
u3	DOPE	5 - 15

Table 1: Critical material attributes and their respective experimental domain.

Design of Experiments

A Roquemore's Hybrid Design was used to select the formulations to be tested (i.e. the trials to be carried out). Each experimental condition was applied in triplicate (3 mice/treatment). Each lipid's molar percentage takes five values, and the design is composed of 11 different experimental conditions (Table 2). This experimental protocol was carried out for three different choices of PEG-lipid. This design is particularly suited to the identification of quadratic response surface models (see next section) and more economic than a central composite design (15 assays) or Box-Behnken design (13 assays).

N°Exp	IonizLipid	PEGLipid	DOPE
	%	%	%
1	50	1.25	15
2	50	1.25	5
3	40.5	0.78	12.24
4	59.5	0.78	12.24
5	40.5	1.72	12.24
6	59.5	1.72	12.24
7	36.6	1.25	7.76
8	63.4	1.25	7.76
9	50	0.58	7.76
10	50	1.92	7.76
11	50	1.25	10

Table 2: Roquemore's Hybrid Design of Experiments

Investigation Model

The investigation model used to optimize the LNP composition is described by a quadratic response surface model structure:

$$Y_k = b_0 + \sum_{i=1}^{3} b_i \, u_{i,k} + \sum_{i=1}^{3} b_{ii} \, u_{i,k}^2 + \sum_{i=1}^{2} \sum_{j=2}^{3} b_{ij} \, u_{i,k} \, u_{j,k} + E_k$$

with:

- k=1,⋯,n: is the index of the experimental condition in the experimental design ;
- n: is the total number of experiments to be carried out;
- Y_k: value of %E7-specific T cells in blood for the k-th assay of the design;
- b_0: value of the mean response;
- b_i: additive effect of the i-th factor;
- b_{ii}: quadratic effect of the i-th factor;
- b_{ij}: interaction effect between the i-th and j-th factors on the response;
- $E_k \sim N(0,\sigma 2)$: random error describing modeling residual.

All the model coefficients b_i, b_{ii} and b_{ij} have to be estimated from the experimental data collected after experimentation.

Bayesian estimation of the model parameters

After obtaining data on the T-cell stimulatory capacity (%E7-specific CD8 T cells) of the LNP formulations in mice, the data was used to construct a quadratic response surface model. The Hamiltonian Monte Carlo (HMC) algorithm, a generalization of the Metropolis algorithm[3], was used to compute the posterior distributions of the model parameters. Simulations from the HMC are determined by Bayes' rule, in which the posterior distribution of the parameters is proportional to the prior distribution of the parameters multiplied by the likelihood. Main percentile values characterizing dispersion and uncertainty of the model parameters are given in Table 3 (and interpreted in section "Tests of significance and criticality")

A

	mean	sd	25%	50%	75%
(Intercept)	113.08	76.53	62.61	113.02	162.87
u1	0.65	2.04	-0.67	0.63	1.95
u2	-137.65	39.89	-164.07	-137.60	-111.73
u3	-4.14	5.22	-7.48	-4.15	-0.81
I(u1^2)	0.00	0.02	-0.01	0.00	0.02
I(u2^2)	29.73	10.53	22.92	29.76	36.79
I(u3^2)	0.13	0.20	0.00	0.13	0.26
u1:u2	-0.03	0.52	-0.38	-0.03	0.32
u1:u3	-0.08	0.07	-0.13	-0.08	-0.03
u2:u3	3.79	1.62	2.73	3.83	4.86
sigma	8.56	1.32	7.61	8.40	9.34

B

	mean	sd	25%	50%	75%
(Intercept)	11.53	90.95	-47.29	13.29	72.37
u1	2.58	2.47	0.99	2.45	4.18
u2	-52.95	44.04	-81.36	-52.61	-24.63
u3	-6.19	6.42	-10.50	-6.07	-1.84
I(u1^2)	-0.01	0.02	-0.02	-0.01	0.01
I(u2^2)	29.61	11.63	22.06	29.66	37.39
I(u3^2)	-0.31	0.24	-0.46	-0.31	-0.15
u1:u2	-1.89	0.63	-2.32	-1.90	-1.47
u1:u3	0.12	0.09	0.06	0.12	0.18
u2:u3	4.83	1.84	3.62	4.86	6.06
sigma	10.06	1.53	9.00	9.88	10.96

C

	mean	sd	25%	50%	75%
(Intercept)	-167.89	135.06	-260.62	-161.43	-71.64
u1	6.80	3.96	3.92	6.57	9.52
u2	-15.39	49.51	-47.11	-13.98	16.03
u3	6.65	7.80	1.40	6.53	11.91
I(u1^2)	-0.06	0.04	-0.08	-0.05	-0.03
I(u2^2)	-17.33	14.27	-26.91	-17.15	-7.90
I(u3^2)	-0.58	0.31	-0.79	-0.57	-0.37
u1:u2	-0.06	0.69	-0.50	-0.06	0.39
u1:u3	0.00	0.10	-0.06	0.00	0.07
u2:u3	4.14	2.26	2.62	4.14	5.59
sigma	12.51	1.95	11.11	12.30	13.71

Table 3: Mean, standard deviation and main percentile values characterizing dispersion and uncertainty of the model parameters. A: DMG-PEG2000 model; B: DSG-PEG2000 model and C: DSPE-PEG1000 model.

Posterior predictive check

The posterior predictive check (PPC)[4] is a Bayesian technique to assess the appropriateness of the model to fit data.[3] A “good” model is able to simulate data close to the observations as illustrated in Figure 2.

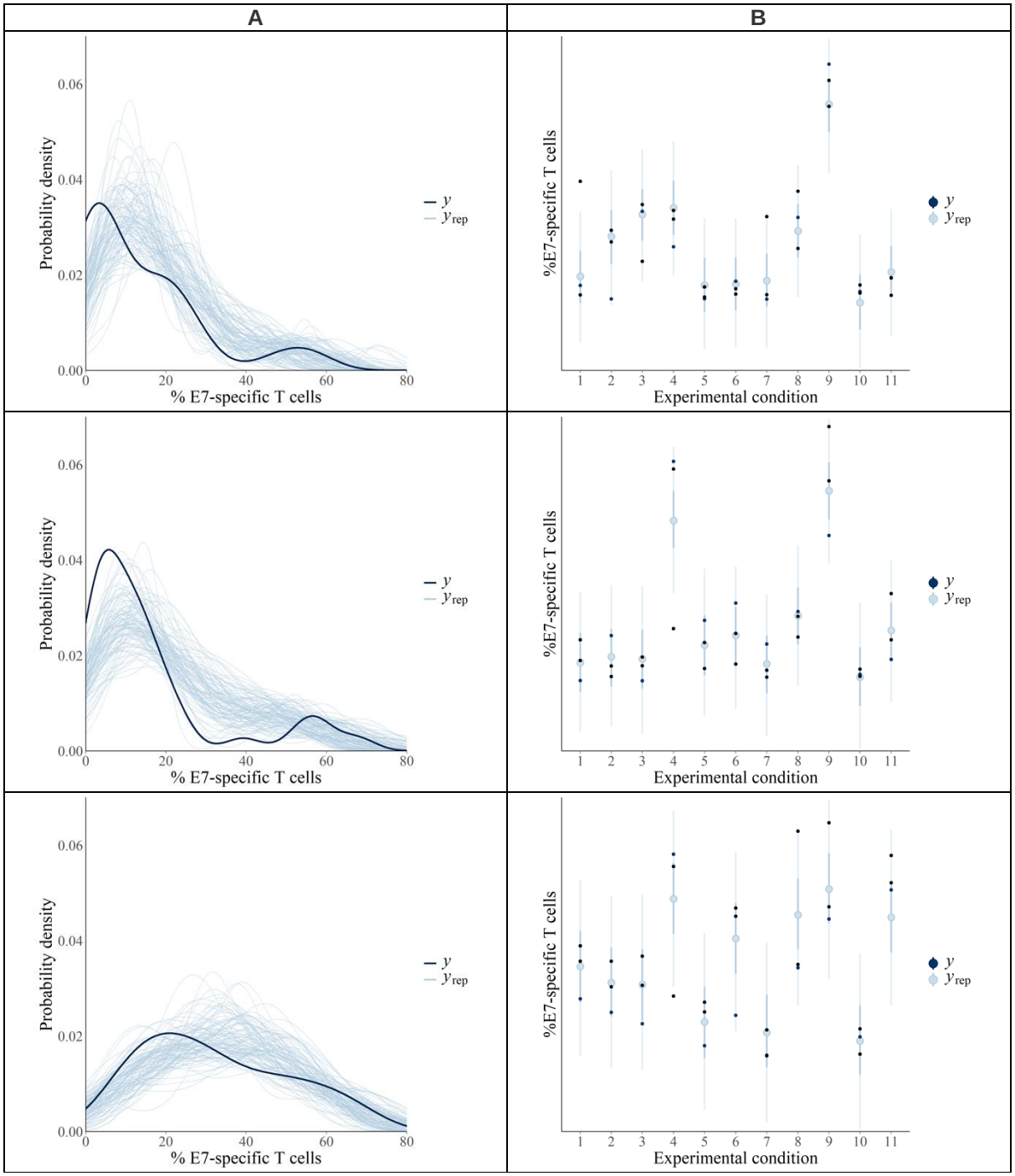

Figure 2: A) Observed vs replicated data densities for E7-specific T cell response. The density line in dark blue indicates the smooth density of observed data compared to overlaid smooth densities of 100 replicated data in light blue. B) Points in dark indicate observations of the 11 conditions tested in triplicate. Each line in light blue represents the posterior predictive distribution for each condition. Top to bottom DMG-PEG2000 model, DSG-PEG2000 model and DSPE-PEG1000 model.

To summarize data fitting performance a Bayesian version of the coefficient of determination (R^2) was computed. This coefficient uses draws from the residual distribution and is defined as the variance of the predicted values divided by the variance of the predicted values plus the variance of residuals (differences between fitted values and observed data)[5]. Figure 3 shows Bayesian R^2 mean values larger for DMG-PEG2000 and DSG-PEG2000 (≈0.72) than DPSE-PEG1000 (≈0.59).

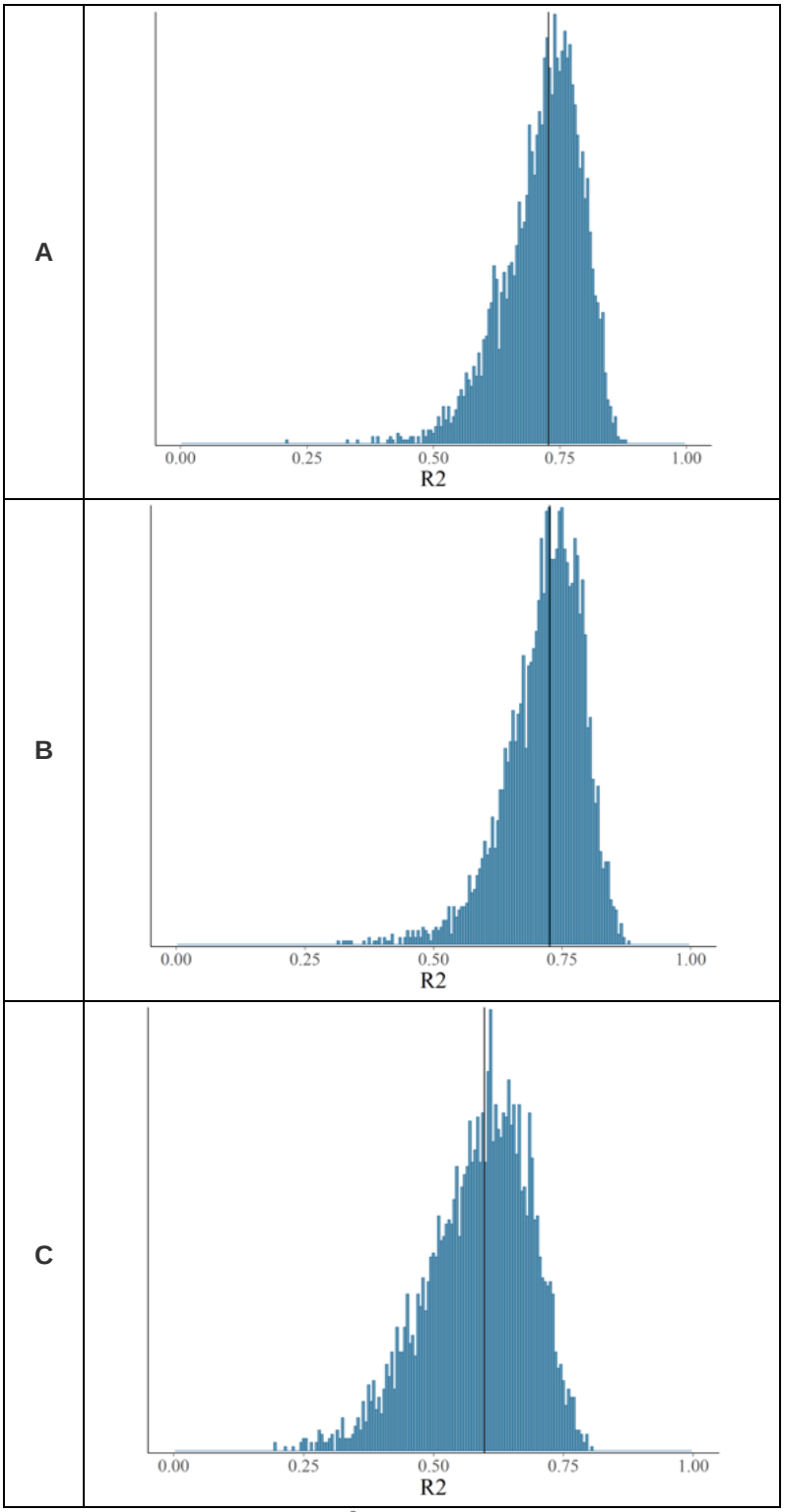

Figure 3: Histogram of the Bayesian version of the R^2 coefficient of determination computed over 4000 replicated data of CD8 T cell response. A: DMG-PEG2000 model; B: DSG-PEG2000 model and C: DSPE-PEG1000 model.

Analysis of posterior distributions related to the model parameters

Tests of significance and criticality

Effect analysis is often implemented as statistical tests applied to each model parameter, in which p-values play a key role. Nevertheless, several controversialities have recently emerged about their use and interpretation[6–8]. The way that p-values have been informally defined and interpreted appears to have led to tremendous confusion and controversy regarding their place in statistical analysis. To avoid those trick questions, posterior distributions of model parameters were directly used to estimate their criticality. The *modus operandi* implemented to analyze effects of each factor (i.e. lipid component of the LNPs) is described in Figure 4. Each subfigure is composed of a posterior distribution of a model parameter b (see investigation model) describing either single, quadratic or interaction effects. Two different aspects have to be examined: significance and criticality of effects.

- Significance of the effect (test of nullity): Examining the position of the distribution with respect to the origin of the X-axis:
  $$\begin{cases} H0s: & b = 0 \\ H1s: & b \neq 0 \end{cases} \quad (1)$$
  We used the equation $p_s = P[H0s]$. If $p_s < \pi_s$, significance of the effect b is accepted. π_s is a threshold probability of significance.
- Criticality of the effect is assessed by examining the position of the same distribution with respect to a threshold d: the smallest mean value of the effect considered as critical.
  $$\begin{cases} H0c: & |b| > d \\ H1c: & |b| \not> d \end{cases} \quad (2)$$
  We used the equation $p_c = P[H0c]$. If $p_c > \pi_c$, criticality of the effect b is accepted. π_c is a threshold probability of criticality.

Six situations can occur and are illustrated in Figure 4. In cases 1 and 4, posterior distributions are beyond the threshold d, showing critical effects even if uncertainty on the effect magnitude is greater in case 4. On the contrary, cases 2 and 3 do not show any critical effects. The trickiest situation is presented in cases 5 and 6, where two contradictory conclusions may be drawn. In those both risky cases, the effect b is classified “at-risk” until more informative data is collected to definitively conclude.

According to the type of effect (simple, interaction of quadratic) different threshold values can be chosen. In this application, d was fixed to 5, i.e., a variation of 5% of the E7-specific T cell response caused by a 1% change in u_i, u_iu_j or u_i^2 respectively. Note that each factor was normalized before the estimation step. After normalization, all factors take values between -1 and +1 associated with minimal and maximal values in their real scale. Consequently, 1% of change for u_i corresponds to 1% of variation in lipid percentage within its experimental domain presented above in Table 1.

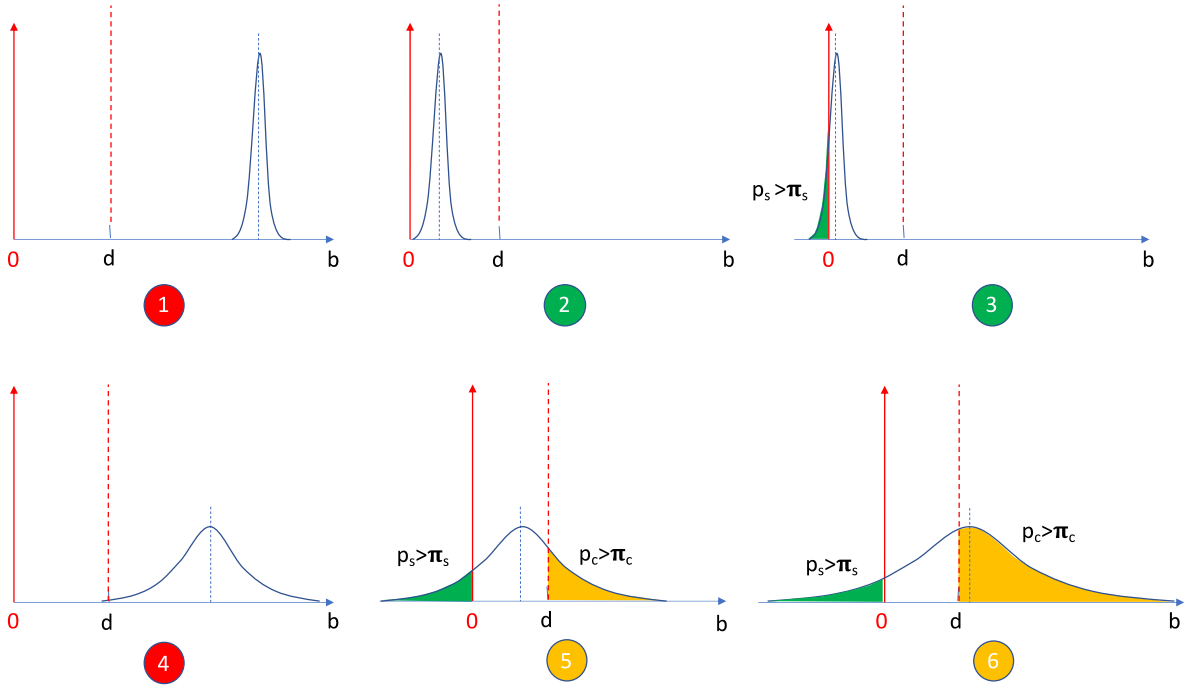

1 - b is both **significant** and **critical**.	2- b is **significant** ($p_s<\pi_s$) but **not critical**.	3 - b is neither **significant** ($p_s>\pi_s$) nor **critical**
4 - b is both **significant** and **critical**.	5 – Uncertain situation: conclusions on **significance** ($p_s>\pi_s$) and **criticality** ($p_c>\pi_c$) are contradictory.	6 - Uncertain situation: conclusions on **significance** ($p_s>\pi_s$) and **criticality** ($p_c>\pi_c$) are contradictory.

b: estimated effect, d: critical effect (threshold)

Figure 4: Schematic showing differences between significance and criticality of effects.

DMG-PEG2000

Figure 5A shows a critical single effect of the %PEG-lipid (u2) and emphasizes a meaningful risk for the %ionizable lipid (u1) and %DOPE (u3) to have a critical impact on the T cell response. Figure 5B points out a critical interaction between %DMG-PEG2000 and %DOPE and potentially between %ionizable lipid and %DOPE. The risk of an interaction between %ionizable lipid and %PEG-lipid impacting the T cell response still exists but is less likely. Figure 5C presents the quadratic effects and confirms the same conclusions drawn for the single effects, i.e. a critical influence of %DMG-PEG2000, and likely impacts of the two other lipids.

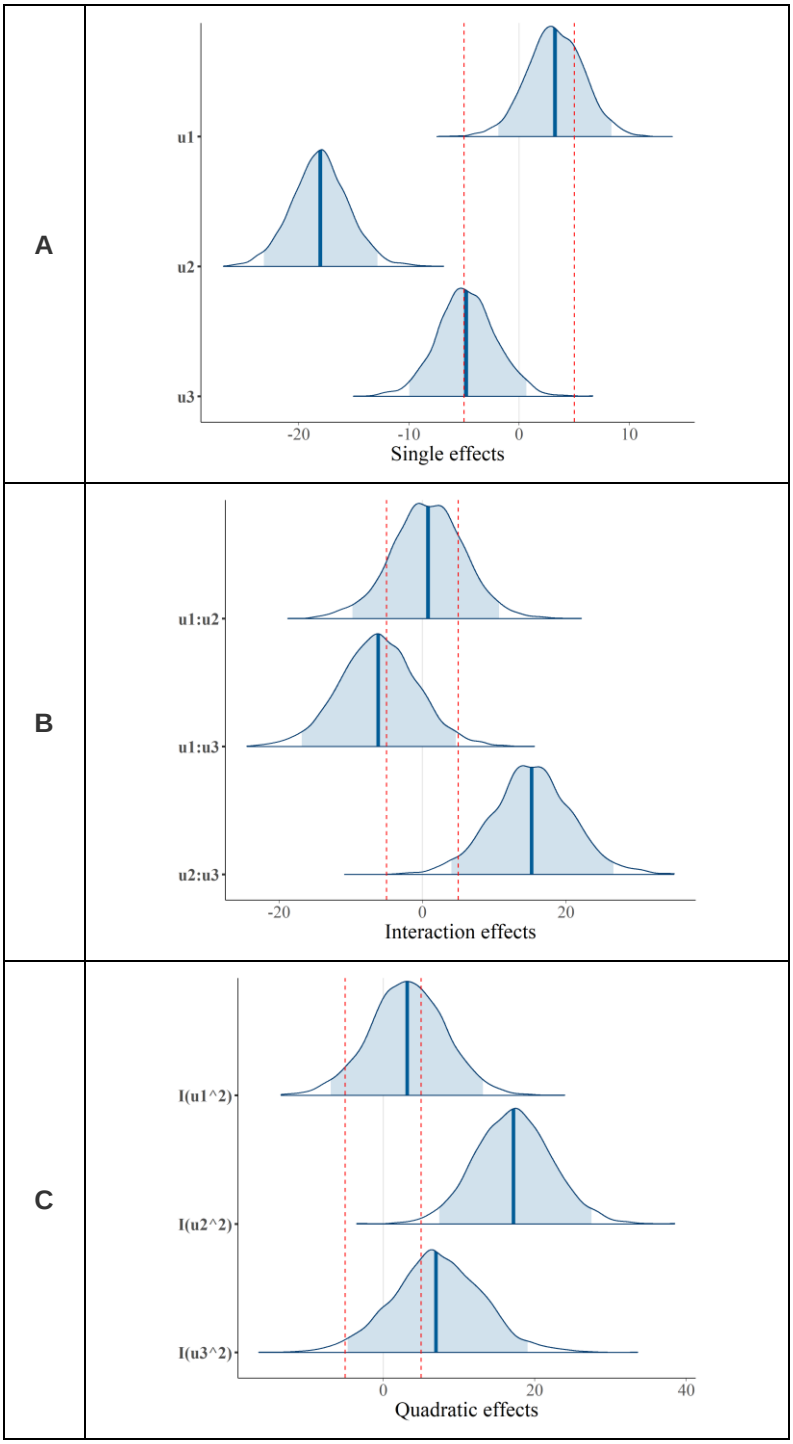

Figure 5: Analysis of individual lipid effects on T cell responses for DMG-PEG2000-based LNPs. Posterior distributions with 95% confidence interval of additive effects for the three studied factors. B: Posterior distributions of interactions effects between factors. C: Posterior distrbutions of quadratic effects. Red dashed lines indicate threshold d to detemine criticality of the effect.

DSG-PEG2000

Figure 6A confirms the critical impact of the %PEG-lipid (u2), already observed for DMG-PEG2000 LNPs (Figure 5a). It concerns both single (Figure 6A) and quadratic effects (Figure 6C) but also interactions with the two other lipid proportions (Figure 6B). Figure 6A also reveals a single effect of %ionizable lipid (u1), which is more critical than estimated for DMG-PEG2000 LNPs (Figure 5a). On the contrary, %DOPE (u3) does not show any critical single effect, but an important interaction with the %PEG-lipid and %ionizable lipid (Figure 6B) and a potential quadratic influence (Figure 6C) on the T cell response.

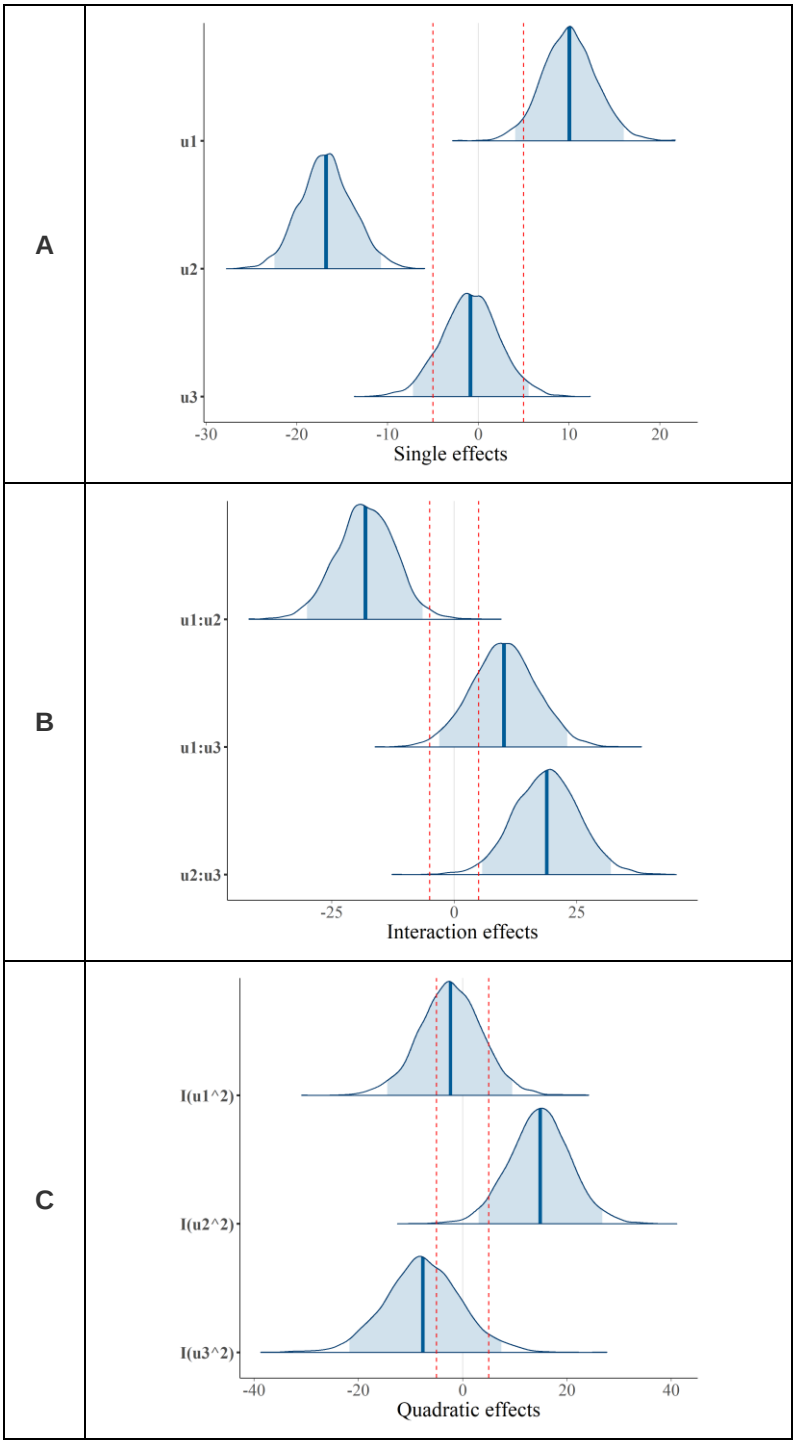

Figure 6: Analysis of individual lipid effects on T cell responses for DSG-PEG2000-based LNPs. Posterior distributions with 95% confidence interval of additive effects for the three studied factors. B: Posterior distributions of interactions effects between factors. C: Posterior distrbutions of quadratic effects. Red dashed lines indicate threshold d to detemine criticality of the effect.

DSPE-PEG1000:

Single effects presented in Figure 7A are very similar to the ones observed in Figure 6A for DSG-PEG2000 LNPs and identify %PEG-lipid (u3) and % ionizable lipid (u1) as critical. Only one interaction seems to be critical and involves %PEG-lipid and %DOPE. On the contrary, all lipid proportions have a critical quadratic influence on the T cell response.

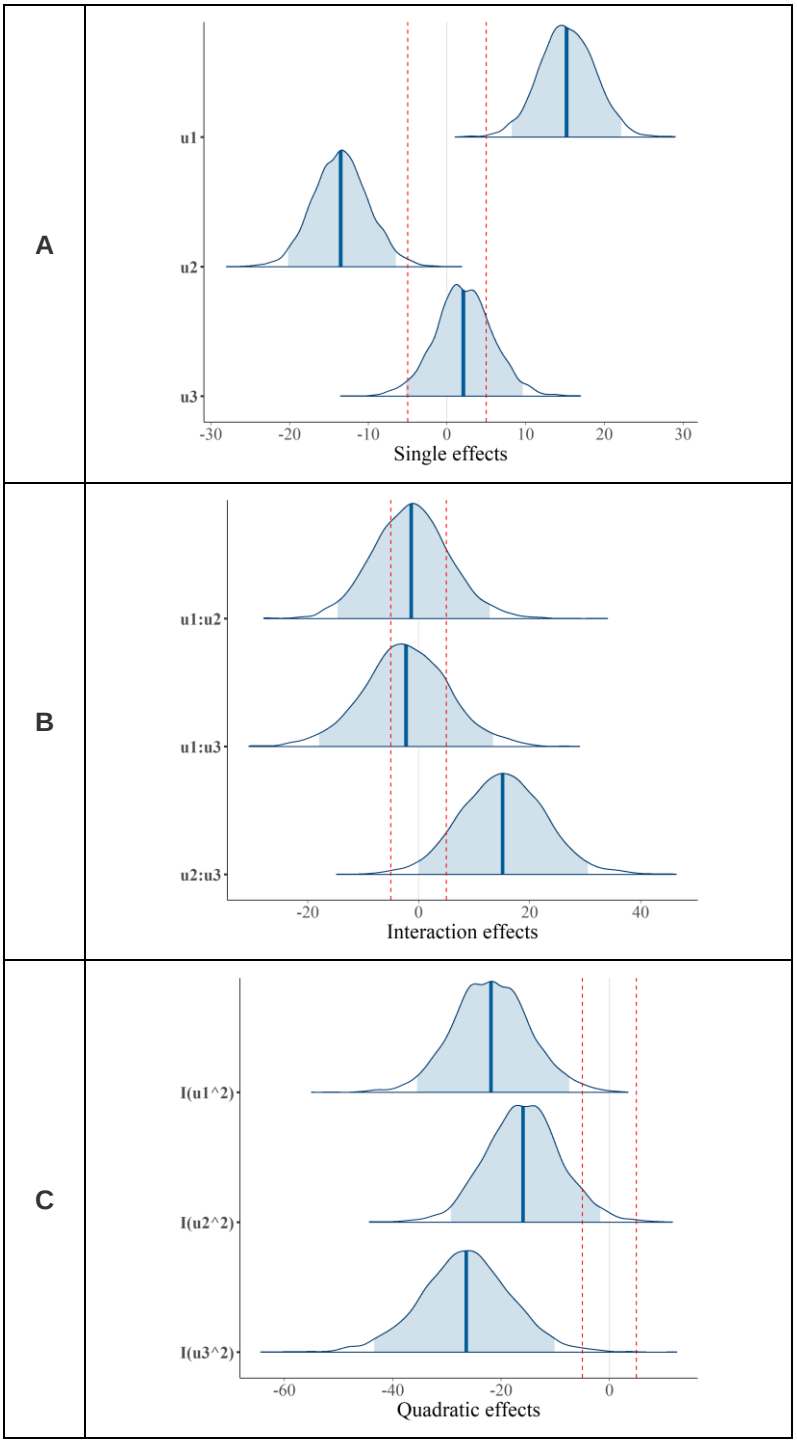

Figure 7: Analysis of individual lipid effects on T cell responses for DSPE-PEG1000 based LNPs. Posterior distributions with 95% confidence interval of additive effects for the three studied factors. B: Posterior distributions of interactions effects between factors. C: Posterior distributions of quadratic effects. Red dashed lines indicate threshold d to detemine criticiality of the effect.

To conclude on the effect analysis, critical effects that are very likely are as follows (listed in order of strength of the effect within the effect type and PEG-lipid type):

- Single effects
    - DMG-PEG2000: PEG-lipid
    - DSG-PEG2000: PEG-lipid and ionizable lipid
    - DSPE-PEG1000: PEG-lipid and ionizable lipid
- Interaction effects
    - DMG-PEG2000: PEG-lipid and DOPE
    - DSG-PEG2000: PEG-lipid and DOPE; ionizable lipid and PEG-lipid; ionizable lipid and DOPE
    - DSPE-PEG1000: PEG-lipid and DOPE
- Quadratic effects
    - DMG-PEG2000: PEG-lipid
    - DSG-PEG2000: PEG-lipid
    - DSPE-PEG1000: DOPE, ionizable lipid, PEG-lipid

To summarize and compare their global effects on the T cell response, results of a global sensitivity analysis are presented in the next section.

Global sensitivity analysis

Single, quadratic and interaction effects can sometimes offset each other. To globally test their impact on the response, a global sensitivity analysis was performed. This global analysis accounts for all types of effect (single, quadratic and interaction). Sensitivity indices of the %E7-specific T cells with respect to the three lipid proportions were computed based on a Monte Carlo estimation of the Sobol' indices[9]. Results are shown in Figure 8.

A

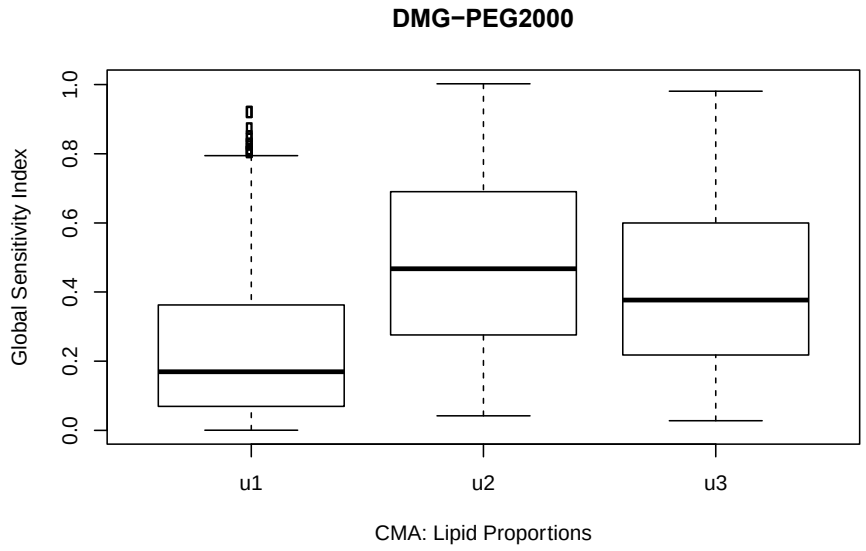

B

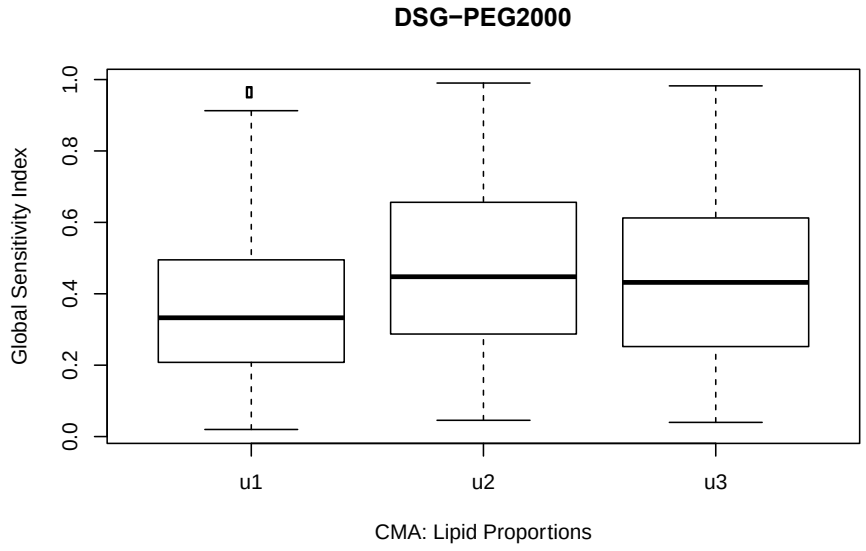

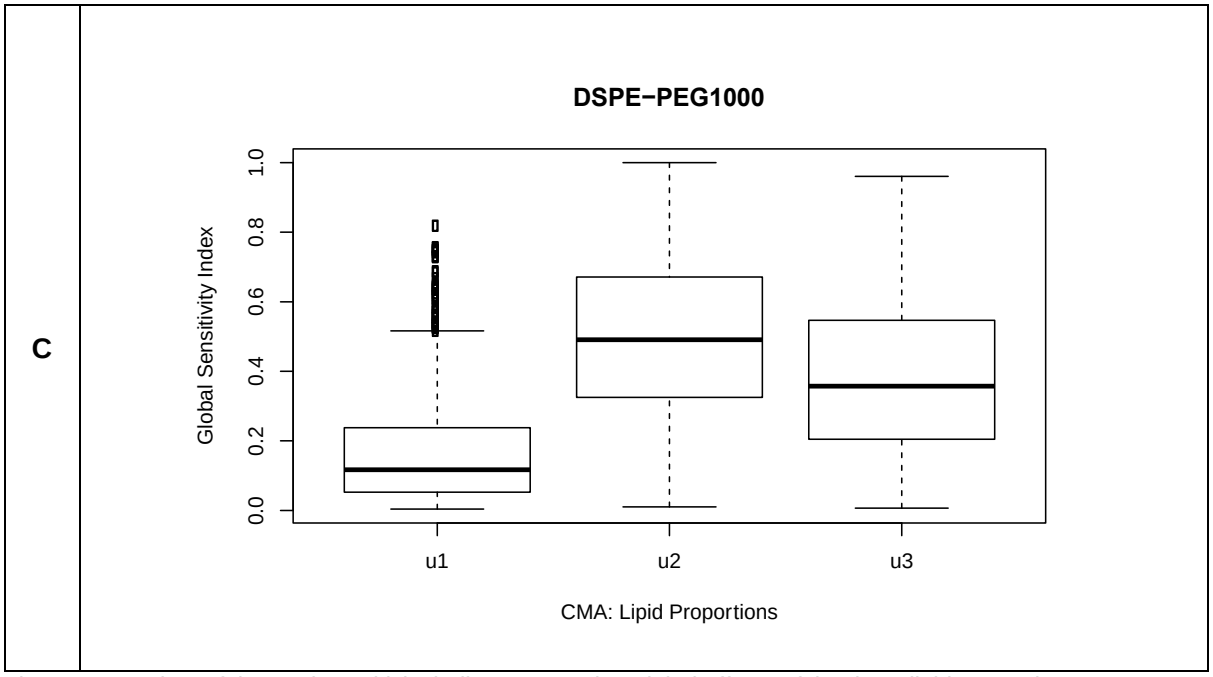

Figure 8: Boxplots of the total sensitivity indices comparing global effects of the three lipid proportions: %ionizable lipid (u_1), %PEG-lipid (u_2) and DOPE (u_3) on the %E7-specific T cell response. A: DMG-PEG2000, B: DSG-PEG2000 and C: DSPE-PEG1000. A boxplot is a standardized way of displaying the dataset based on a five-number summary: the minimum, the maximum (two whiskers), the sample median (horizontal bold black bar), and the first and third quartiles (box). Dots correspond to values estimated as outliers.

For DMG-PEG2000 based LNPs (Fig. 8A), estimated values of mean global sensitivity indices are: S1≈21% for u1, S2≈42% for u2 and S3≈ 37% for u3. For DSG-PEG2000 based LNPs (Fig. 8B), estimated values of mean global sensitivity indices are: S1≈27% for u1, S2≈37% for u2 and S3≈ 36% for u3. For DSPE-PEG1000 based LNPs (Fig. 8C), estimated values of mean global sensitivity indices are: S1≈16% for u1, S2≈49% for u2 and S3≈ 35% for u3.

Regardless of what type of PEG lipid was incorporated in the LNPs, we systematically observed that the T cell response is most sensitive to changes in %PEG-lipid, followed by changes in %DOPE and %ionizable lipid respectively. Changes in %ionizable lipid have a bigger mean impact on T cell response for DSG-PEG2000 LNPs (S= 27%) than for DMG-PEG-2000 (S=21) and DSPE-PEG1000 LNPs (S=16). The ratio of T cell response sensitivity to changes in %PEG-lipid over changes in %ionizable lipid is highest for DSPE-PEG1000LNPs (49/16 = 3), followed by DMG-PEG2000 (42/21 =2) and DSG-PEG2000 (37/27=1.4). We observe a quasi-constant sensitivity of the immune response with respect to %DOPE (around 36%), only the ratio %PEG-lipid/%ionizable lipid depends on the PEG-lipid type.

Response Prediction

After the qualification of the models for all three PEG-lipid types, we used the models to predict mean responses (%) for all combinations of the three factors (%ionizable lipid, %PEG-lipid, %DOPE). All predictions are gathered in Figure 9. The green region corresponds to the set of lipid proportions predicted to lead to the highest %E7-specfic T cell repsonse.

A	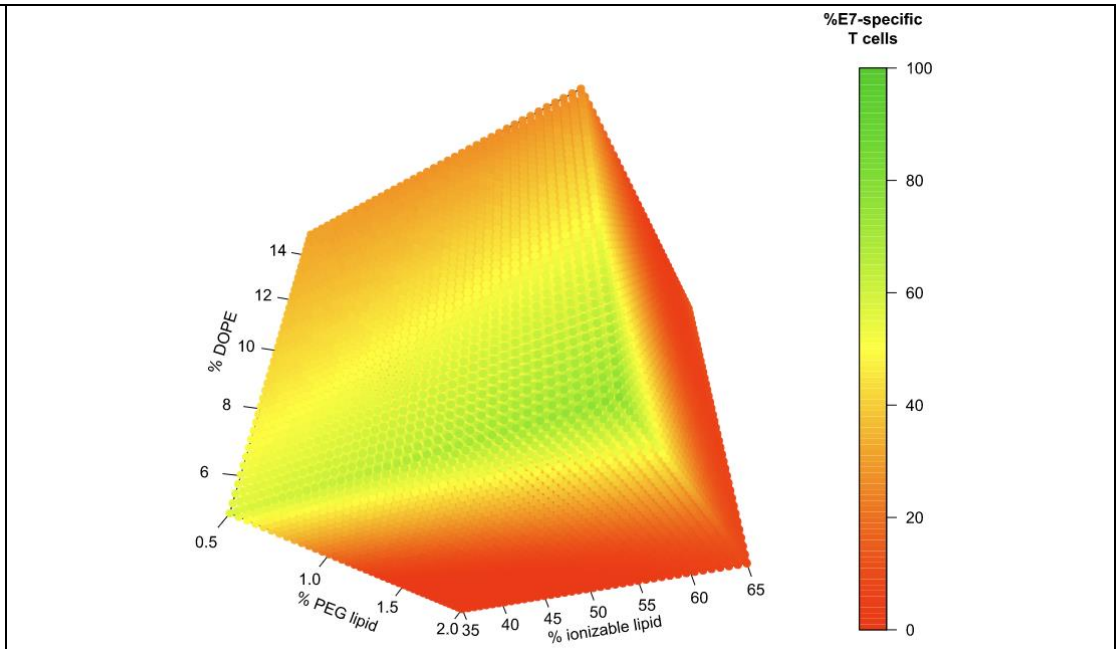
B	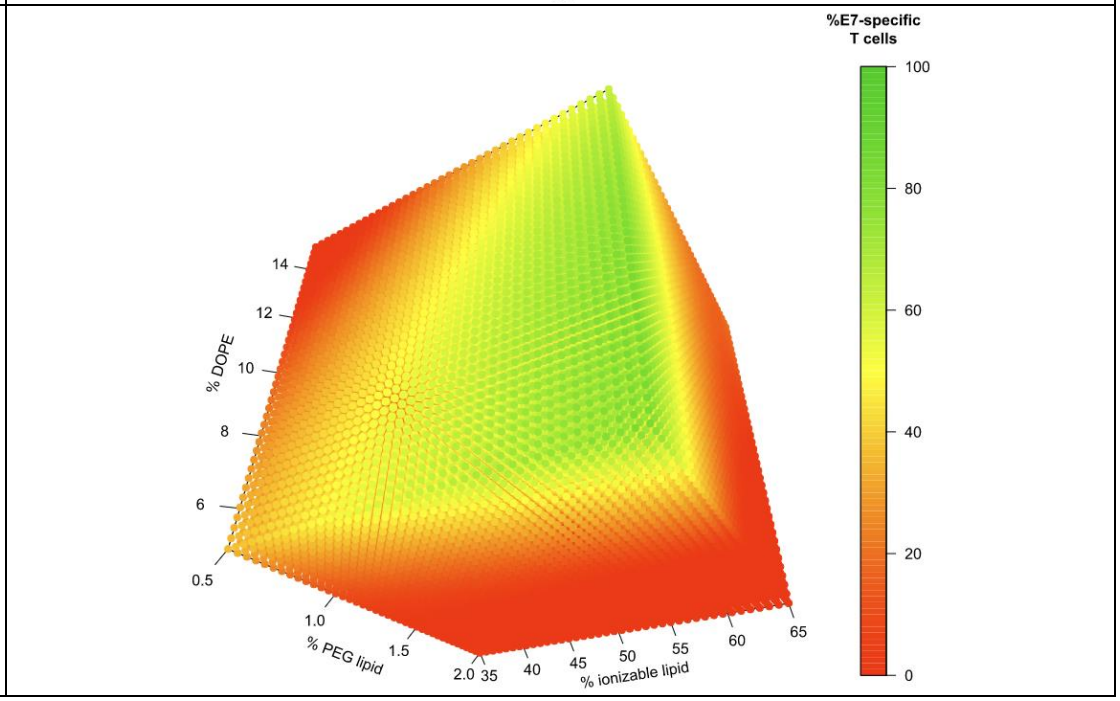

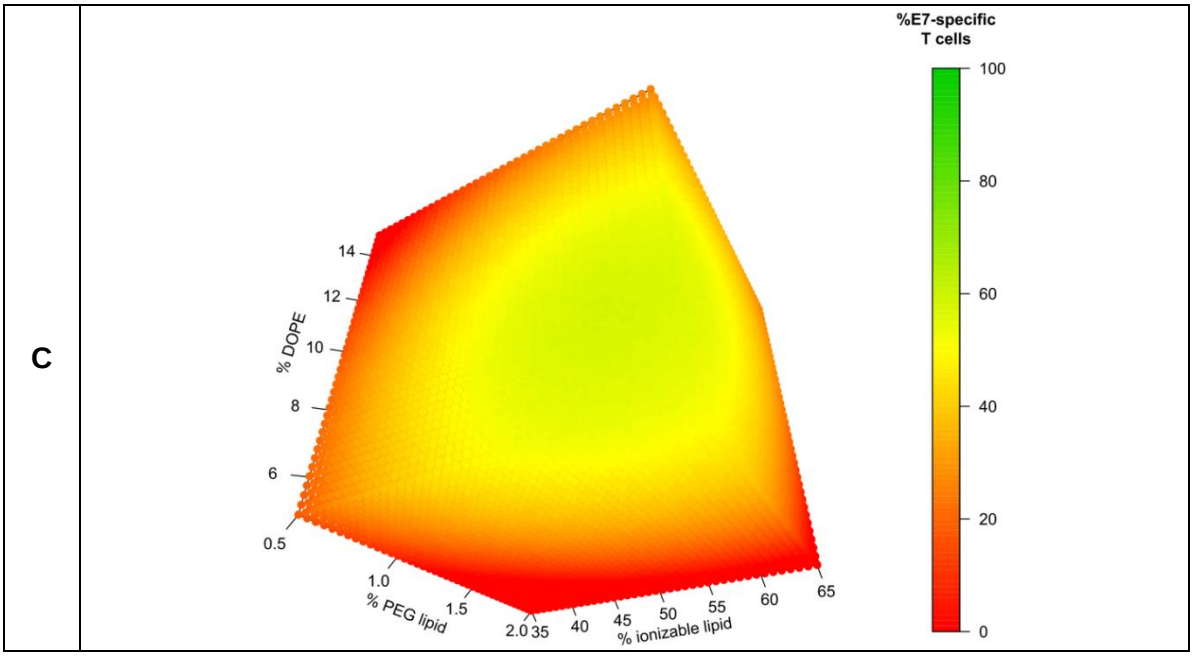

Figure 9: 3D model of mean predictions of the %E7-specific T cells in respect to %ionizable lipid, %PEG-lipid and DOPE. A: DMG-PEG2000, B: DSG-PEG2000 and C: DSPE-PEG1000.

For all PEG-lipid types, the optimal response region corresponds to high percentage of ionizable lipid and small percentages of PEG-lipid and DOPE.

Design Space (Risk mapping)

A Design Space is a multidimensional risk mapping in which probabilities to fulfill CQA specifications are split up into three regions: NOR (Normal Operating Region), PAR (Proven Acceptance Region) and OOS (Out Of Specification) denoting respectively: the desired region of interest, the domain where the product is still acceptable but corrections should be made and the area where the level of risk is not acceptable. In this study, region NOR has a probability to respect the specification of at least 50% E7-specific T cells greater than 90%. Region PAR has a probability between 70% and 90% while the last region, OOS has a probability lower than 70% to respect the specification. In practice, design spaces were determined from simulations carried out from posterior predictive distributions of the CD8 T cell response. Those response distributions were themselves obtained using Hamiltonian Monte Carlo, a family of Markov chain Monte Carlo (MCMC) algorithms.[10] Design spaces for each PEG-lipid type are given in Figure 10.

A	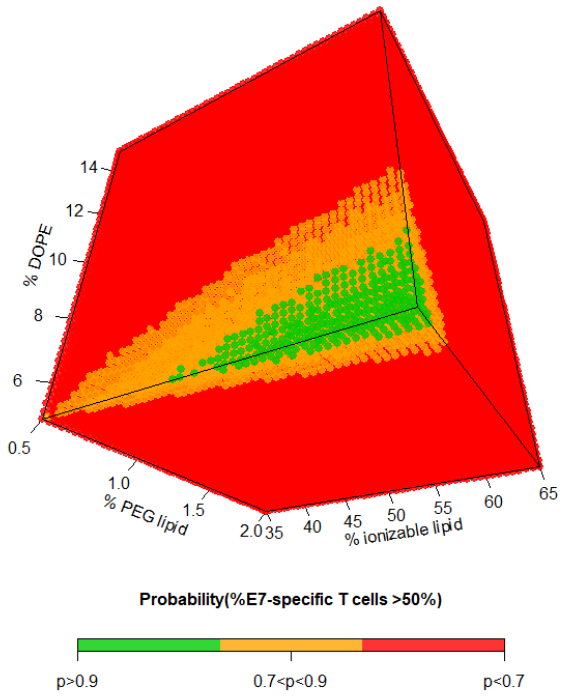 % DOPE 14 12 10 8 6 0.5 1.0 1.5 2.0 % PEG lipid 35 40 45 50 55 60 65 % ionizable lipid Probability(%E7-specific T cells >50%) p>0.9 0.7<p<0.9 p<0.7
B	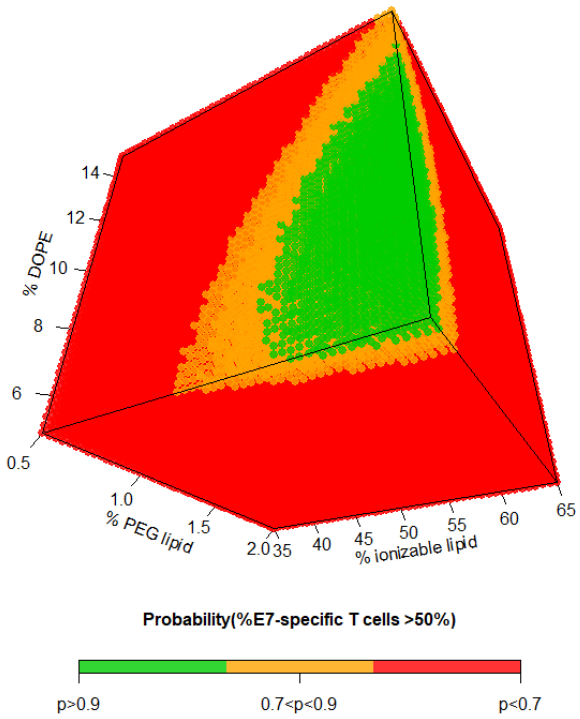 % DOPE 14 12 10 8 6 0.5 1.0 1.5 2.0 % PEG lipid 35 40 45 50 55 60 65 % ionizable lipid Probability(%E7-specific T cells >50%) p>0.9 0.7<p<0.9 p<0.7

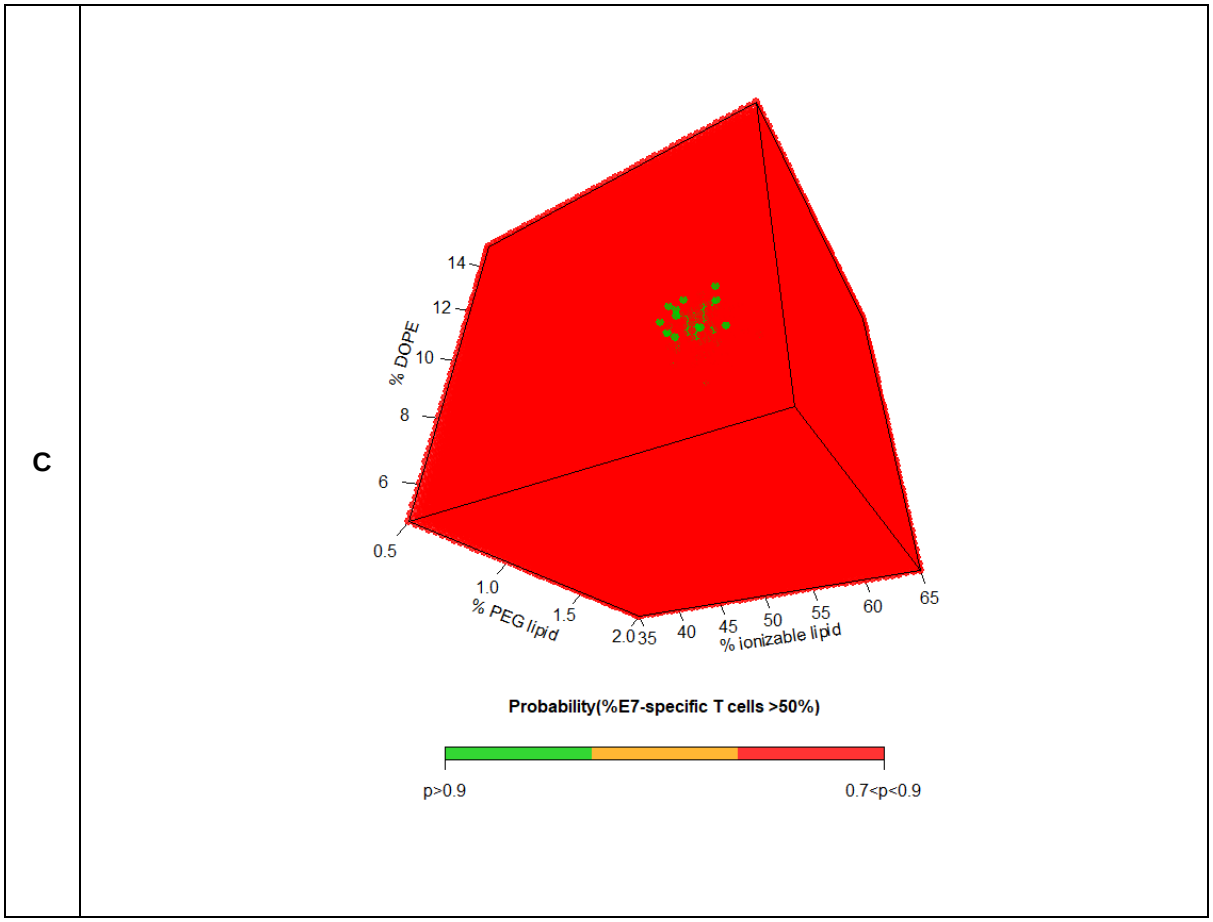

Figure 10: Design Spaces for DMG PEG2000 (A), DSG PEG2000 (B) and DSPE PEG-1000 (C). Green: NOR (Normal Operating Region), Orange: PAR (Proven Acceptance Region) and Red: OOS (Out Of Specification)

Risk assessment of the optimal LNP compositions

Based on the models described above, for each PEG-lipid a predicted optimal and predicted suboptimal LNP composition was chosen (LNPs 34-39), different from the compositions in the initial LNP library, and tested in 4-5 mice each. Table 4 presents the results of this cross-validation test. Four measured T cell responses out of 26 were out of the 95% confidence interval, which is acceptable in this *in vivo* context despite some gaps between predicted and observed mean values of the E7-specific T cells response.

		Lipid proportion (%)				Predicted E7-specific T cells (%)		Observed E7-specific T cells (%)	
PEG-lipid type	**LNP number**	**Ionizable lipid**	**DOPE**	**Cholesterol**	**PEG-lipid**	**Mean**	**95% confidence interval**		**Mean**
DMG-PEG2000	34	56.5	5.25	37.75	0.5	70	[43;95]	40, 67, 62, 57	59
	35	42	12	44.5	1.5	3	[0;21]	8, 4, 8, 10	8
DSG-PEG2000	36	64.4	8	27.1	0.5	82	[51;100]	65, 41, 53, 52	53
	37	42	12	44.5	1.5	6	[0 ;28]	7, 16, 1, 9, 3	8
DSPE-PEG1000	38	64.6	6.6	28.3	0.52	56	[15 ;95]	84, 36, 48, 49, 50	54
	39	42	12	44.5	1.5	26	[0 ;54]	61, 44, 38, 59, 54	51

Table 4: LNP compositions selected for the three types of PEG-lipid with their predicted responses (mean values and 95% confidence interval).

References

(1) *Committee for Human Medicinal Products, "ICH Guideline Q8 (R2) on Pharmaceutical Development," Tech. Rep. Step 5, European Medicine Agency, June 22 2017*.

(2) Hornik, K. The Comprehensive R Archive Network. *Wiley Interdisciplinary Reviews: Computational Statistics*. **2012**. https://doi.org/10.1002/wics.1212.

(3) Gelman, A.; Carlin, J. B.; Stern, H. S.; Dunson, D. B.; Vehtari, A.; Rubin, D. B. *Bayesian Data Analysis*; **2013**. https://doi.org/10.1201/b16018.

(4) Gabry, J.; Simpson, D.; Vehtari, A.; Betancourt, M.; Gelman, A. Visualization in Bayesian Workflow. *J. R. Stat. Soc. Ser. A Stat. Soc.* **2019**. https://doi.org/10.1111/rssa.12378.

(5) Gelman, A.; Goodrich, B.; Gabry, J.; Vethari, A. R-Squared for Bayesian Regression Models - The Problem Defining R 2 Based on the Variance of Estimated Prediction Errors. *Am. Stat.* **2018**.

(6) Wellek, S. A Critical Evaluation of the Current "p-Value Controversy." *Biometrical Journal*. **2017**. https://doi.org/10.1002/bimj.201700001.

(7) Wasserstein, R. L.; Lazar, N. A. The ASA's Statement on p-Values: Context, Process, and Purpose. *American Statistician*. **2016**. https://doi.org/10.1080/00031305.2016.1154108.

(8) Kuffner, T. A.; Walker, S. G. Why Are P-Values Controversial? *Am. Stat.* **2019**. https://doi.org/10.1080/00031305.2016.1277161.

(9) Salteli, A.; Ratto, M.; Andres, T.; Campolongo, F.; Cariboni, J.; Gatelli, D.; Saisana, M.; Tarantola, S. Global Sensitivity Analysis. *Biometrics* **2009**, *65* (4), 1311–1312. https://doi.org/10.1111/j.1541-0420.2009.01343_7.x.

(10) Gelman, A.; Carlin, J. B.; Stern, H. S.; Dunson, D. B.; Vehtari, A.; Rubin, D. B. *Bayesian Data Analysis, Third Edition*; 2013.

Supplementary Method: Adsorption of plasma proteins on LNPs

Incubation of LNPs with plasma

10 µl of LNPs (conc.=100 µg mRNA/ml) were mixed with 90 µl of 10% plasma in PBS adjusted to 10 mM sodium citrate to prevent coagulation. The mixure was incubated for 1 h at 37 ℃. The LNP-corona complexes were spun at 20,000 × g at 4 °C for 1h, supernatant discarded, and the pellet resuspended in 100 µl PBS. The LNP-corona pellet was washed twice with PBS using the same procedure then resuspended in 20 µl PBS and protein content was measured using Micro BCA™ protein assay kit (ThermoFisher, USA).

Sample preparation for proteomics

Proteins (3 µg) were precipitated with the trichloroacetic acid deoxycholate (TCA/DOC) method, as described elsewhere [1]. Protein pellets were suspended in 7 M urea / 2 M thiourea, 100 mM ABC, 20 mM methylamine solution, followed by disulfide reduction and cysteine alkylation with 5 mM DTT and 10 mM chloroacetamide for 60 min each at room temperature. Proteins were predigested with 1:50 (enzyme to protein) Lys-C (Wako Chemicals) for 4 h, diluted 5 times with 100 mM ABC and further digested with trypsin (Sigma Aldrich) overnight at room temperature. Peptides were desalted with in-house made C18 StageTips.

Nano-LC/MS/MS measurement

Samples were injected to an Ultimate 3000 RSLCnano system (Dionex) using a C18 trap-column (Dionex) and an in-house packed (3 µm C18 particles, Dr Maisch) analytical 50 cm x 75 µm ID emitter-column (New Objective). Peptides were eluted at 200 nl/min with a 8-40% B 120 min gradient (buffer B: 80% acetonitrile + 0.1% formic acid, buffer A: 0.1% formic acid) to a Q Exactive Plus (Thermo Fisher Scientific) mass spectrometer (MS) using a nano-electrospray source (spray voltage of 2.5 kV). The MS was operated with a top-10 data-dependent acquisition strategy. Briefly, one 350-1400 m/z MS scan at a resolution setting of R=70 000 at 200 m/z was followed by higher-energy collisional dissociation fragmentation (normalized collision energy of 26) of 10 most intense ions (z: +2 to +6) at R=17 500. MS and MS/MS ion target values were 3e6 and 5e4 with 50 ms injection times. Dynamic exclusion was limited to 40 s.

Raw Data Processing

Mass spectrometric raw files were analyzed the with the MaxQuant software (version 1.6.15.0) [2]. Methionine oxidation and protein N-terminal acetylation were set as variable modifications, while cysteine carbamidomethylation was defined as a fixed modification. Search was performed against UniProt (www.uniprot.org) *Mus musculus* reference proteome database (downloaded on 04.01.2021) using the tryptic digestion rule (including cleavages after proline). Only identifications with minimally 1 peptide 7 amino acids long were accepted and transfer of identifications between runs was enabled. Label-free normalization with MaxQuant LFQ algorithm was also applied. Protein and LFQ ratio count (i.e. number of quantified peptides for

reporting a protein intensity) was set to 1. Peptide-spectrum match and protein false discovery rate (FDR) was kept below 1% using a target-decoy approach. All other parameters were default.

Proteomics data analysis

Differential enrichment analysis was performed on the LFQ Intensity values by using Differential Enrichment analysis of Proteomics data (DEP) Version 1.10.0 [3], R Version 4.0.2 and RStudio version 1.3.1073. The figures were modified with GraphPad Prism Version 9 (GraphPad Software, Inc., La Jolla, CA, USA), if applicable.

References

(1) Using Deoxycholate and Trichloroacetic Acid to Concentrate Proteins and Remove Interfering Substances. *Cold Spring Harb. Protoc.* **2006**. https://doi.org/10.1101/pdb.prot4258.

(2) Cox, J.; Mann, M. MaxQuant Enables High Peptide Identification Rates, Individualized p.p.b.-Range Mass Accuracies and Proteome-Wide Protein Quantification. *Nat. Biotechnol.* **2008**, *26* (12), 1367–1372. https://doi.org/10.1038/nbt.1511.

(3) Zhang, X.; Smits, A. H.; Van Tilburg, G. B. A.; Ovaa, H.; Huber, W.; Vermeulen, M. Proteome-Wide Identification of Ubiquitin Interactions Using UbIA-MS. *Nat. Protoc.* **2018**, *13* (3), 530–550. https://doi.org/10.1038/nprot.2017.147.

Supplementary Method: TC-1 tumor experiment (Figure S2)

TC-1 cells were obtained from Leiden University Medical Center. 0.5 million TC-1 cells in 50 µl PBS were injected subcutaneously in the right flank of the mice. Tumor measurements were performed using a caliper. Tumor volume was calculated as (smallest diameter^2 x largest diameter)/2. At a mean tumor volume of 55mm^3, mice were injected i.v. via the tail vein with TBS or 5 µg of either E7-TriMix mRNA, Fluc-TriMix mRNA or Fluc mRNA in LNP36. Immunizations were performed weekly for a total of 3 times. At day 15 (n=4/group) and day 35 (n=6), tumors were isolated and placed in a 24-well plate filled with MACS tissue storage buffer (Miltenyi Biotec) for flow cytometry analysis.

Flow cytometry

Tumors were cut into 3mm^3 pieces and transferred to MACS C tubes containing digestion buffer prepared according to protocol of Tumor Dissociation Kit, mouse (Miltenyi Biotec). The content of enzyme R was reduced to 20% in the enzyme mix to help preserve cell surface epitopes. Single-cell suspensions were generated by use of a gentleMACS Octo dissociater (program 37C_m_TDK_2). Samples were immediately filtered through a 70 µm cell strainer, followed by lysis of red blood cells. Next, samples were split over two 96-well plates to stain with 2 different antibody cocktails. For both plates the cells were first incubated with FcR block and viability dye. After 20' incubation at 4°C both plates were washed. Next, an antibody mixture for surface molecules CD45, Thy1.2, CD19, MHCII, CD11c, CD11b, Ly6G, F4/80 and CD206 (Table S3) was added to the cells of plate 1 and incubated for 30 minutes at 4 °C. To plate 2, APC labelled E7 (RAHYNIVTF)-tetramer was added and incubated at RT for 30 minutes. Hereafter, excess tetramer was washed away and an antibody mixture for surface molecules CD45, CD4, CD8 and PD-1 (Table S3) was added and incubated for 30 minutes at 4 °C. Excess antibodies were washed off. Before proceeding with intracellular staining, cells were fixated and permeabilized with FoxP3 Fixation/Permeabilization solution (eBioscience) according to manufacturer protocol. Cells were kept in Fixation/Permeabilization solution overnight at 4 °C. The next morning, cells were washed with permeabilization buffer followed by addition of an antibody mixture of FoxP3, granzyme B and Ki67 antibodies (in permeabilization buffer) (Table S3). Samples were acquired on a 3-laser AttuneNxt flow cytometer. Analysis was done using FlowJo software. Gating strategies are provided in the next section of Supplementary information.

RT-qPCR

Tumors of mice that had reached a volume of 1000 mm^3 (for TBS, Fluc-TriMix and Fluc groups, n=11-12) or tumors that had relapsed at day 35 (for the E7-TriMix group, n=3) were washed in MACS tissue storage buffer, blotted dry, snap-frozen in liquid nitrogen and stored at -80˚C. Pieces of approximately 100mg were cut off, weighed and mixed with 1 mL TRIzol Reagent per 100 mg tissue (Thermo Fisher Scientific) in tubes containing 1.4 mm ceramic beads (Qiagen). Tissues were homogenized for 60 seconds at 4°C in a a Mini-BeadBeater-8 (BioSpec) at full speed for 60s at 4˚C. Homogenates were stored at -20˚C, thawed, centrifuged at 10.000 x g for 10 min at 4˚C to remove beads and debris, and 500 µL of supernatants were transferred to clean tubes. Phase-separation and RNA isolation was carried out according to manufacturer's instructions. RNA was dissolved in 150 µL nuclease-free water (Ambion) and stored at -80°C. Reverse transcription was performed using an iScript cDNA Synthesis Kit (Bio-Rad) in 10 µL reactions containing 375ng of RNA according to manufacturer's instructions. Resulting cDNA was diluted with 90 µL of nuclease-free water. Three microliters of each sample were used as input for 10 µL reactions containing 1X iQ™ SYBR® Green Supermix (Bio-Rad) and 250 nM of forward and reverse primers. Reactions were run on a CFX96 Touch Real-Time thermocycler (Bio-Rad) using the following cycling parameters: 3 min 95°C, 45 cycles of 40s 60°C and 15s 95°C, followed by melting curve analysis. Ct values of E7 and housekeeping gene beta-2-microglobulin (B2m)

were converted to fold changes compared to TBS-treated mouse values using the ΔΔCt method. Primer sequences were

E7_Fw: 5’- TCAGAGGAGGAGGATGAAATAGATGGTC-3',
E7_Rv: 5’- GCACAACCGAAGCGTAGAGTCAC-3',

Supplementary Method: Ex vivo LNP opsonization experiment

LNP34 and LNP36 were formulated with Fluc mRNA and Cy5-Fluc mRNA in a 1:9 ratio and diluted to an mRNA concentration of 0.1 mg/mL. Twenty-five microliters of each LNP were mixed with 1µg of rabbit anti-PEG IgG (Abcam, clone RM105) and incubated for 30 min at room temperature. LNPs were then mixed with 100 µL of pooled mouse serum obtained from wild-type C57Bl/6 mice and incubated for 30 or 120 min at 37°C. Mixtures were loaded onto a XK16/20 column (Cytiva) packed with Sepharose CL-4B resin equilibrated with PBS. Size exclusion chromatography (SEC) was performed using a refrigerated ÄKTA Start chromatography system (Cytiva) at a flow rate of 1 mL/min, while 1mL fractions were collected. LNP-containing fractions were pooled and aliquots were analysed by Dynamic Light Scattering as described in the main text. As controls for proper separation of LNPs and unbound anti-PEG, anti-PEG was incubated with serum in the absence of LNPs, subjected to SEC and typical LNP-containing fractions were collected. All samples were concentrated on Amicon Ultra-4 Centrifugal Filter Units with 100 kD molecular weight cut-off to volumes of approximately 50µL. LNP concentrations were normalized based on Cy5 fluorescence, which was measured using a SpectraMax iD3 platereader (Molecular Devices). Equal quantities of LNP-derived fluorescence were mixed with sample buffer containing dithiothreitol (DTT), heated to 95°C for 10 min, and subjected to SDS-PAGE using 4-12% Bis-Tris polyacrylamide gels (Thermo Fisher Scientific). Proteins were electrotransferred to Immobilon-FL polyvinylidene difluoride (PVDF) membranes (Merck Millipore). Membranes were blocked, probed with IRDye® 800CW Goat anti-Rabbit IgG secondary antibodies (LI-COR) and imaged using an Odyssey M Imaging System (LI-COR). Band intensities were quantified using Emperia Studio 2.1 (LI-COR).

Supplementary Method: Flow cytometry gating strategies

Flow cytometry gating strategies of all stainings performed in this work. Clone and catalog numbers of the used antibodies are summarized in Supplementary table 3.

Gating strategy of spleens (wild-type mice) to determine cellular Cy5-mRNA association

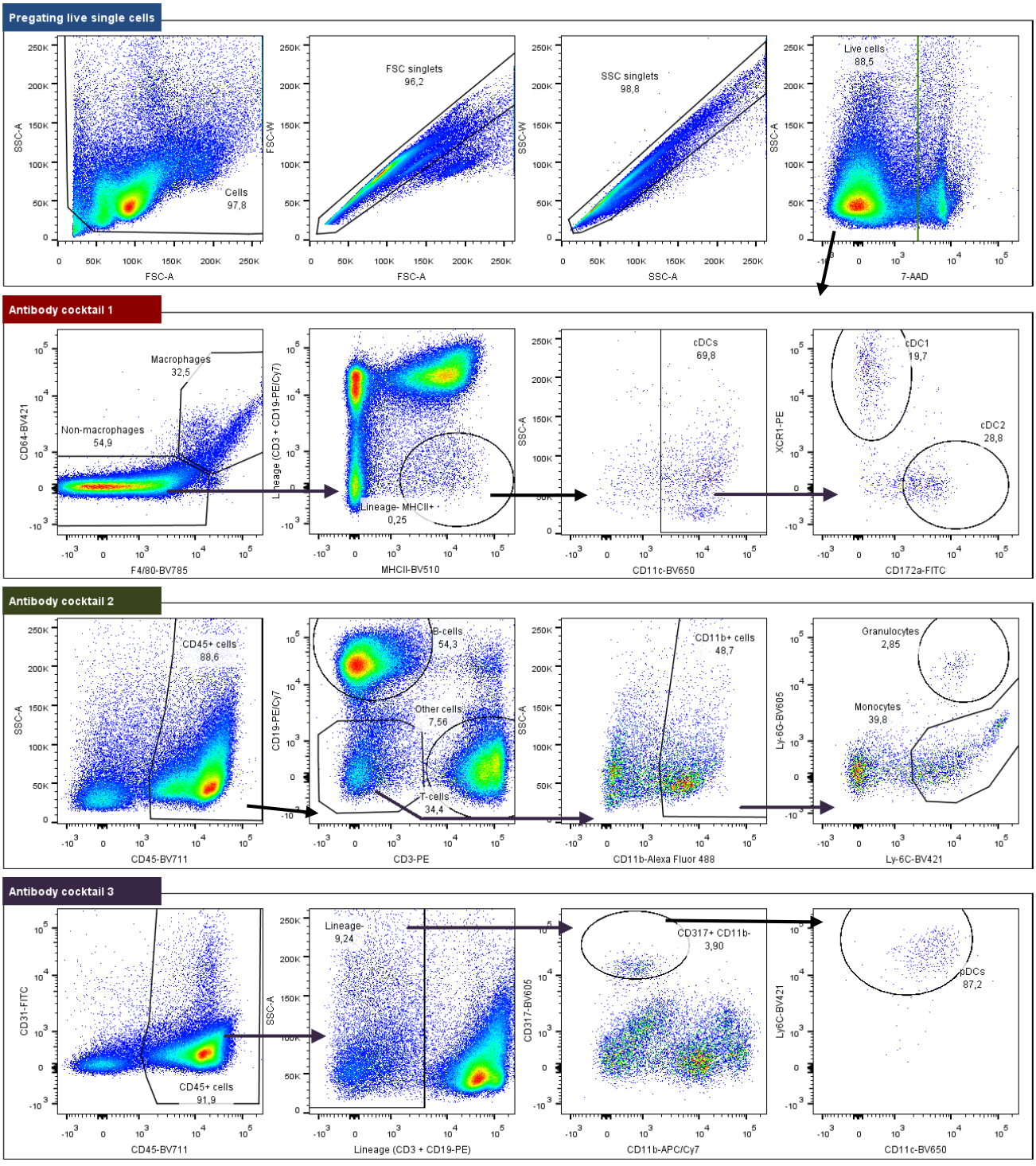

Gating strategy of livers (wild-type mice) to determine cellular Cy5-mRNA association

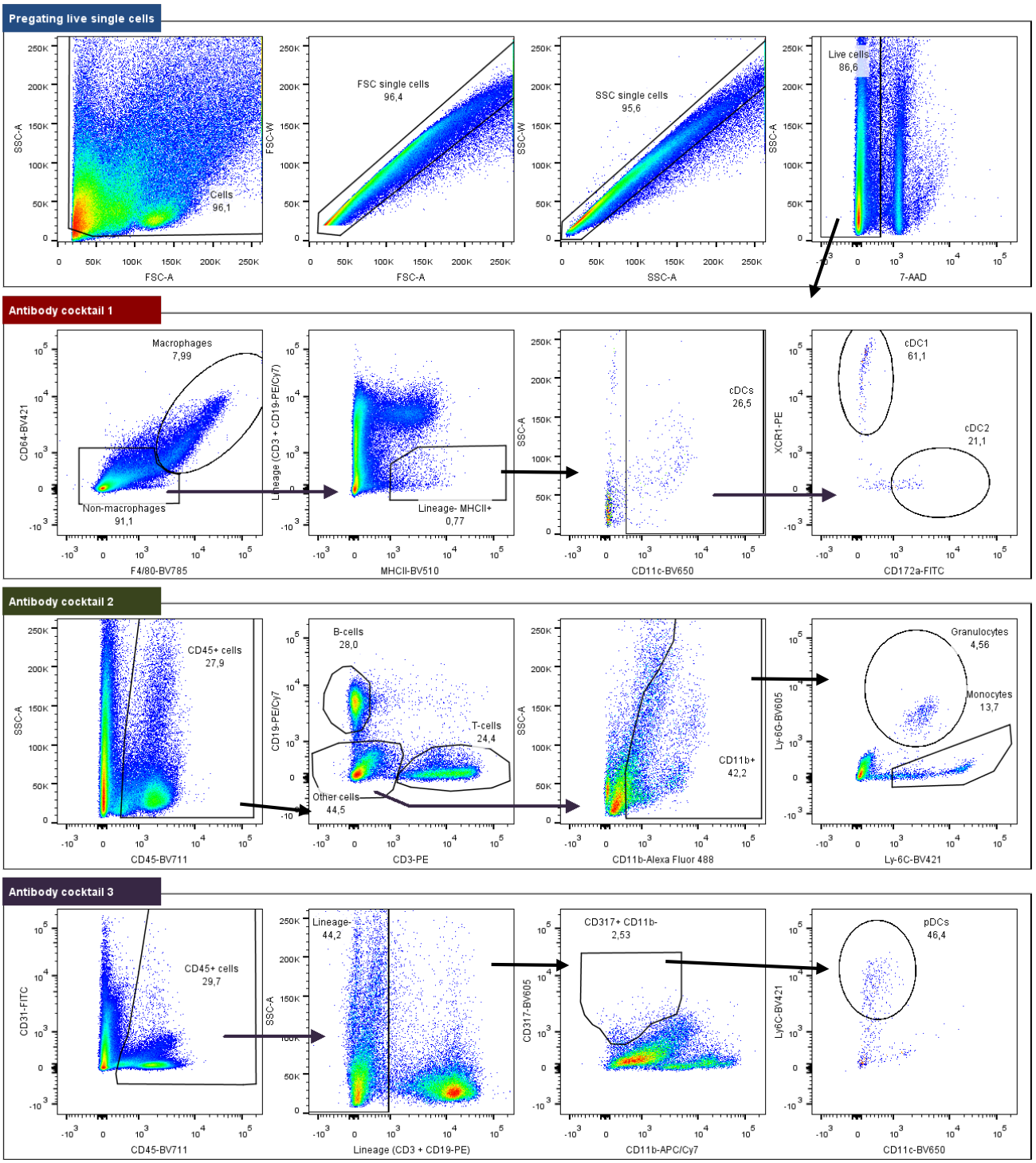

Gating strategy of spleens (Ai9; Cre reporter mice) to determine cellular tdTomato expression

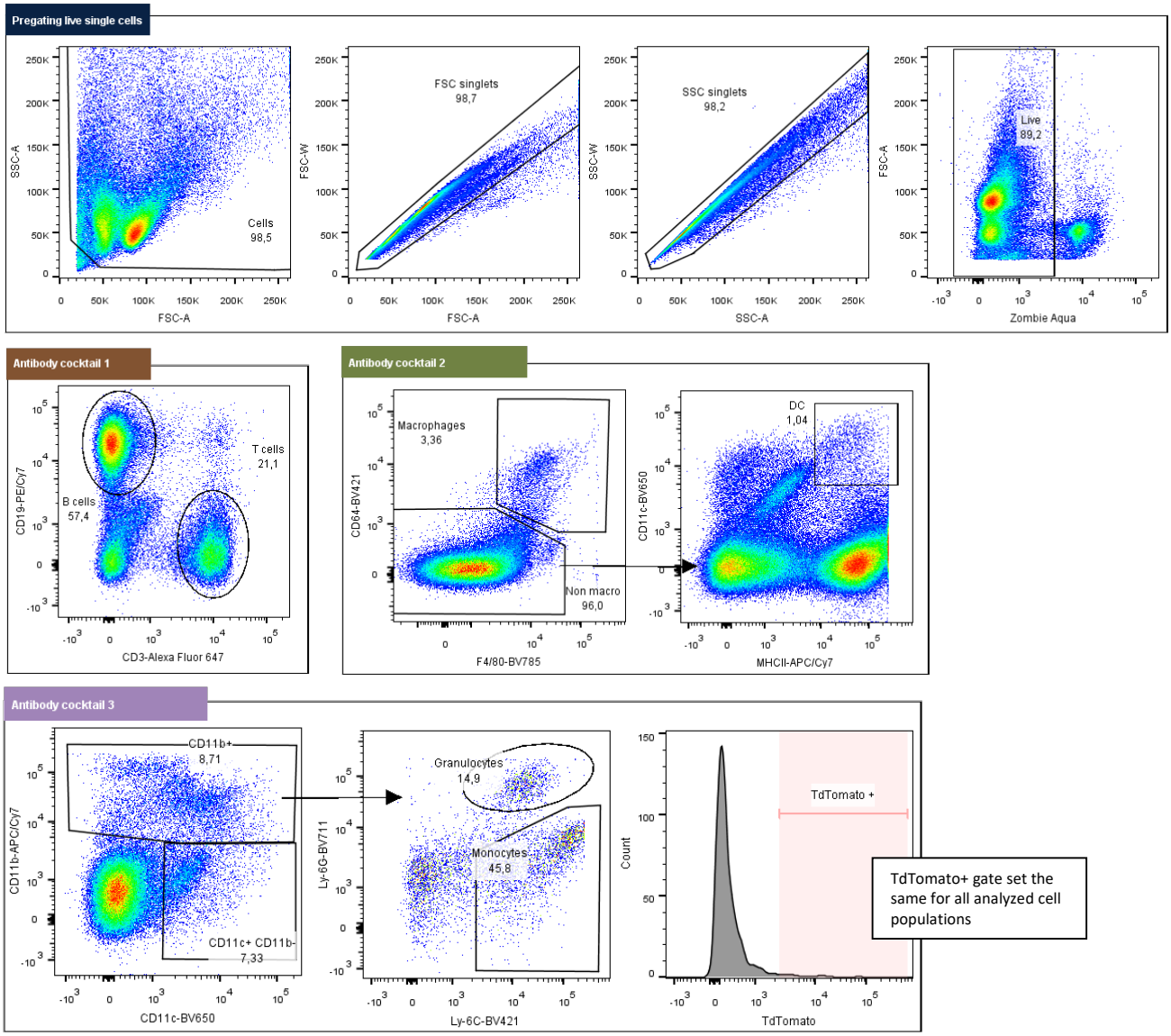

Gating strategy of CD8 T cells in mouse blood to determine E7-specificity and phenotype

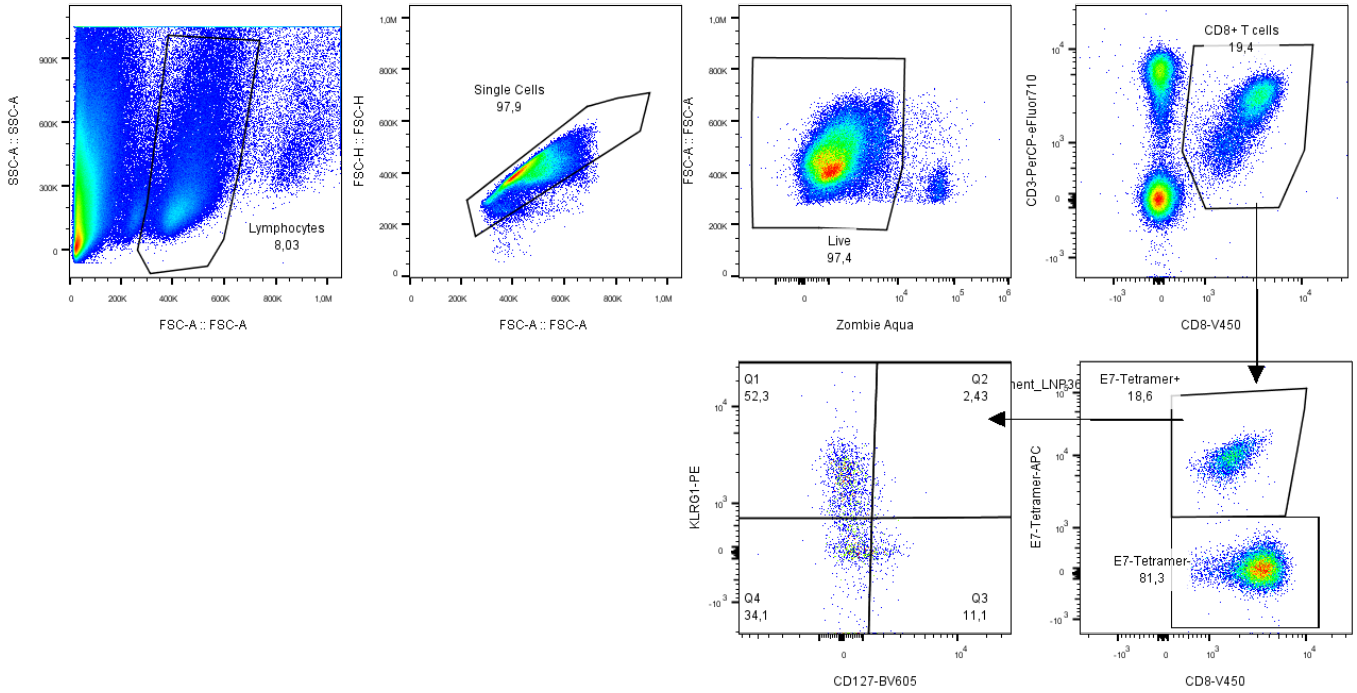

Gating strategy of spleens (wild-type mice) to determine activation status of B cells

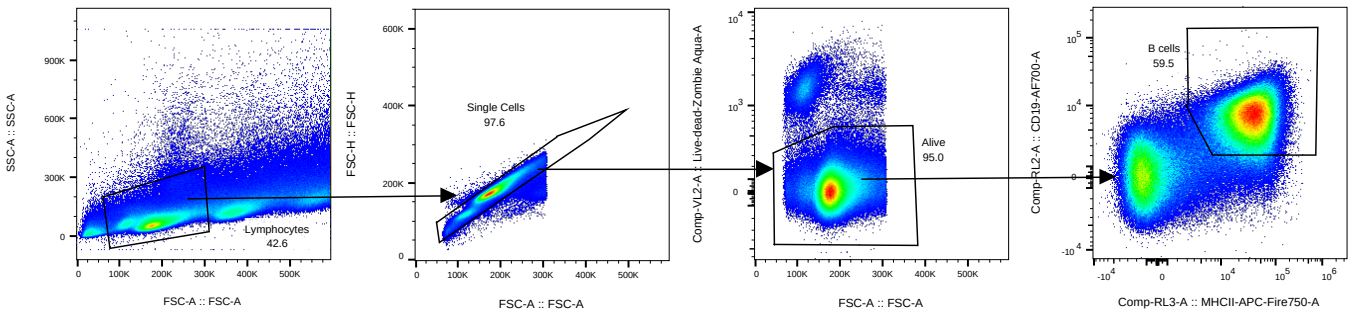

Gating strategy of spleens (wild-type mice) to determine activation status of cDC1 and cDC2

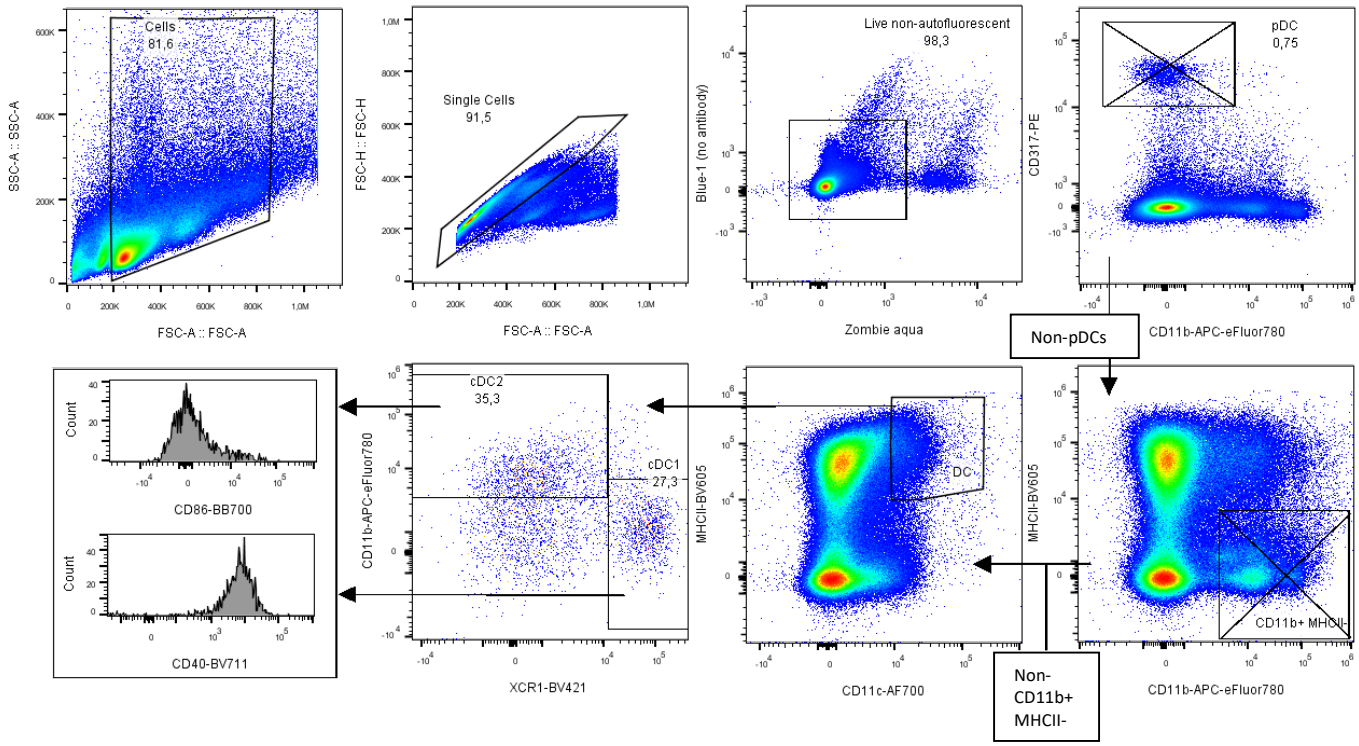

Gating strategy of spleens (wild-type mice) to determine CD8 T cell cytokine secretion

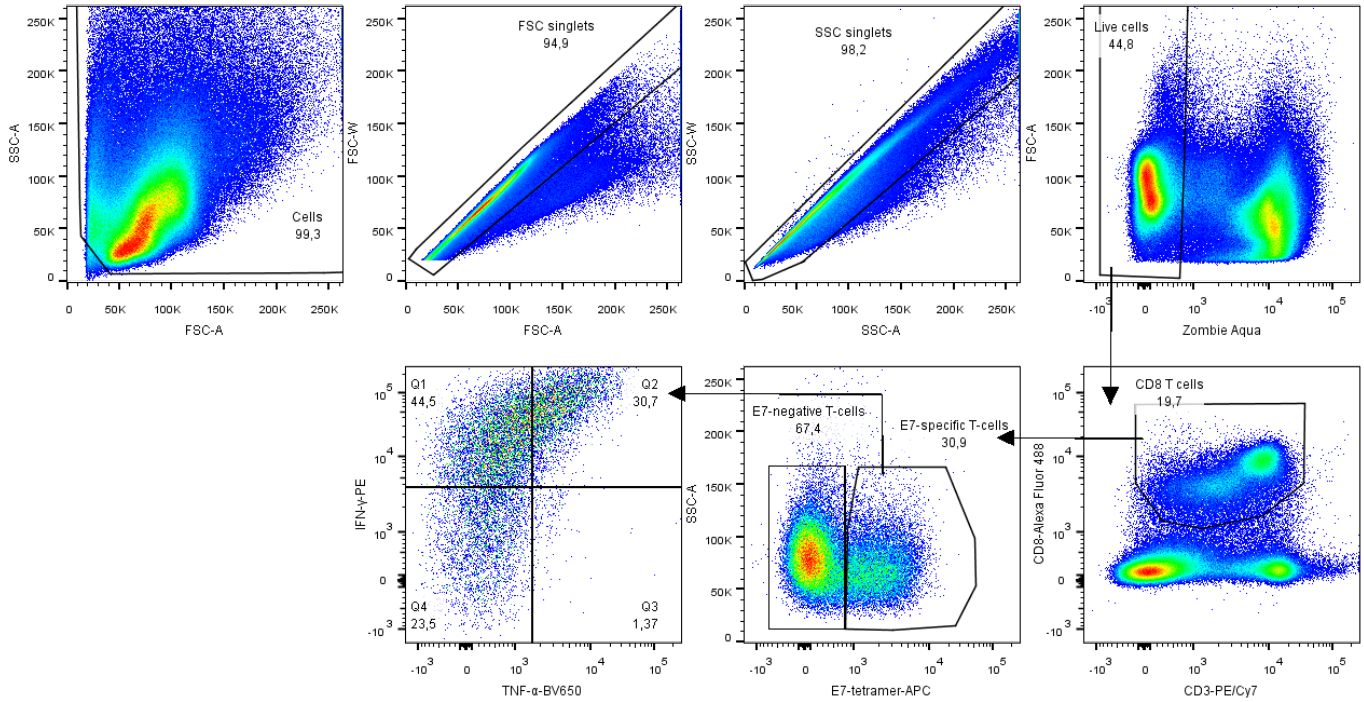

Gating strategy of TC-1 tumors to quantify infiltrating CD8 T cells (for figure 2)

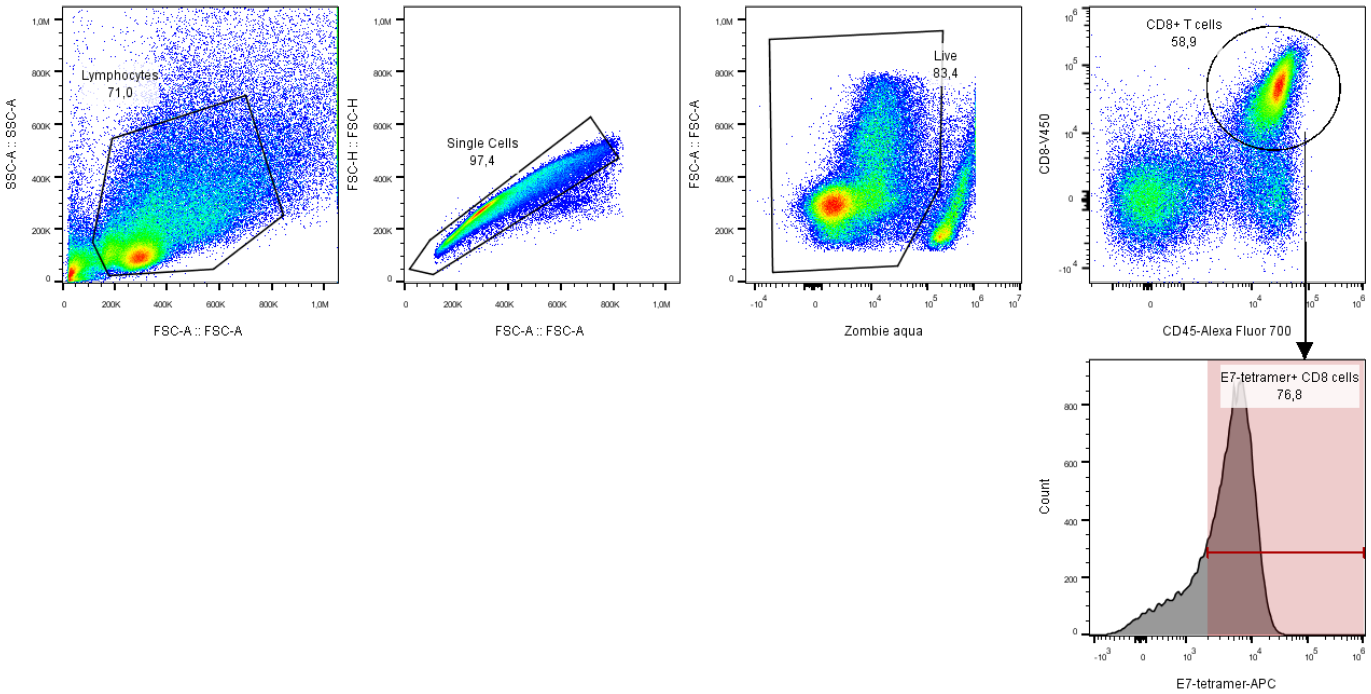

Gating strategy of TC-1 tumors to quantify and characterize infiltrating CD8 T cells (for figure S2)

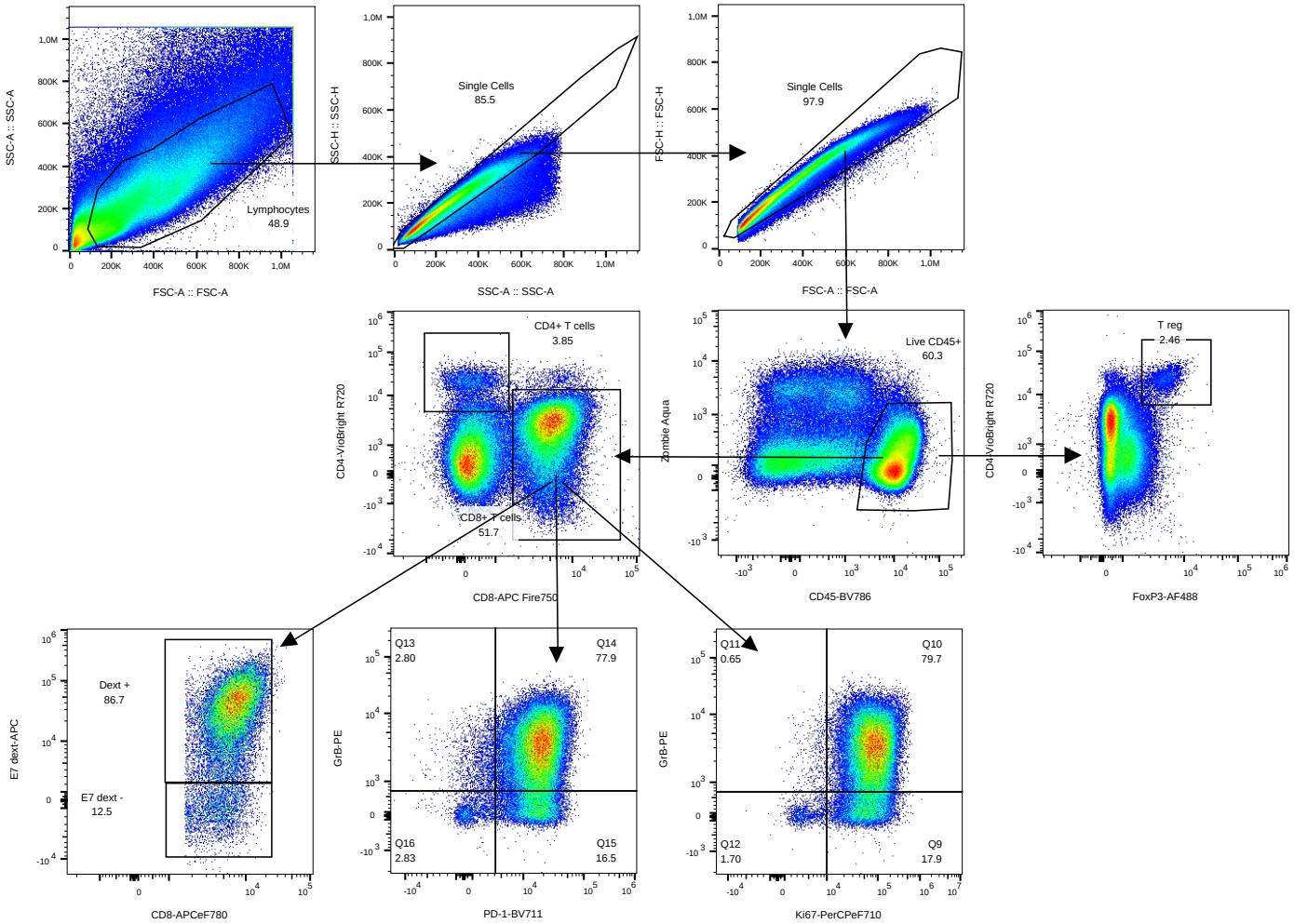

Gating strategy of TC-1 tumors to quantify infiltrating immune cells (for figure S2)

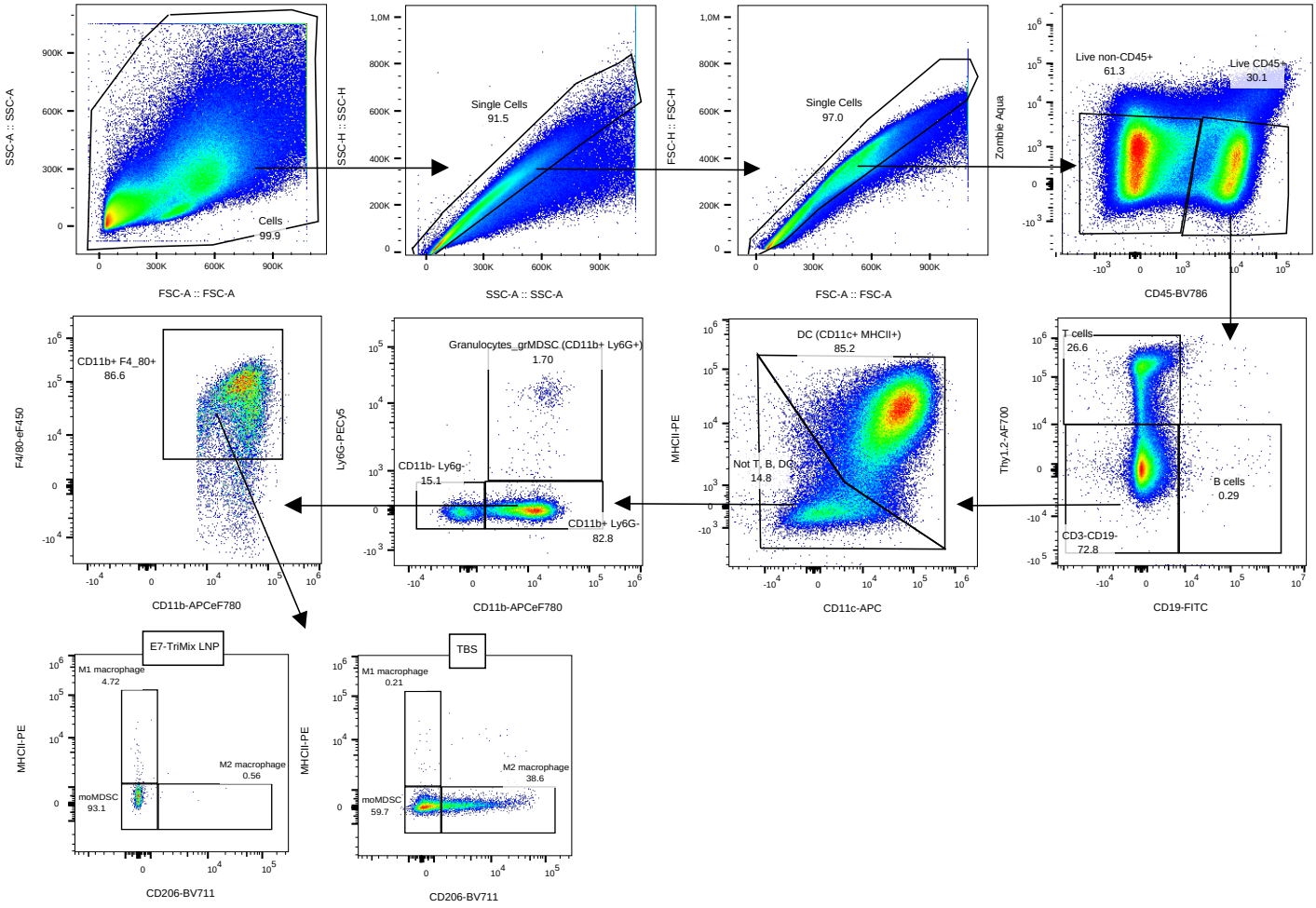

Supplementary Tables

Table S1. LNP properties

Lipid composition (molar percentages), size, polydispersity index (PDI), %mRNA encapsulation and zeta potential of all LNPs used in this work.

		Composition (molar %)						Size (nm)	PDI	%mRNA encapsulation	Zeta potential (mV)
Library	LNP number	SS-EC	DOPE	Cholesterol	DMG-PEG2000	DSG-PEG2000	DSPE-PEG1000				
DOE	1	50	15	33.75	1.25			73	0.12	97	4
	2	50	5	43.75	1.25			86	0.09	96	-2
	3	40.5	12.24	46.48	0.78			89	0.09	96	0
	4	59.5	12.24	27.48	0.78			107	0.07	94	5
	5	40.5	12.24	45.54	1.72			66	0.14	97	1
	6	59.5	12.24	26.54	1.72			83	0.12	97	3
	7	36.6	7.76	54.39	1.25			71	0.09	97	-1
	8	63.4	7.76	27.59	1.25			112	0.09	96	7
	9	50	7.76	41.66	0.58			111	0.09	95	-3
	10	50	7.76	40.32	1.92			76	0.15	96	0
	11	50	10	38.75	1.25			83	0.08	97	2
	12	50	15	33.75		1.25		80	0.13	97	4
	13	50	5	43.75		1.25		93	0.07	96	-1
	14	40.5	12.24	46.48		0.78		92	0.07	95	-1
	15	59.5	12.24	27.48		0.78		128	0.08	93	4
	16	40.5	12.24	45.54		1.72		66	0.09	97	0
	17	59.5	12.24	26.54		1.72		93	0.07	96	3
	18	36.6	7.76	54.39		1.25		78	0.10	97	-2
	19	63.4	7.76	27.59		1.25		123	0.05	76	-2
	20	50	7.76	41.66		0.58		116	0.07	94	-3
	21	50	7.76	40.32		1.92		82	0.11	96	1
	22	50	10	38.75		1.25		87	0.07	96	2
	23	50	15	33.75			1.25	95	0.08	93	0
	24	50	5	43.75			1.25	99	0.07	94	-4
	25	40.5	12.24	46.48			0.78	118	0.07	92	-8
	26	59.5	12.24	27.48			0.78	135	0.07	89	-1
	27	40.5	12.24	45.54			1.72	81	0.10	96	-7
	28	59.5	12.24	26.54			1.72	98	0.09	95	1
	29	36.6	7.76	54.39			1.25	100	0.05	91	-8
	30	63.4	7.76	27.59			1.25	133	0.02	94	-1
	31	50	7.76	41.66			0.58	163	0.06	89	-7
	32	50	7.76	40.32			1.92	88	0.13	93	-4
	33	50	10	38.75			1.25	100	0.07	94	-6
Validation	34	56.49	5.25	37.76	0.5			122	0.05	97	-8
	35	42	12	44.5	1.5			68	0.13	99	-3
	36	64.41	7.97	27.12		0.5		136	0.06	96	-4
	37	42	12	44.5		1.5		70	0.12	99	-4
	38	64.59	6.62	28.27			0.52	153	0.07	89	-7
	39	42	12	44.5			1.5	79	0.08	90	-15

Table S2. Correlations between LNP size, T cell response and splenic expression.

Significant positive or negative correlations as assesed by Pearson correlation test are marked in green or red respectively. Significant positive correlations were present between LNP size and %E7-specific T cells in blood after 3 weekly immunizations with E7 mRNA encapsulating DMG-PEG2000 or DSG-PEG2000 LNPs. In addition, LNP size significantly correlated with relative expression in the spleen (as % of total luciferase activity in all analyzed organs) 4h after single administration of Fluc mRNA LNPs. The %E7-specific T cell response (3 immunizations) moreover significantly correlated with relative (DMG-PEG2000) or absolute (DSG-PEG2000) fluc mRNA expression (1 administration) in spleen, whereas there is no correlation with total mRNA expression and a negative correlation with mRNA expression in liver.

DMG-PEG2000 LNPs

		%E7-specific T cells	Relative spleen luciferase activity
LNP size	Pearson r	0.910	0.944
	p value	1.03E-04	1.26E-05
Relative spleen luciferase activity	Pearson r	0.691	
	p value	0.019	
Absolute spleen luciferase activity	Pearson r	0.286	
	p value	0.394	
Relative liver luciferase activity	Pearson r	-0.685	
	p value	0.020	
Absolute liver luciferase activity	Pearson r	-0.520	
	p value	0.101	
Total luciferase activity	Pearson r	-0.457	
	p value	0.158	

DSG-PEG2000 LNPs

		%E7-specific T cells	Relative spleen luciferase activity
LNP size	Pearson r	0.805	0.667
	p value	0.003	0.025
Relative spleen luciferase activity	Pearson r	0.262	
	p value	0.436	
Absolute spleen luciferase activity	Pearson r	0.888	
	p value	3.00E-04	
Relative liver luciferase activity	Pearson r	-0.201	
	p value	0.553	
Absolute liver luciferase activity	Pearson r	0.166	
	p value	0.627	
Total luciferase activity	Pearson r	0.289	
	p value	0.389	

Table S3. Flow cytometry antibodies used in this work
List of all antibodies, including clone number, catalog number and manufacturer, used for flow cytometry analyses.

Name	Fluorophore	Manufacturer	Clone
Live/Dead	Zombie Aqua	BioLegend	-
Live/Dead	Zombie NIR	BioLegend	-
Live/Dead	7-AAD		-
CD16/32 (Fc block)	-	BD	2.4G2
CD16/32 (Fc block)	-	Biolegend	93
E7-Tetramer	APC	MBL International	-
CD11c	AF700	BD Biosciences	HL3
CD11c	BV650	BD Biosciences	HL3
CD11c	BV650	BioLegend	N418
CD11c	APC	BioLegend	N418
CD127	BV605	BioLegend	A7R34
CD11b	APC-eF780	Invitrogen	M1/70
CD11b	AF488	eBioscience	M1/70
CD11b	APC-Cy7	BioLegend	M1/70
CD172a	FITC	BioLegend	P84
CD19	FITC	BD Biosciences	1D3
CD19	AF700	BD Biosciences	1D3
CD19	FITC	BioLegend	6D5
CD19	PE-Cy7	BioLegend	6D5
CD19	PE	BioLegend	6D5
CD31	FITC	BD Pharmingen	MEC 13.3
CD317	PE	BioLegend	129C1
CD317	BV605	BioLegend	927
CD3	PerCPeF710	Invitrogen	17A2
CD3ε	FITC	BD Biosciences	145-2C11
CD3ε	PE-Cy7	BioLegend	145-2C11
CD3ε	PE	BioLegend	145-2C11
CD3ε	AF647	BioLegend	145-2C11
CD4	Viobright R720	Miltenyi Biotec	REA604
CD40	BV711	BD Biosciences	3/23
CD45	AF700	Invitrogen	30-F11
CD45	BV711	BioLegend	30-F11
CD45	BV786	BD Biosciences	30-F11
CD64	BV421	BioLegend	X54-5/7.1
CD69	BV650	BD Biosciences	H1.2F3
CD8	APC-Fire750	BioLegend	53-6.7
CD8	V450	BD Biosciences	53-6.7
CD86	BB700	BD Biosciences	GL1
CD206	BV711	BioLegend	C068C2
F4/80	eF450	Invitrogen	BM8
F4/80	BV785	BioLegend	BM8
FoxP3	AF488	Invitrogen	150D/E4
Granzyme B	PE	Invitrogen	GB12
IFN-γ	PE	BioLegend	4S.B3
Ki67	PerCP-eF710	Invitrogen	SolA15
KLRG1	PE	BioLegend	2F1/KLRG1
Ly6c	BV650	BioLegend	HK1.4
Ly6c	eF450	Invitrogen	HK1.4
Ly6C	BV421	BioLegend	HK1.4
Ly6G	BV605	BioLegend	1A8
Ly6G	BV785	BioLegend	1A8
Ly6G	PE-Cy5	BioLegend	1A8
MHCII	BV510	BioLegend	M5/114.15.2
MHCII	APC-Fire750	BioLegend	M5/114.15.2
MHCII	BV605	BD Biosciences	M5/114.15.2
MHCII	APC-Cy7	BioLegend	M5.144.15.2
MHCII	PE	Invitrogen	M5/114.15.2
PD-1	BV711	BioLegend	29F.1A12
Thy1.2	AF700	BioLegend	53-2.1
TNF-α	BV650	BioLegend	MP6-XT22
XCR1	BV421	BioLegend	ZET
XCR1	PE	BioLegend	ZET

Supplementary Figures

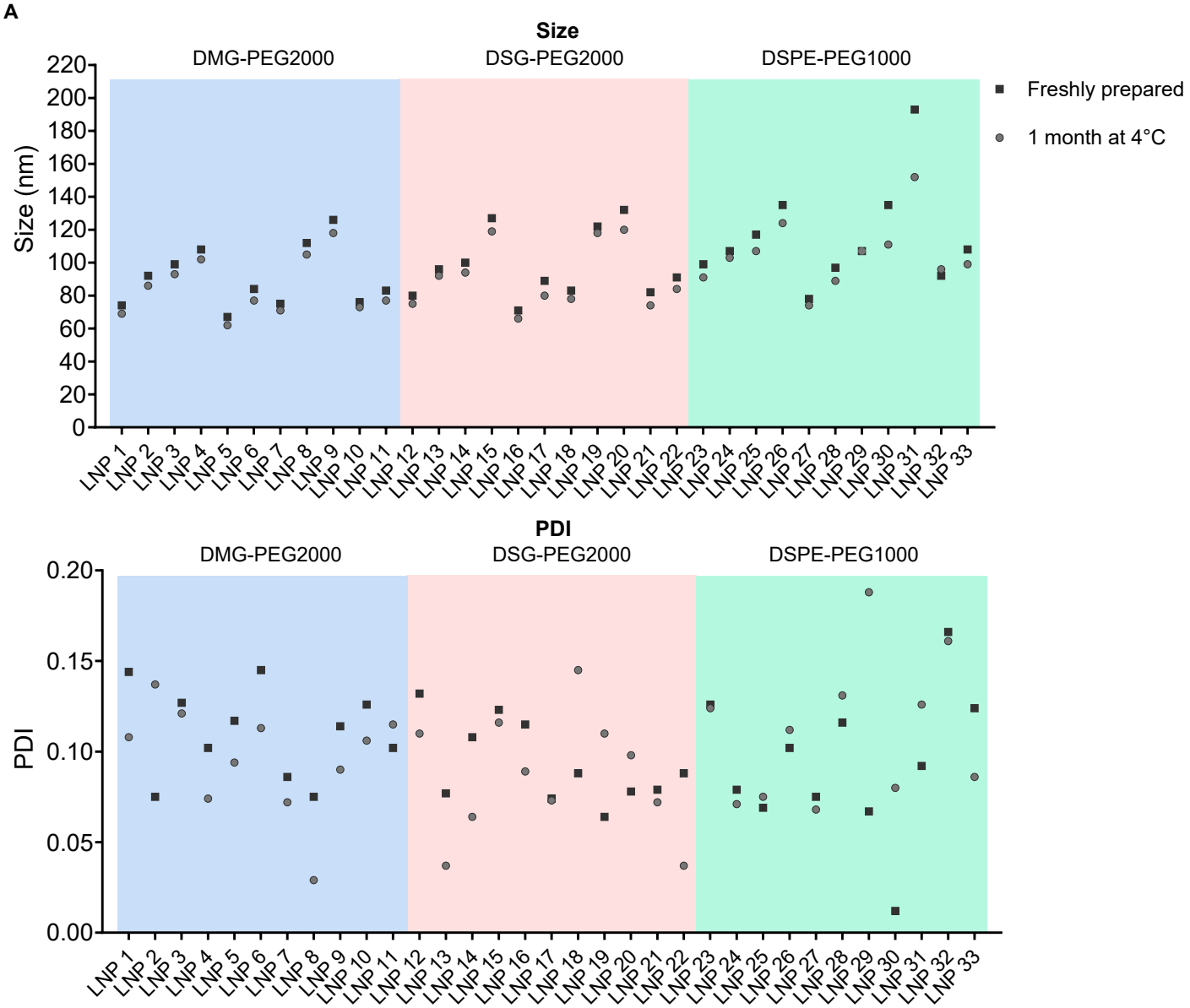

Figure S1. Size and polydispersity index of LNPs remains stable during storage at 4°C.
A) Size and PDI of E7 LNPs used in DOE experiment. B) Size and PDI of E7 LNPs used for validation of the model.
For all LNPs tested, size of LNPs after storage at 4°C (grey circles) does not deviate more than 10% of the size of freshly prepared LNPs (black squares) except for LNP30 and LNP31 which decreased in size by 18% and 21% respectively. PDI remained low (<0.2) during storage at 4°C for all LNPs tested.
Blue background: DMG-PEG2000 LNPs, pink background: DSG-PEG2000 LNPs, green background: DSPE-PEG1000 LNPs

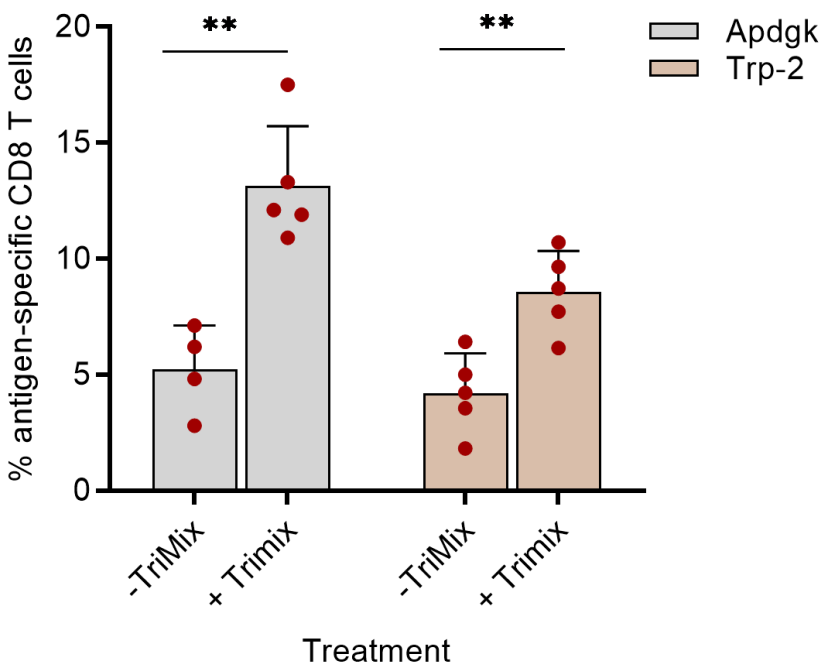

Figure S2. Strong T cell responses are achieved after two immunizations with LNP36 encapsulating mRNA encoding Apdgk or Trp-2 in combination with TriMix.
Mice were injected intravenously two times with weekly interval with 10 µg of mRNA encapsulated in LNP36. mRNA comprised either antigen-encoding mRNA (- Trimix) or a 1:1 mixture of antigen-encoding and TriMix (+ TriMix). Percentages of antigen-specific CD8 T cells in blood were assessed 5 days after the second administration. Data is presented as mean ± SD with individual data points in red, n=4-5. Statistical differences were assessed using two-way Student's t test. **: $p<0.01$.

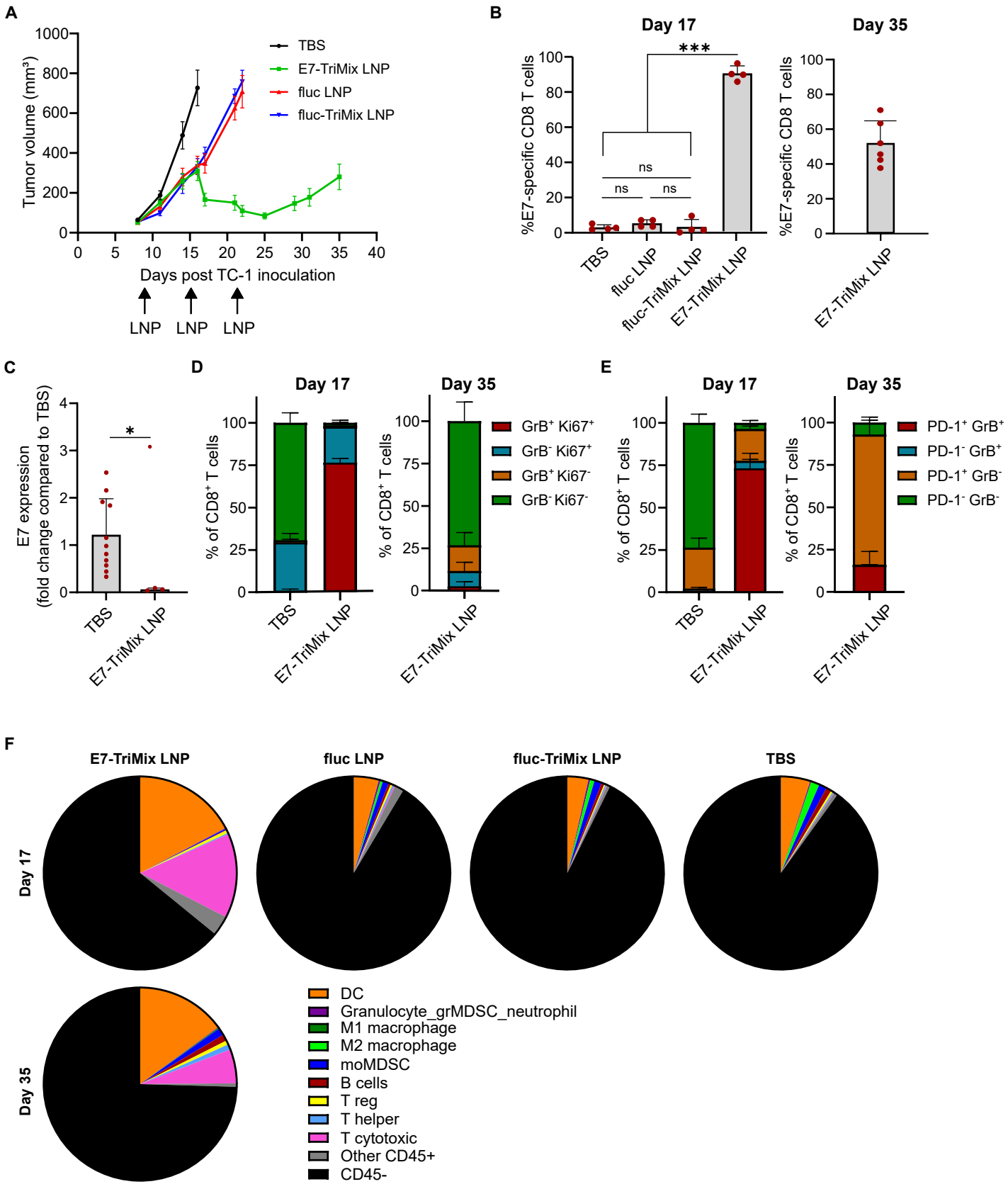
A
Tumor volume (mm³)
Days post TC-1 inoculation
LNP LNP LNP
TBS
E7-TriMix LNP
fluc LNP
fluc-TriMix LNP
B
Day 17
Day 35
%E7-specific CD8 T cells
***
ns
ns
ns
TBS
fluc LNP
fluc-TriMix LNP
E7-TriMix LNP
C
E7 expression
(fold change compared to TBS)
*
D
Day 17
Day 35
% of CD8⁺ T cells
GrB⁺ Ki67⁺
GrB⁻ Ki67⁺
GrB⁺ Ki67⁻
GrB⁻ Ki67⁻
E
PD-1⁺ GrB⁺
PD-1⁻ GrB⁺
PD-1⁺ GrB⁻
PD-1⁻ GrB⁻
F
E7-TriMix LNP
fluc LNP
fluc-TriMix LNP
TBS
Day 17
Day 35
DC
Granulocyte_grMDSC_neutrophil
M1 macrophage
M2 macrophage
moMDSC
B cells
T reg
T helper
T cytotoxic
Other CD45+
CD45-

Figure S3. TC-1 tumors relapse due to decreased TIL infiltration, T cell exhaustion and reduced E7 antigen expression

Mice were injected 3 times i.v. with 5µg fluc, 5µg E7-TriMix (1:1 ratio) or 5µg fluc-TriMix (1:1 ratio) encapsulated in LNP36 or with TBS at a weekly interval. First injection was given at a mean tumor volume of 55mm³. Tumors were harvested at day 17 (all groups) and day 35 (only E7-TriMix LNP group remaining alive) after TC-1 inoculation. **A**: TC-1 tumor growth curves shown as mean ± SEM (n=12). Despite some initial reduced growth rate induced by aspecific immune activation by fluc LNP or fluc-TriMix LNP administration, only E7-TriMix LNP induced tumor regression. **B**: %E7-specific CD8 T cells of the total tumor infiltrating CD8 T cells shown as mean ± SD with individual data points (n=4-6) shown in red. Only after E7-TriMix LNP vaccination a significant infiltration of E7-specific CD8 T cells was noted, which reduced from day 17 to day 35. Statistical differences were assessed using One-Way ANOVA with Tukey's multiple comparison test. **C**: E7 expression in tumors was assessed by RT-qPCR when they reached maximal size (around 1000mm³) for TBS, fluc LNP and fluc-TriMix groups or at day 35 for E7-TriMix LNP. E7 expression was substantially reduced in day 35 tumors of E7-TriMix treated mice. Mean± SD is shown. Statistical differences were assessed using two-tailed t test. **D, E**: Phenotyping of CD8 T cells in the tumor at day 17 (n=4) and day 35 (n=6). CD8 T cells in tumors of E7-TriMix treated mice are mostly Granzyme B^+ $Ki67^+$ (D) and Granzyme B^+ $PD\text{-}1^+$ (E) at day 17, but have lost proliferative and cytolytic capacity at day 35 (tumor relapse). Mean ± SD is shown. **F**: Characterization of the immune cell infiltrate in the tumor at day 17 (average of 4 tumors per group) and day 35 (average of 6 tumors). At day 17, the percentage of CD8 T cells and DC is significantly increased compared to other groups (no significant differences are present between TBS, fluc LNP and fluc-TriMix LNP treatments). At day 35, percentage of CD8 T cells in the tumor is significantly reduced compared to day 17. Statistical differences were assessed using Two-Way ANOVA with Sidak's multiple comparison test. *: $p<0.05$, ***: $p<0.001$, ns: not significant.

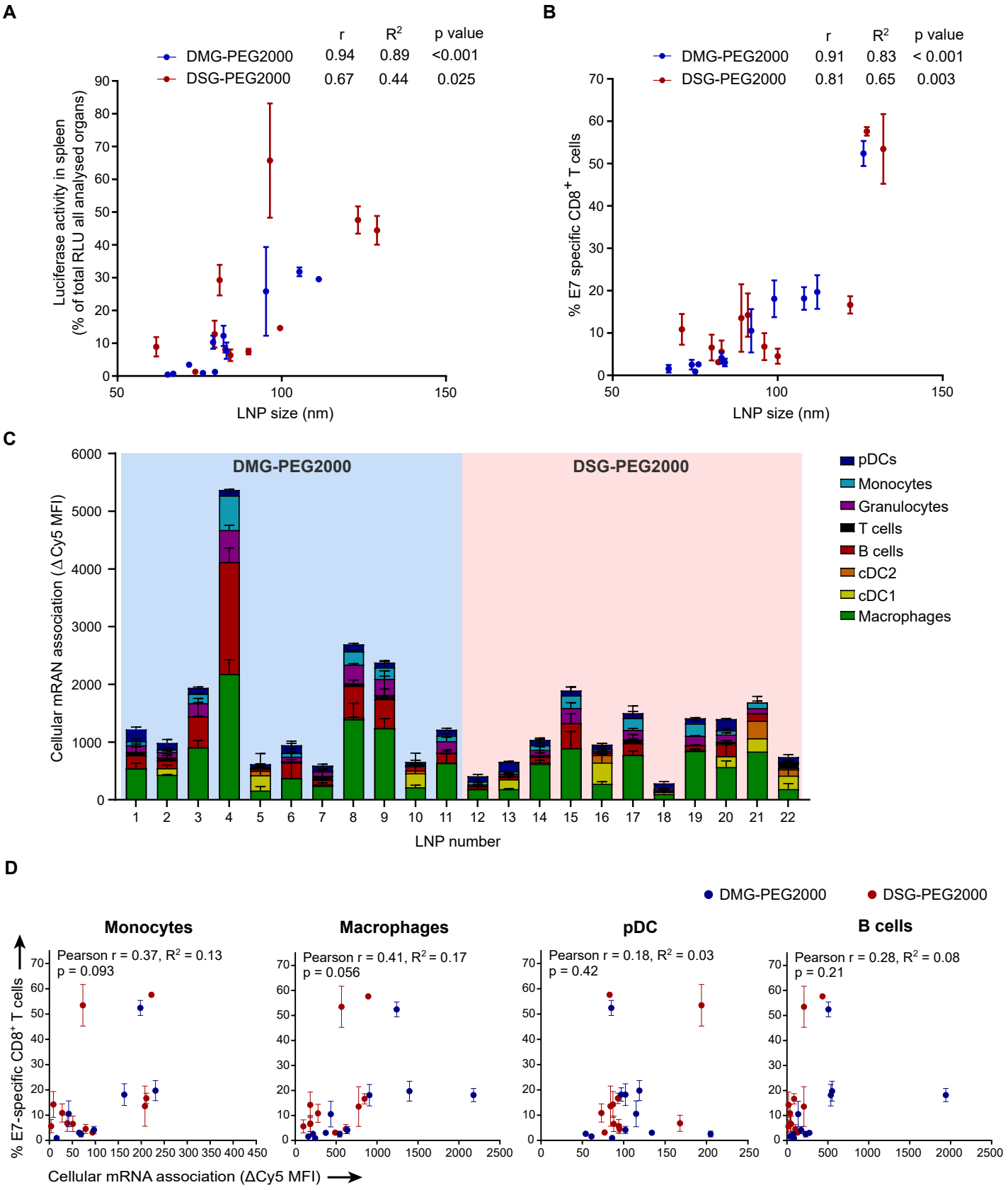
A
r
R²
p value
DMG-PEG2000
0.94
0.89
<0.001
DSG-PEG2000
0.67
0.44
0.025
Luciferase activity in spleen
(% of total RLU all analysed organs)
LNP size (nm)
B
r
R²
p value
DMG-PEG2000
0.91
0.83
< 0.001
DSG-PEG2000
0.81
0.65
0.003
% E7 specific CD8+ T cells
LNP size (nm)
C
DMG-PEG2000
DSG-PEG2000
Cellular mRAN association (ΔCy5 MFI)
LNP number
pDCs
Monocytes
Granulocytes
T cells
B cells
cDC2
cDC1
Macrophages
D
DMG-PEG2000
DSG-PEG2000
Monocytes
Pearson r = 0.37, R² = 0.13
p = 0.093
Macrophages
Pearson r = 0.41, R² = 0.17
p = 0.056
pDC
Pearson r = 0.18, R² = 0.03
p = 0.42
B cells
Pearson r = 0.28, R² = 0.08
p = 0.21
% E7-specific CD8+ T cells
Cellular mRNA association (ΔCy5 MFI)

Figure S4. LNP size and spleen-specific transfection capacity correlate with T cell responses.
A: LNP from the DOE library loaded with Cy5-labeled Fluc mRNA were injected i.v. in mice (n=2-4). After four hours, kidneys, lungs, heart, liver and spleen were isolated, homogenized and assayed for luciferase activity. Luciferase activity in spleen, expressed as percentage of luciferase activity/mg in all assayed organs (Fig. 3C), positively correlated with the size of the injected LNPs based on Pearson correlation coefficients. **B**: E7 mRNA-LNPs were administered intravenously (n=3) three times with a weekly interval. Percentages of E7-specific CD8 T cells in blood after three immunizations (Fig. 1C), as determined by flow cytometry, positively correlated with the size of the injected LNPs, based on Pearson correlation coefficients. **C,D**: Cy5-labeled Fluc mRNA in LNPs was injected i.v. in mice (n=2-4). After four hours, liver non-parenchymal cells were analyzed by flow cytometry to assess Cy5 association with multiple cell types (C). Cellular Cy5 association is expressed as difference between Cy5 mean fluorescence intensity of LNP injected mice and vehicle injected mice (ΔCy5 MFI). In contrast to splenic cell types (Fig. 3E), ΔCy5 MFI of hepatic monocytes, macrophages, pDC and B cells did not correlate with the T cell response after 3 immunizations (D). A,B,C,D: Mean ± SD is shown. RLU=relative light unit. Blue background: DMG-PEG2000-based LNPs, Pink background; DSG-PEG2000-based LNPs.

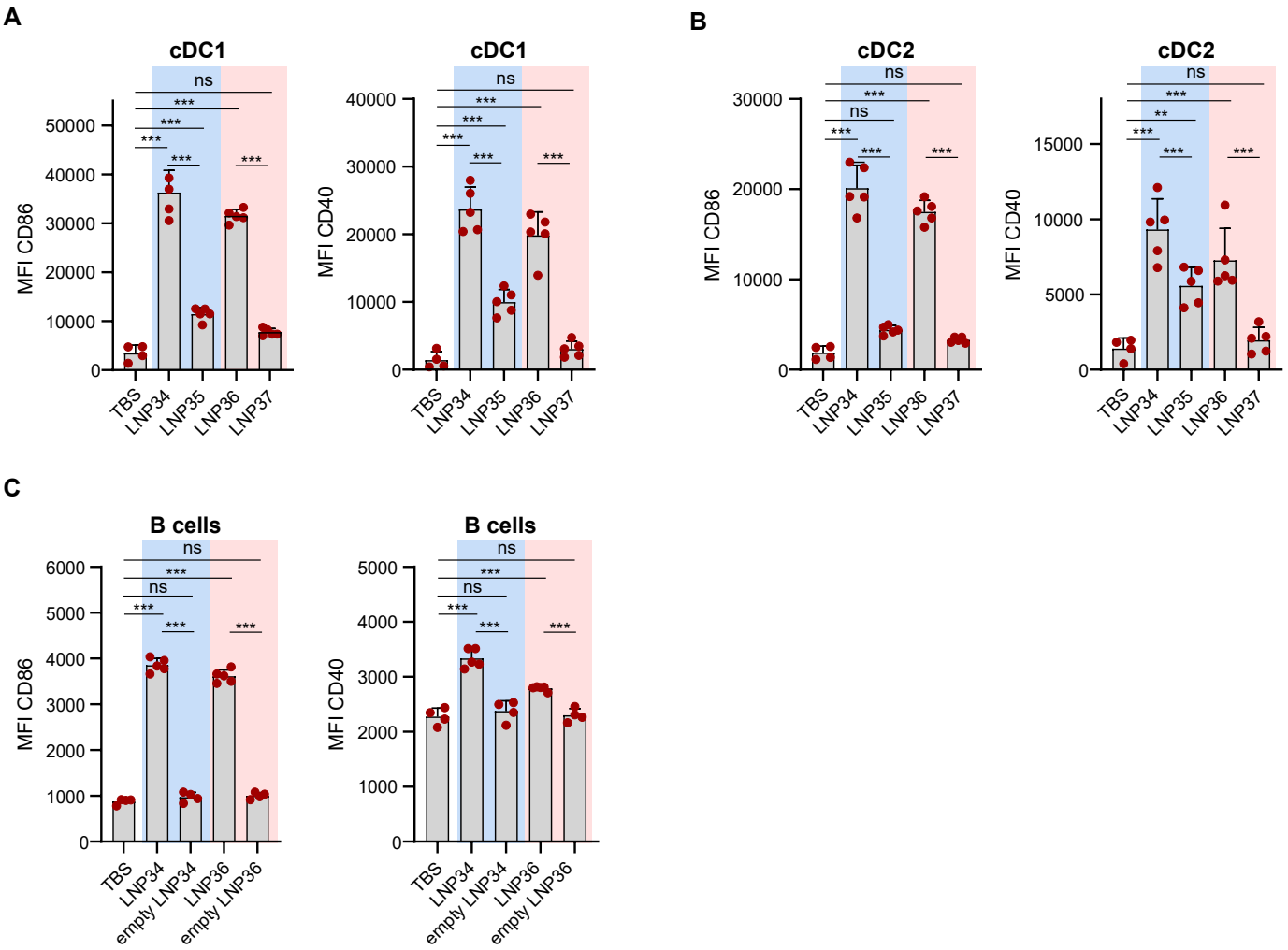

Figure S5. LNP administration induces activation of B cells and DCs.
A,B: E7-TriMix mRNA-LNPs or vehicle controls (TBS) were administered intravenously (n=4-5) and spleens were isolated 4h later for flow cytometry analysis. Geometric Mean Fluorescence Intensity (MFI) of CD86 and splenic cDC1 (A) and cDC2 (B) is strongly upregulated by optimal LNPs (LNP34 and LNP36) and to a lesser extent by non-optimal LNPs (LNP35 and LNP37). **C**: E7-TriMix LNPs or empty LNPs (no mRNA encapsulated) were administered intravenously (n=4-5) and spleens were isolated 4h later for flow cytometry analysis. Geometric Mean Fluorescence Intensity (MFI) of CD86 and CD40 on B cells is significantly upregulated by optimal mRNA-LNPs, but not by optimal empty LNPs. A,B,C: Mean ± SD is shown, with individual data points in red. Statistics were assessed by One-Way ANOVA with Tukey's multiple comparison test. ***: $p<0.001$; ns=not significant. Blue background: DMG-based LNPs, Pink background; DSG-PEG2000-based LNPs.

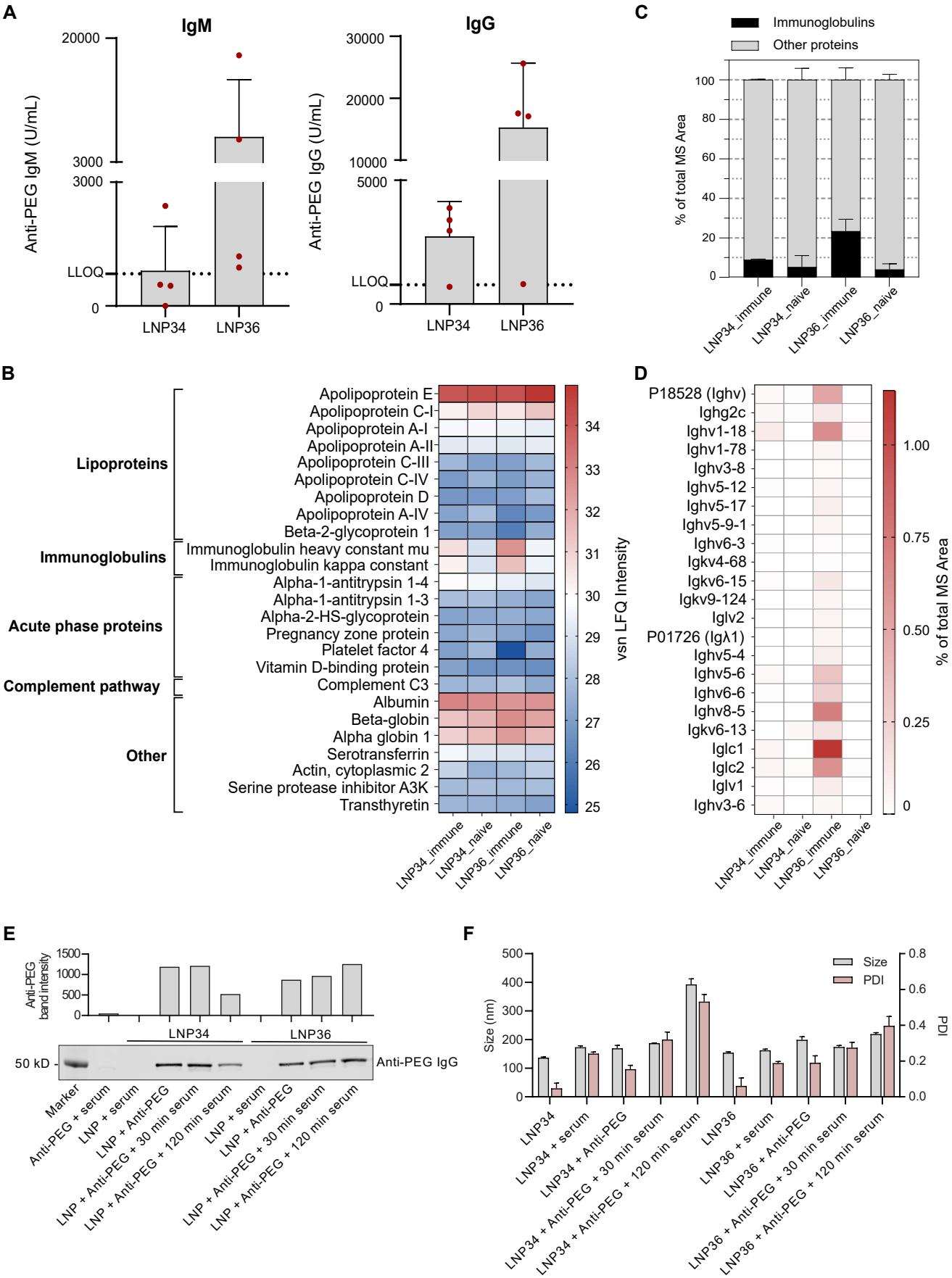
A
IgM
IgG
Anti-PEG IgM (U/mL)
Anti-PEG IgG (U/mL)
20000
3000
LLOQ
0
30000
10000
5000
LNP34
LNP36
B
Lipoproteins
Immunoglobulins
Acute phase proteins
Complement pathway
Other
Apolipoprotein E
Apolipoprotein C-I
Apolipoprotein A-I
Apolipoprotein A-II
Apolipoprotein C-III
Apolipoprotein C-IV
Apolipoprotein D
Apolipoprotein A-IV
Beta-2-glycoprotein 1
Immunoglobulin heavy constant mu
Immunoglobulin kappa constant
Alpha-1-antitrypsin 1-4
Alpha-1-antitrypsin 1-3
Alpha-2-HS-glycoprotein
Pregnancy zone protein
Platelet factor 4
Vitamin D-binding protein
Complement C3
Albumin
Beta-globin
Alpha globin 1
Serotransferrin
Actin, cytoplasmic 2
Serine protease inhibitor A3K
Transthyretin
vsn LFQ Intensity
34
33
32
31
30
29
28
27
26
25
LNP34_immune
LNP34_naive
LNP36_immune
LNP36_naive
C
Immunoglobulins
Other proteins
% of total MS Area
100
80
60
40
20
0
D
P18528 (Ighv)
Ighg2c
Ighv1-18
Ighv1-78
Ighv3-8
Ighv5-12
Ighv5-17
Ighv5-9-1
Ighv6-3
Igkv4-68
Igkv6-15
Igkv9-124
Iglv2
P01726 (Igλ1)
Ighv5-4
Ighv5-6
Ighv6-6
Ighv8-5
Igkv6-13
Iglc1
Iglc2
Iglv1
Ighv3-6
1.00
0.75
0.50
0.25
0
% of total MS Area
E
Anti-PEG band intensity
1500
1000
500
0
LNP34
LNP36
50 kD
Anti-PEG IgG
Marker
Anti-PEG + serum
LNP + serum
LNP + Anti-PEG
LNP + Anti-PEG + 30 min serum
LNP + Anti-PEG + 120 min serum
F
Size
PDI
Size (nm)
500
400
300
200
100
0
0.8
0.6
0.4
0.2
0.0
LNP34
LNP34 + serum
LNP34 + Anti-PEG
LNP34 + Anti-PEG + 30 min serum
LNP34 + Anti-PEG + 120 min serum
LNP36
LNP36 + serum
LNP36 + Anti-PEG
LNP36 + Anti-PEG + 30 min serum
LNP36 + Anti-PEG + 120 min serum

Figure S6. LNPs induce anti-PEG antibodies and show differential interactions with mouse plasma proteins. **A**: Mice were immunized three times with E7 mRNA, encapsulated in LNP34 or LNP36, on days 0, 7 and 14 to induce T cell responses. On day 54 (40 days after the last immunization), serum was collected anti-PEG IgM andIgG titers were analyzed by ELISA. When in a separate experiment mice were boosted with mRNA-LNPs at day 55, high percentages of E7-specific T cells were observed (Fig. 2A). It is therefore unlikely that anti-PEG antibodies interfere with the boostability of the mRNA-LNP vaccines. Mean ± SD is shown, with individual data points in red. LLOQ = lower limit of quantification. **B,C,D**: Mice were immunized twice with a weekly interval with E7-TriMix mRNA encapsulated in LNP34 or LNP36. Blood plasma was collected 6 days after the last immunization. Additionally, plasma from naive (non-immunized) mice was collected. LNPs were incubated with plasma of naive mice or mice immunized with the same LNPs, followed by centrifugation of the complexes, precipitation of proteins, digestion to peptides and analysis by mass spectrometry. Details on method/analysis are included in Supplementary methods. **B**:Identified proteins were sorted by the average LFQ (label-free quantification) intensity values over all samples (LNP34 and LNP36 incubated with immune or naive plasma). Figure shows the 25 proteins with the highest average intensities, grouped by functionality. These proteins consist mainly of common serum proteins (e.g. albumin), lipoproteins, immunoglobulins, acute phase proteins and complement. Mean of replicates (n=3) is used to construct heatmap. **C**: The percentage of the total MS area (sum of LFQ intensity values of all identified proteins) classified as immunoglobulins is clearly increased in samples obtained from incubation of LNP36 with immune plasma compared to naive plasma. Mean ± SD is shown. **D**: The percentage of the total MS area of the differentially enriched (DE) immunoglobulins in LNP34 (only Ighv3-6) and LNP36 samples. DE proteins H1-2 and Gm8797, which are reduced in intensity in LNP36 immune plasma compared to naive plasma (Fig. 5F), are excluded from the heatmap. Several immunoglobulins are clearly more abundant in samples obtained from incubation of LNP36 with the respective immune plasma than from LNP34 incubation. Median of replicates (n=3) is used for heatmap. **E**: Western blot and band intensity quantification of LNPs incubated with anti-PEG antibodies and/or mouse serum and subjected to size-exclusion chromatography to remove free antibodies. In control lane 'anti-PEG + serum', typical LNP-containing fractions of a serum/antibody sample without LNPs was loaded to show the capacity of the column to separate LNPs from free anti-PEG. Anti-PEG opsonization of LNP34, but not of LNP36, is reduced after 2h incubation with serum. **F:** Size and polydispersity index (PDI) of LNPs after incubation in serum and/or anti-PEG antibodies. Size of LNP34, but not of LNP36, is increased after 2h incubation with serum and antibodies. Mean ± SD of 3 replicate measurements is shown.

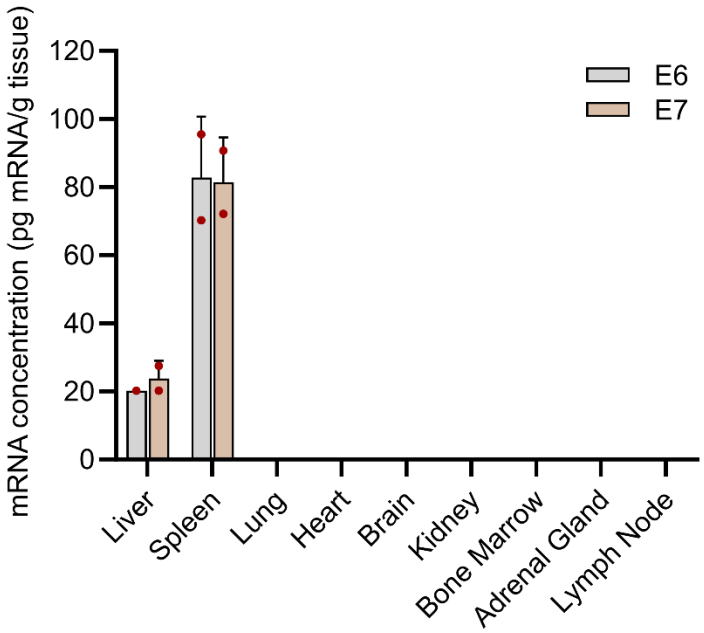

Figure S7. mRNA-LNPs distribute mainly to spleen in non-human primates at lower doses.
After 2 intravenous immunizations with 40µg of mRNA (formulated as a mixture of LNP36 containing either E6 or E7 mRNA and TriMix), mRNA strongly accumulated in spleen of non-human primates, similar to when a 100µg dose was administered (Fig. 5G). Mean ± SD is shown, with individual data points in red (n=2).

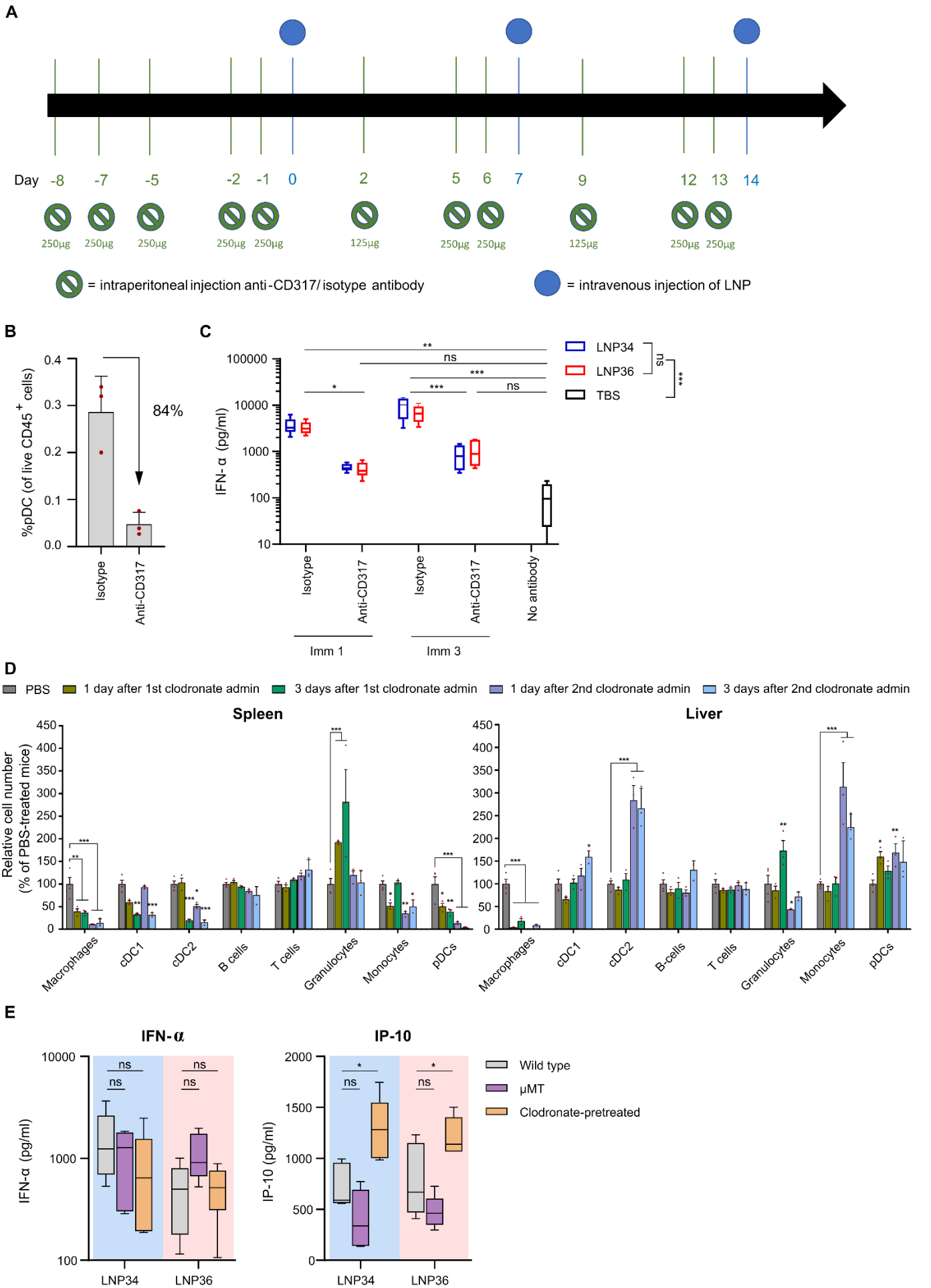
A
Day -8 -7 -5 -2 -1 0 2 5 6 7 9 12 13 14
250µg 250µg 250µg 250µg 250µg 125µg 250µg 250µg 125µg 250µg 250µg
= intraperitoneal injection anti-CD317/ isotype antibody
= intravenous injection of LNP
B
%pDC (of live CD45+ cells)
84%
Isotype
Anti-CD317
C
IFN-α (pg/ml)
LNP34
LNP36
TBS
ns
***
Isotype
Anti-CD317
Isotype
Anti-CD317
No antibody
Imm 1
Imm 3
D
PBS
1 day after 1st clodronate admin
3 days after 1st clodronate admin
1 day after 2nd clodronate admin
3 days after 2nd clodronate admin
Spleen
Liver
Relative cell number (% of PBS-treated mice)
Macrophages
cDC1
cDC2
B cells
T cells
Granulocytes
Monocytes
pDCs
B-cells
E
IFN-α
IP-10
IFN-α (pg/ml)
IP-10 (pg/ml)
LNP34
LNP36
Wild type
µMT
Clodronate-pretreated

Figure S8. Validation of pDC and phagocyte depletion models.
A: Treatment regimen used for depleting pDCs, by intraperitoneal injection of anti-CD317 or isotype control antibody. **B**: Six control mice were included in the experiment to confirm successful pDC depletion. At typical days of LNP immunization (day 0, 7 and 14), spleens of the control mice injected with isotype or anti-CD317 (scheme in A) were isolated and the percentage of pDCs was analyzed using flow cytometry. pDC percentage within the live CD45+ cell population was on average (at all three timepoints) 84% lower in anti-CD317-treated mice compared to isotype-treated mice. **C**: IFN-α levels after immunization with E7-TriMix-loaded LNPs were significantly reduced in pDC depleted mice compared to isotype control antibody injected mice, but remained elevated (not significant) compared to TBS buffer injected mice, indicating there are also other cell types than pDC producing IFN-α. Statistical differences were assessed by Two-Way ANOVA with Tukey's multiple comparison test **D**: Depletion of phagocytes in spleen and liver after intravenous injection of clodronate liposomes was assessed by flow cytometry 1 and 3 days after first and second administration (1 week interval) of clodronate liposomes. Macrophages were significantly depleted in both organs at all assessed timepoints, but also reduced numbers of DCs and monocytes were observed in spleen. Statistical differences were assessed by One-Way ANOVA with Dunnett's multiple comparison test. **E**: IFN-α cytokine levels were not significantly different in μMT and clodronate-treated mice compared to wild type mice after LNP immunization. IP-10 was slightly increased in clodronate-treated mice, but similar in μMT mice, compared to wild type mice, as determined by One-Way ANOVA with Dunnett's multiple comparison test. *: $p<0.05$, **: $p<0.01$, ***: $p<0.001$, ns: not significant.